Master's thesis

NTNU
Norwegian University of Science and Technology
Faculty of Medicine and Health Sciences
Department of Clinical and Molecular Medicine

Daniel Margarido Galán

Investigating the immunomodulatory effects of SARS-CoV-2 proteins ORF3a, ORF6 and ORF9b on the inflammatory response of human lung epithelial cells

Master's thesis in Molecular Medicine
Supervisor: Markus Haug
Co-supervisor: Claire Louet
June 2022

NTNU
Norwegian University of Science and Technology

Daniel Margarido Galán

Investigating the immunomodulatory effects of SARS-CoV-2 proteins ORF3a, ORF6 and ORF9b on the inflammatory response of human lung epithelial cells

Master's thesis in Molecular Medicine
Supervisor: Markus Haug
Co-supervisor: Claire Louet
June 2022

Norwegian University of Science and Technology
Faculty of Medicine and Health Sciences
Department of Clinical and Molecular Medicine

NTNU
Norwegian University of
Science and Technology

Abstract

The COVID-19 pandemic has taken an unprecedented number of lives and brought incredibly high social costs across the globe. The disease severity is associated with a strong innate immune dysregulation characterised by low or inexistent levels of type I and type III IFNs early in disease as well as an overall heightened inflammatory response. Several proteins of SARS-CoV-2, the causative agents of COVID-19 have been identified as important contributors to the immunopathology. These viral proteins may interfere with innate immune functions of the host cell and thus enable immune evasion of the virus. Most of the research on immune evasion of SARS-CoV-2 has been centred on type I IFN rather than type III IFN responses, which are the family of IFNs that are mainly produced by lung epithelial cells, the main target and replication site of SARS-CoV-2. Moreover, these studies have been mostly performed on cell models that are not as relevant in the context of SARS-CoV-2 infection. In this project, we focused on studying the effects of SARS-CoV-2 proteins on the production of type III IFNs and other inflammatory cytokines in lung epithelial cells. A549 human lung epithelial cells transduced with plasmids for the SARS-CoV-2 proteins ORF3a, ORF6 and ORF9b under a doxycycline-inducible promotor were used for this study. We analysed the production of type III IFNs, pro-inflammatory cytokine IL-6 and chemokine IL-8 after stimulation of the RIG-I/MDA5 signalling pathway by poly(I:C) treatment. We found IL-6 to be upregulated at the mRNA transcript level in cells expressing SARS-CoV-2 proteins. This suggests a possible role of these SARS-CoV-2 proteins in the enhancement of the inflammatory response in the organism that is linked to complications in the patients' outcome. However, ORF3a, ORF6 and ORF9b induced no significant changes in the production of type III IFNs, IL-6 and IL-8 at the protein level. As of today, the precise functions of these and other SARS-CoV-2 proteins are yet to be completely unveiled. Our study indicates that ORF3a, ORF6 and ORF9 do not significantly alter the outcome of stimulation of the RIG-I/MDA5 pathway in human epithelial cells. Further studies on virus-host interactions with other SARS-CoV-2 proteins or in other model systems might deepen our knowledge on the immunomodulatory functions of CoV-2 proteins and contribute to develop therapeutical tools for the treatment of COVID-19 and other similar outbreaks that could arise in the future.

Acknowledgements

This Master Thesis project was conducted in the Mycobacterial and HIV-1 Infections Research Group led by Prof. Trude Helen Flo at the Centre of Molecular Inflammation Research (CEMIR), included in the Faculty of Medicine and Health Sciences of the Norwegian University of Science and Technology (NTNU) in Trondheim.

First of all, I would like to thank my main supervisor, Dr. Markus Haug for allowing me to join this research group and giving me the opportunity to work on such an interesting project. I can say that I have acquired a deeper of knowledge of the field during the course of this Master Thesis thanks to his invaluable guidance and experience. I would also like to express my gratitude to my co-supervisor Claire Louet, who has constantly supported me throughout the entirety of this project by checking up on me and giving me the most useful and earnest advice on my work inside and outside the laboratory. She made sure that not only I understood the experiments I was performing, but also how to adapt them for future research when the conditions of the study might have changed. Also, I would like to acknowledge Alexandre, Anne, Ragnhild, Ingvild, Sindre, Marit and all the other members of our group and of CEMIR, who have had the kindness of dedicating their time to helping me learn the different methods as well as navigate the laboratory environment with ease.

Likewise, I would like to thank my fellow classmates and friends for sharing great experiences with me and contribute to making my student life in Trondheim a memorable one. I truly appreciate and cherish all the connections that I have made thanks to this master's degree, as they have given me an incredible amount of joy over the past two years.

Last but not least, my gratitude goes to my family for being supportive and encouraging me in all my endeavours, for always guiding me and trusting me in my decisions. They provide me with a great deal of love and strength, which allow me to move forward and pursue my ambitions.

Daniel Margarido Galán Trondheim, June 2022

Table of Contents

List of Figures

List of Tables

List of Abbreviations

ACE2 Angiotensin-Converting Enzyme 2

ANOVA Analysis of variance

ARDS Acute respiratory distress syndrome

AP-1 Activator protein 1

ATCC American Type Culture Collection

BSA Bovine Serum Albumin

CARD Caspase activation recruitment domains

CCM Complete culture media

COVID-19 Coronavirus disease-19

CXCL Chemokine (C-X-C) Ligand

DAMP Damage-associated molecular pattern

DMEM Dulbecco's Modified Eagle's Medium

DMSO Dimethyl sulfoxide

DPBS Dulbecco's Phosphate Buffered Saline

DPP4 Dipeptidyl peptidase 4

DTT dithiothreitol

EDTA Ethylenediaminetetraacetic acid

ELISA Enzyme-linked Immunosorbent Assay

FBS Foetal Bovine Serum

FCS Foetal Calf Serum

GAPDH Glyceraldehyde 3-phosphate dehydrogenase

GFP Green fluorescent protein

HAECs human air-liquid airway epithelial cells

HEK293T Human embryonic kidney 293T cells

HIV-1 Human immunodeficiency virus 1

HRP Horseradish peroxide

IFN Interferon

IFNAR Interferon Alpha Receptor

IFNLR Interferon Lambda Receptor

IKK IκB kinase

IL Interleukin

IRF Interferon regulatory factor

ISG Interferon-stimulated gene

ISGF3 Interferon-stimulated gene factor 3

ISRE Interferon-stimulated Response Element

JAK Janus kinases

LDH Lactate Dehydrogenase

MAMs Mitochondrial associated membranes

MAVS Mitochondria antiviral-signaling protein

MDA5 Melanoma differentiation-associated gene 5

MDM Monocyte-derived macrophages

MERS Middle Eastern Respiratory Syndrome

MERS-CoV Middle Eastern Respiratory Syndrome Coronavirus

MTS 3-(4,5-dimethylthiazol-2-yl)-5-(3-carboxymethoxyphenyl)-2-(4-sulfophenyl)-2H-tetrazolium

MTT 3-(4,5-dimethylthiazol-2-yl)-2,5-diphenyltetrazolium bromide

NADH Nicotinamide adenine dinucleotide hydrogen

NF-κB Nuclear factor kappa-light-chain enhancer of activated B cells

NK cell Natural Killer cell

NLRP Nucleotide-binding oligomerization domain

NSP Non-structural protein

OAS 2',5'-oligoadenylate synthetase

ORF Open Reading Frame

SDS-PAGE sodium dodecyl sulphate–polyacrylamide gel electrophoresis

PAMP Pathogen-associated molecular pattern

PBMC Peripheral blood mononuclear cells

PBS Phosphate Buffered Saline

RT-qPCR Reverse Transcriptase Quantitative Polymerase Chain Reaction

PRR Pattern Recognition Receptor

iPSC induced pluripotent stem cell

PVDF polyvinylidene difluoride

RIG-I Retinoic-acid inducible gene I

RLR RIG-I like receptor

RNA Ribonucleic acid

RT Reverse Transcriptase

RTC Replicase/transcriptase complex

SARS-CoV Severe Acute Respiratory Syndrome-Coronavirus

SARS-CoV-2 Severe Acute Respiratory Syndrome-Coronavirus 2

STAT Signal transducers and activators of transcription

TBK1 TANK-binding kinase 1

TBS-T Tris Buffered Saline with Tween-20

TEER Transepithelial electrical resistance

TLR Toll-like Receptor

TNF Tumour-necrosis factor

TOM70 Mitochondrial surface receptor

TRIF TIR-domain-containing adapter-inducing interferon-β

TYK2 Tyrosine kinase 2

WHO World Health Organization

WT Wild-type

1. Introduction

1.1. COVID-19 and the Innate Immune System

In the past two decades, coronaviruses have been responsible for major zoonotic outbreaks of highly lethal respiratory diseases in humans characterised by a pronounced proinflammatory response[1-4]. Namely, 2002 was the year that saw the first severe acute respiratory syndrome (SARS) epidemic, which affected over 8,000 people in Asia and presented a mortality rate of around 10%[3]. A decade later, in 2012, another epidemic caused by the Middle East respiratory syndrome coronavirus (MERS-CoV) emerged, involving more than 2,000 infections and 800 deaths and being still active to this day[5, 6]. Today, yet another health crisis, the infamous coronavirus disease 19 (COVID-19) pandemic, is being confronted at a truly global scale. The COVID-19 pandemic is attributed to the latest form of coronavirus, the severe acute respiratory syndrome coronavirus 2 (SARS-CoV-2), and after its emergence in late December 2019 it has been responsible for over 500 million confirmed cases with a cost of 6.2 million deaths worldwide (as of April 27th, 2022)[1, 7-9].

As evidenced over the course of these past two years, COVID-19 has proven to be a highly pathogenic disease in humans, threatening the lives of mainly the elder population and those individuals afflicted by underlying medical conditions such as cardiovascular disease, hypertension, obesity, diabetes, chronic respiratory disease and cancer[8-12]. Individuals with these conditions are at higher risk of severe COVID-19 due to systemic inflammation innate and adaptive immune response disorder and tissue damages[9]. SARS-CoV-2 produces a wide spectrum of diseases, predominantly infecting the respiratory tract and causing a broad array of respiratory symptoms. In the majority of cases, COVID-19 patients are either asymptomatic or experience mild to moderate airway symptoms consisting of sore throat, cough, fever, anosmia and dyspnoea, recovering without the need of special treatments. However, up to 10 to 15 % of patients (mainly those with the aforementioned comorbidities) manifest severe pneumonia and some develop hypoxia and acute respiratory distress syndrome (ARDS). The outcome of these cases deeply depends on critical care facilities with mechanical ventilation, still existing a high mortality risk. "Long-COVID" is also significantly recurrent among patients, in which pneumonia causes long-lasting symptoms and morbidity[8, 13]. In

addition, other disorders observed in the progression of severe COVID-19 include thrombocytic lung damage, disseminated intravascular coagulation, acute kidney injury and multi-organ failure[8, 9, 14-18].

Notably, severe COVID-19 and death have been associated with a dysregulated innate immune response to SARS-CoV-2 infection, characterised by inappropriate hyperinflammation with unbalanced production of C-reactive protein and lactate dehydrogenase, low and delayed antiviral interferon-responses, overexuberant release of pro-inflammatory cytokines, lymphopenia and infiltration of mononuclear cells in infected tissues[9, 18-21]. All these hallmarks are part of a systemic inflammatory state in the organism that worsens the outcome of those patients afflicted by severe COVID-19.

1.1.1. General structure, tropism and life cycle of SARS-CoV-2

Coronaviruses are not only a threat for public health, but also for companion animals, livestock and the economy in general, since they are able to infect other mammals and avian species[4]. In humans, 10 to 35 % of upper respiratory tract infections falling under the umbrella of common-cold are attributed to coronaviruses[22]. This branch of viruses was first discovered in the 1930s and is classified in the family *Coronaviridae* and subfamily *Orthocoronavirinae*, which comprises the four major genera *Alphacoronavirus, Betacoronavirus, Gammacoronavirus and Deltacoronavirus*[4]. They present single-stranded positive-sense RNAs ((+)ssRNAs), ranging from 26 kb to 32 kb, being the biggest known viral RNA genome size, and feature spikes on their surfaces resembling the shape of a crown[12, 23]. SARS-CoV-2 belongs to the genus *betacoronavirus* together with SARS-CoV and MERS-CoV, which have roughly 80% and 50% homology to SARS-CoV-2, respectively[23]. Inside this genus, SARS-CoV and SARS-CoV-2 are placed in the *Sarbecovirus* subgenus (B lineage) and infect host cells via the angiotensin-converting enzyme 2 (ACE2), whereas MERS-CoV is identified within the *Merbecovirus* subgenus (C lineage), infecting host cells via the dipeptidyl peptidase (DPP4)[4].

The genome of SARS-CoV-2 is 29.9 kb in length, features 14 open reading frames (ORFs) and codes for 27 proteins, which can be classified into structural proteins, non-structural proteins and accessory proteins[1, 12]. In detail, there are four structural proteins coded in the genome that are crucial for the formation of

virions: the spike (S), envelope (E), membrane (M) and nucleocapsid (N) proteins. There are also 16 non-structural proteins (NSPs) coded in the genome, which constitute the replication-transcription complex and ensure viral RNA replication [9, 12, 23]. Furthermore, it has been proposed that 7 interspersed open reading frames (ORF3a, ORF3b, ORF6, ORF7a, ORF7b, ORF8, and ORF9) code for accessory proteins, which carry out modulatory functions to enhance virulence and contribute to viral immune evasion strategies[1, 9, 23-26]. The NSPs are coded by two large ORFs (ORF1a and ORF1b) that make up two-thirds of the SARS-CoV-2 genome and are situated at its 5′ end, whereas the structural and accessory proteins are transcribed from the 3′ end and make up for the remaining one-third of the genome[4] (**Figure 1**).

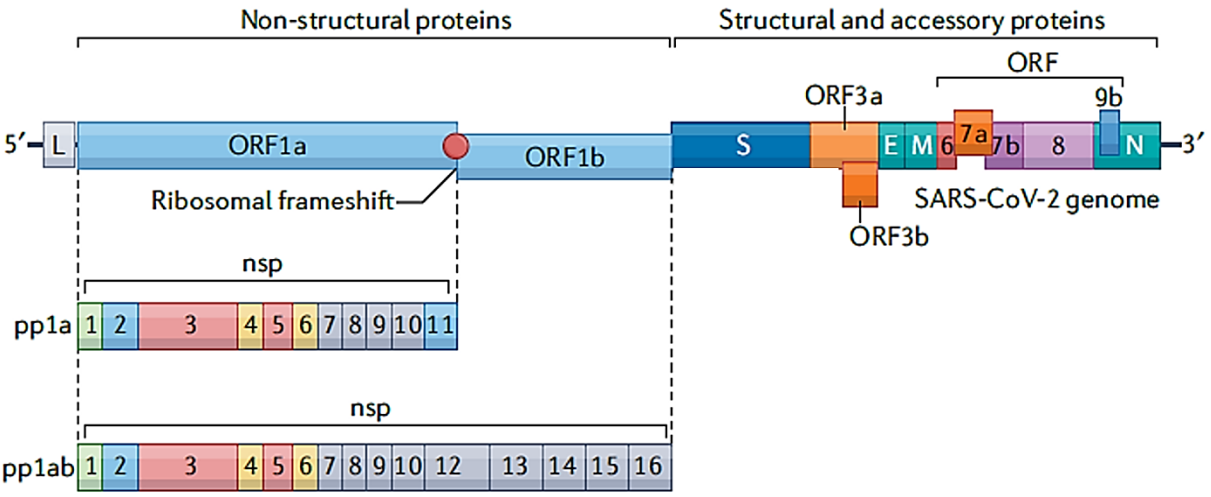

Figure 1. Configuration of the SARS-CoV-2 genome. *The viral genome of SARS-CoV-2 features a leader sequence (L) in its 5′ end. Polyprotein 1a (pp1a) and pp1ab are encoded in the open reading frame 1a (ORF1a) and ORF1b. Non-structural proteins Nsp1-11 are encoded by pp1a, whereas nsp12-16 are encoded by pp1ab and expressed upon ribosomal frameshift at the junction of nsp11 and nsp12. Downstream, these genes are followed by the spike (S), the envelope (E), the membrane (M) and the nucleoprotein (N) structural proteins coding genes, which present inserted in between them the ORF3a, ORF3b, ORF6, ORF7a, ORF7b, ORF8 and ORF9b coding for accessory proteins. Figure adapted from Wong et al., Nature Reviews Immunology, 2022 [1].*

The viral envelope of SARS-CoV-2 is composed of M, E and S proteins, the latter determining the tropism and entry of the virus into the host cells. The reason why SARS-CoV-2 is known to have higher transmissibility than its predecessor SARS-CoV is based on the stronger affinity of its S protein receptor-binding domain (RBD) for ACE 2, the virus entry receptor on host cells[27]. ACE2 is predominantly expressed on lung, liver, gastrointestinal tract and kidney cells (proteinatlas.org). There is less than 75% shared nucleotide identity between the S protein of SARS-

CoV-2 and SARS-CoV[23] and these differences modify the structure of the RBD, making it more or less successful in recognising and binding the target receptor as well as initiating viral entry into the host cell. Additionally, the presence of the transmembrane protease serine 2 (TMPRSS2) is also necessary to efficiently infect the host cell, as it primes the S protein[4, 28]. The other structural protein, the N protein, creates complexes with the genomic RNA (gRNA) inside the viral particle and has been demonstrated to enhance the infectivity of the S protein, contributing to the spread of SARS-CoV-2[29].

SARS-CoV-2's primary means of transmission is via respiratory droplets or direct contact with an infected individual[12, 23]. The virus predominantly infects ciliated epithelial cells in nasal mucosa and bronchus as well as type II alveolar pneumocytes in lung alveoli, which express both ACE2 and TMPRSS2[30-33]. Once the coronavirus particles are bound to cellular attachment factors, the RBD in the S protein establishes specific S interactions with the cellular receptor ACE2 promoting viral uptake by receptor-mediated endocytosis in most cases. This process is followed by endosomal acidification, activating the S protein after proteolytical cleavage by cathepsin B and cathepsin L. The activated S protein enables the fusion of SARS-CoV-2 with the endosomal membrane and release of the viral genome into the cytosol of the host cell[12, 31]. From this moment on, the transcription and replication cycles begin, being highly regulated in space and time. First, ORF1a and ORF1b are translated into pp1a and pp1ab respectively. These are two large polyproteins that produce sixteen NSPs after undergoing auto-proteolytic cleavage by NSP3 (papain-like protease) and NSP5 (3C-like protease), two viral cysteine proteases[4]. NSPs are cleaved and released in order, starting with NSP1, which recruits the host cell translation machinery. Subsequently, NSP2-16 creates the viral replicase/transcriptase complex (RTC), where NSP12 is the RNA-dependent RNA polymerase (RdRP), having NSP7 and NSP8 as cofactors. The RTC then generates new copies of gRNA and transcribes them into a nested set of sub-genomic mRNAs that are eventually translated into the accessory proteins ORF3a, ORF4, ORF6, ORF7a, ORF7b, ORF8, ORF9b and ORF10[4, 34]. Interestingly, the replication and transcription processes occur within a protective microenvironment delimitated by small open double-membrane spherules, convoluted membranes and characteristic perinuclear double-membrane vesicles, constituting viral replication organelles[4, 35]. The structural proteins are the last to be expressed and

they are translated by ribosomes attached to the endoplasmic reticulum (ER), translocating into the ER membranes and transiting via the ER-to-Golgi compartment, where viral assembly around the N-encapsulated gRNA takes place [4, 12]. Finally, the newly produced virions are budded into the lumen of secretory vesicular compartments and released from the host cell by exocytosis, budding or cell death, after which they will continue to infect neighbouring cells, allowing SARS-CoV-2 to disseminate throughout the organism [4, 12, 26, 31, 36].

1.1.2. Induction of innate immune responses against Coronaviruses

When viruses and bacteria establish contact with the host, the innate immune system is the first line of defence that they encounter, initiating immunological responses as soon as infection occurs. These first responses are then detected and magnified by immune cells (e.g. dendritic cells, monocytes/macrophages, neutrophils, cytotoxic T cells, helper T cells, B cells/plasma cells)[37]. Upon coronavirus infection, pattern recognition receptors (PRRs) recognise viral ssRNA, dsRNA intermediaries and protein structures, which constitute pathogen-associated molecular patterns (PAMPs). Further, PRRs will trigger the expression of chemokines, pro-inflammatory cytokines and type I and III interferons (IFNs)[38-40]. Namely, it has been shown that numerous antiviral effectors are induced by IFN responses in the infected host and neighbouring cells. As a result, all these molecules foster the humoral and cell-mediated immune responses that are essential in the fight against infections that cannot be contained by the initial innate immune mechanisms. The adaptive immune response will eventually establish long-term immune memory against the pathogen[40].

PRRs are present in different subcellular locations. On the one hand, Toll-like receptors (TLRs) are PRRs embedded in cell membranes and located in the endosomal membranes (e.g. TLRs 3, 7, 8 and 9) or in the surface of the cell (e.g. TLRs 1, 2, 4, 5 and 6)[41-43]. In detail, endosomal TLRs sense the presence of internalised viral nucleic acids and recruit Toll interleukin-1 (IL-1) receptor (TIR)-domain-containing adapter-inducing interferon (TRIF) and Myeloid differentiation primary response 88 (MyD88)[43, 44]. However, there are exceptions as in the case of dsDNA sensing TLR3, which only recruits TRIF and not MyD88. These are two adapter proteins that bind the cytoplasmic section of the TLRs through homophilic interactions with their TIR domains. Once recruited, they mediate the activation of several transcription factors including interferon regulatory factors (IRFs),

activator protein 1 (AP-1) and nuclear factor kappa-light-chain enhancer of activated B cells (NF-κB)[38, 39, 43]. Interestingly, it has been found that TLR2 recognises the E protein from SARS-CoV-2 on the surface of human bone marrow-derived macrophages and human peripheral mononuclear cells (PBMCs)[45]. On the other hand, apart from their location in the cell surface or endosomal membranes, PRRs are also found in the cytosol, as is the case for NOD-like receptors (NLRs), retinoic-acid inducible gene I (RIG-I)-like receptors (RLRs), AIM2-like receptors and the cyclic guanosine monophosphate–adenosine monophosphate synthase (cGAS). These PRRs can detect PAMPs, damage associated molecular patterns (DAMPs) and viral material such as RNA and DNA in the cytosol[46, 47]. The RLR family is comprised of 3 members: RIG-I, melanoma differentiation-associated gene 5 (MDA5) and laboratory of genetics and physiology 2 (LGP2). All RLRs have a carboxy-terminal domain and a DECH-box helicase domain that work in consonance to bind and detect foreign RNA[48]. In the context of SARS-CoV-2 infection, the RLR RIG-I and melanoma differentiation gene 5 (RIG-I/MDA-5) is particularly important for the detection of dsRNA[49-51].

1.2. The role of the RIG-I/MDA5 and NF-κB pathways in infection

RIG-I/MDA5 is the primary sensor of SARS-CoV-2 nucleic acids in human epithelial cell lines and the main initiator of innate immune responses against the virus[49-52]. Its activation leads to the induction and production of chemokines, cytokines as well as type I and type III IFNs. In depth, SARS-CoV-2 ssRNA and dsRNA intermediaries are recognised by RIG-I/MDA5, activating the cytosolic receptor and enabling the interaction of its caspase activation recruitment domains (CARD) with the adapter mitochondria antiviral signalling protein (MAVS)[53-55]. From this point, there are two divergent signalling pathways. In one signalling pathway, MAVS recruits TANK-binding kinase 1 (TBK1) and inhibitory-κB (IκB) kinase epsilon (IKKε)[44], two IKK-related kinases that activate IRF3 and IRF7 by phosphorylation. Subsequently, activated IRF3 and 7 are translocated into the nucleus, where they act as transcription factors to promote the expression of type I and III IFN genes[39, 43, 44, 56, 57] (**Figure 2**). In a parallel signalling pathway, MAVS activates AP-1 and NF-κB, the transcription factors responsible for the expression

of chemokines such as chemokine ligand 8 (CXCL8) or IL-8 and inflammatory cytokines such as IL-1, IL-6 and tumour necrosis factor alpha (TNF-α)[39, 56-58]. Of note, one of the most predominant inducers of RIG-I/MDA5 together with other PRRs such as TLR3 used in research is polyinosinic:polycytidylic acid or poly(I:C). Poly(I:C) is a synthetic analogue of viral dsRNA that induces type I IFN and IFN-stimulated gene expression, enhances antiviral activity in the target cells[39, 56, 59-62]. Pure poly(I:C) is taken up by endocytosis and interacts with TLR3, which is located in the endosomal membrane. Thus, poly(I:C) alone mainly stimulates TLR3 responses. In order to activate cytosolic RNA receptors such as RIG-I/MDA5, poly(I:C) delivery needs to be combined with a transfection reagent (TR) (e.g. LyoVec, Lipofectamine RNAiMAX, TransITLT1, X-tremeGENE)[56, 61, 63, 64].

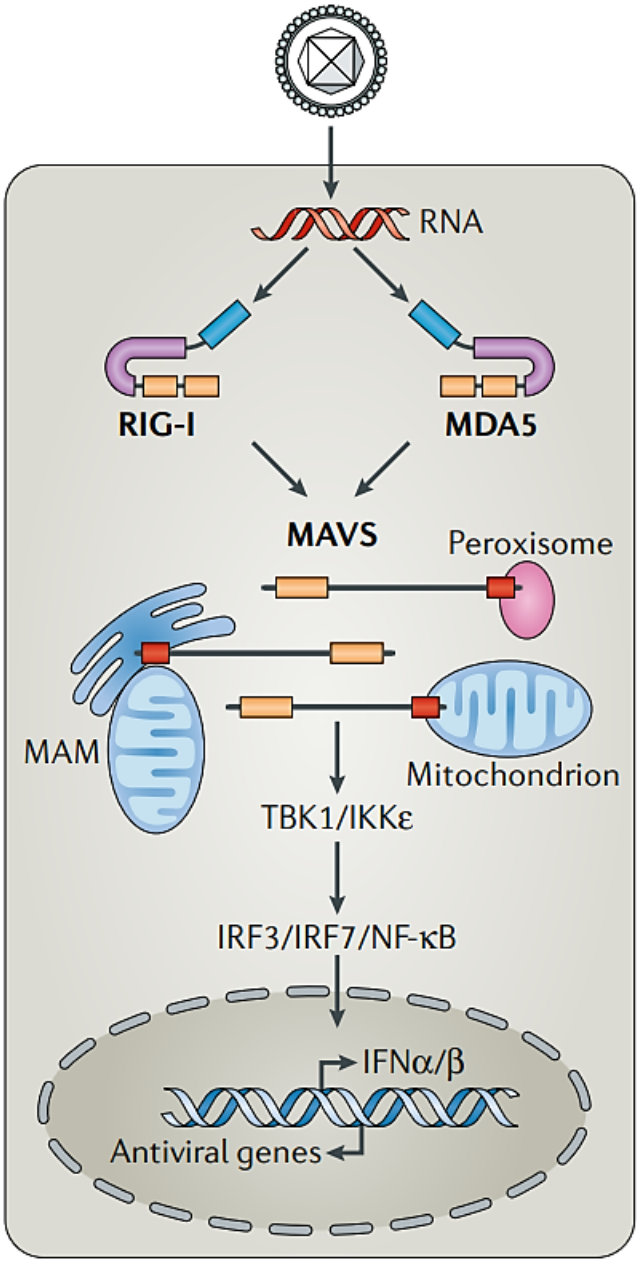

Figure 2. RIG-I/MDA5 signalling pathway. *Immunostimulatory RNA activates RIG-I and MDA5, prompting their interaction with MAVS, which is anchored in the surface of mitochondria, peroxisomes or mitochondrial associated membranes (MAMs). MAVS then transmits the signal to TBK1 and IKKε, which in turn activate IRF3 and IRF7. These transcription factors, together with* MAVS-activated *NF-κB, induce the expression of IFNs and other antiviral genes. Figure obtained from Rehwinkel et al., Nature Reviews Immunology, 2020* [46].

As mentioned before, the main transcription factors responsible for proinflammatory cytokine expression are IRF3/7 and NF-κB. The latter one initiates numerous signalling cascades that are collectively known as the NF-κB pathway. NF-κB comprises a family of transcription factors: NF-κB1

(p50 and its precursor p105), NF-κB2 (p52 and its precursor p100), Reina (p65), ReIB and c-ReI homo/heterodimers with ReIA or ReIB. Notably, not only is the NF-κB pathway triggered by PRRs as it has been previously mentioned, but also by the TNF receptor (TNFR) superfamily, the T-cell and B-cell receptors and ligands of several cytokine receptors. All these receptors respond to a broad range of stimuli such as infectious agents, microbial components, mitogens, growth factors and cytokines, leading to the activation of the multi-subunit IKK complex. The IKK complex then phosphorylates IκBα inducing its proteasomal-mediated degradation. Since IκBs forms a complex with NF-κB blocking its function and ensuring its retention in the cytoplasm, once IκBα is degraded the NF-κB:IκB complex is disrupted and NF-κB is translocated into the nucleus, where it will induce pro-inflammatory cytokine, chemokine and IFN gene expression[9, 65]. Namely, IL-6, IL-8, IFN-λ1 and IFN- λ3 are some of the most relevant cytokines in the innate immune response against SARS-CoV-2. These cytokines will be described in detail in **section 1.3.** Interestingly, some pro-inflammatory cytokines like TNF-α have an autocrine effect on the same cell, further stimulating the NF-κB signalling pathway via TNF receptors in a positive feed-forward loop[66]. The role of NF-κB in the context of an infection is crucial, as evidenced by its regulatory actions on important cellular behaviours including cell growth, inflammatory responses and apoptosis[9]. Indeed, some viruses such as hepatitis B virus, hepatitis C virus and human immunodeficiency virus (HIV-1) have developed immune evasive strategies that interfere with the NF-κB pathway, since it is an integral part of host cell's defence mechanisms against viral infection.[67]. Moreover, regarding SARS-CoV-2, it has been proven that NSP5 is capable of SUMOylating MAVS rendering it more stable and triggering an overall increase in the activation of NF-κB[68]. However, many of the underlying mechanisms that allow SARS-CoV-2 to modulate NF-κB functions have not yet been elucidated.

1.3. Cytokines and IFN responses

Proinflammatory cytokines are important molecules that mobilise host defence. However, they can also be detrimental, as they sometimes drive pathologic inflammation. This is explained by the nature of the inflammatory response, which can have an antiviral effect by restricting viral replication and infection or a proviral

effect by helping the release of virions from the host cell facilitating viral dissemination[1, 69]. Recognition of viral structures by PRRs results in the production of cytokines. RIG-I/MDA5 induces the expression of IL-1, IL-6, TNF-α and IL-8 via NF-κB and IRF3 and 7, whereas it induces the expression of type I and type III IFNs via IRF3 and 7[54, 70]. This cocktail of cytokines is responsible for the development of an antiviral state in the organism. In response, viruses have developed strategies to evade the host cell's inflammatory response. In this project, we focus on the study of IL-8, IL-6 and type III IFNs production because of their crucial role and predominance in the context of SARS-CoV-2 infection in the lung, as reported by numerous studies[8, 18, 71-73].

IL-8, also known as CXCL8, is a critical inflammatory mediator induced by RIG-I/MDA5 via the NF-κB pathway that has been studied extensively. This chemokine has been found in elevated concentrations in serum samples from severe COVID-19 patients[18, 19]. The primary function of IL-8 and other chemokines such as CXCL2 is the chemoattraction of neutrophils, being mainly expressed in macrophages[19, 74, 75]. Additionally, IL-8 also plays a key role in the chemotactic migration and activation of lymphocytes, monocytes, eosinophils and basophils at sites of inflammation[76], and it behaves as an angiogenic factor in human microvascular endothelial cells[77]. When IL-8 binds to the neutrophiles CXC receptor 1 or 2 (CXCR1/2), several intracellular signalling cascades are initiated, of which the most significant is the mitogen-activated protein kinase (MAPK) signalling pathway. This cascade enables the release of effector molecules (lisozymes, defensins, antimicrobial proteins, etc.) by degranulation and promotes cell survival, proliferation and inflammation[74].

IL-6 is a pleiotropic cytokine that is also induced by RIG-I/MDA5 via the NF-κB pathway and is expressed by immune and non-immune cells including fibroblasts, endothelial cells, mononuclear phagocytes, T-cells, B-cells and bone marrow cells [78]. Similarly to IL-8, elevated concentrations of IL-6 have been detected in serum samples from severe COVID-19 patients. IL-6 plays a critical role in the final maturation of B-cells into plasma cells, the activation of T-cells as well as the differentiation and regulation of T regulatory cells (Treg) and T helper 2 (Th2) cells[79, 80]. Consequently, IL-6 is essential in the development of adaptive immunity. Furthermore, it stimulates the secretion of acute phase proteins in the liver[81]. Upon binding the IL-6 receptor (IL-6R), IL-6 initiates the Janus kinase signal transducers

and activators of transcription (JAK-STAT) signalling pathway, which prompts the translocation of STAT3 to the nucleus. STAT3 then promotes cytokine, growth factor and angiogenic factor gene expression, creating feed-forward loops by further activating the JAK-STAT pathway[74, 82, 83]. All these molecules contribute to cytotoxic responses that are vital for the elimination of intracellular pathogens[39]. Thus, both IL-8 and IL-6 constitute central pieces of the innate immune system.

IFNs are another group of antiviral cytokines that have a critical role in the fight against viral infections. IFNs are imperative to virus containment and elimination. Type I and type III IFNs are key members of the IFN family in antiviral immune responses and can signal in an autocrine or paracrine way[40]. Type I IFNs are relevant to the induction and regulation of systemic responses defined by inflammatory features, whereas the role of type III IFN is pivotal to the protection against viral infections in epithelial barriers[84, 85]. Type I and III IFNs are secreted early upon viral infection following the activation of NF-κB and IRFs via the RIG-I/MDA5 pathway. Immune cells such as plasmacytoid dendritic cells and macrophages are the most important type I IFN inducers, whereas epithelial cells are one of the main cell types to produce type III[84, 86, 87]. Since the principal target of SARS-CoV-2 are lung epithelial cells, studying type III IFN responses in these cells is of great interest. Moreover, type III IFN production may be an essential defence pathway for lung epithelial cells in order to signal that they are infected and attract other cells to the site of infection. In humans, the type I IFN family consists of 13 proteins: The type I IFN-α subtypes as well as IFN-β, IFN-ε, IFN-κ and IFN-ω. The type III IFN includes subtypes, IFN-λ1 (IL-29), IFN-λ2 (IL-28A), IFN-λ3 (IL-28B), and IFN-λ4. Interestingly, IFN-λ1, -λ2 and -λ3 have distinct promoters, further illustrating the intricacy of type III IFN transcriptional regulation[88]. Furthermore, it has been demonstrated that the subcellular localization of MAVS determines the type of IFNs produced by the cell upon PRR stimulation. Specifically, mitochondria-located MAVS favours type I IFN production, while peroxisome-located MAVS encourages type III IFN production[89-91]. Notwithstanding, the differential expression of type I and type III IFNs across different cell types remains to be fully characterised. IFNs promote the expression of hundreds of interferon-stimulated genes (ISGs) and other antiviral effectors (e.g. Mx1, OAS, IFIT1, Protein kinase R), which inhibit viral entry, replication, translation and release[1, 40]. In the infected host cell and neighbouring cells, they

induce signalling pathways in an overlapping manner sharing a number of functions through the expression of a wide range of antiviral effector proteins that constrain viral replication and encourage viral clearance[92]. All these findings shed light on the distinct functions that both types of IFN carry out against viral infections.

The signalling pathway that is activated in response to IFNs is the JAK-STAT signalling pathway. Type I IFN signals via its heterodimeric IFN-α/β receptor (IFNAR1/IFNAR2), whereas type III IFN signals via its IFN-lambda receptor IFNLR, which is comprised by subunits IFNLR1 and IL10Rb[84]. Theoretically, all cell types are able to detect and respond to the presence of type I IFN, given that IFNAR1/IFNAR2 is ubiquitously expressed. In contrast, IFNLR is primarily expressed in epithelial cells of the respiratory, gastrointestinal and female reproductive tract as well as in some immune cells to a certain extent (e.g. neutrophils)[84, 88]. Both type I and type III IFNs activate JAK1 and tyrosine kinase 2 (TYK2) promoting downstream phosphorylation of STAT1 and STAT2, which recruit IRF9 leading to the assembly of interferon-stimulated gene factor 3 (ISGF3), a transcription factor complex that translocates to the nucleus[93, 94]. In the nucleus, ISGF3 binds IFN-stimulated response elements (ISREs) in order to activate the expression of ISGs and induce antiviral responses[94] (**Figure 3**). All in all, more extensive research has been conducted on the induction of type I IFNs and their effector responses than on type III IFNs. Consequently, further studies on type III IFNs ought to be performed in order to have a more holistic view of their immunological actions.

Patients and animal models infected with SARS-CoV, MERS-CoV or SARS-CoV-2 present pathologically heightened inflammatory responses with elevated levels of cytokines[1]. Namely, serum analysis of COVID-19 patients has allowed the extensive characterisation of chemokines such as IL-8, proinflammatory cytokines such as IL-1β and IL-6 and TNF-α, which are overabundant throughout the course of the disease[1, 8]. This set of inflammatory mediators have been correlated with disease severity[18, 71-73]. Lung epithelial cells would be the first ones to overexpress these signalling molecules in order to recruit myeloid cells to the site of viral infection, since they constitute the primary site of infection[74]. Therefore, lung epithelial cell models such as Calu-3 and A549 cell lines would be adequate for the study of SARS-CoV-2 infection in the lung.

1.4. Dysregulation of Innate Immunity in (severe) COVID-19

The current pandemic has stressed the importance of the immune system in the fight against COVID-19, illustrating how different individuals may produce differing immunological responses to SARS-CoV-2 infection. Numerous studies have suggested that the main cause of COVID-19 outcomes is not only a marked dysregulation of the host immune response, but also an active viral interference with the immune system[95]. This conditions the patients to have a higher propensity to ARDS and death (i.e. severe cases of coronavirus infection) instead of the symptoms of a mild common cold. Weakened and delayed innate immune and inflammatory responses early during SARS-CoV-2 infection are major determinants of severe COVID-19 cases, in which exhibit deterioration of the patients' condition from day 7-8[20]. This results in the development of hyperinflammation with an excessive production of inflammatory cytokines and an impaired induction of IFN responses. These pathological features that constitute major drivers for the most critical outcomes. Additionally, several viral proteins have been identified as deregulators of innate immunity, being inducers of inflammasome activation and contributing to the impairment of IFN induction and signalling[1, 96]. Overall, for new therapeutic alternatives to be designed rationally, the mechanisms behind the dysregulation of the innate immune system as well as the evasion strategies of SARS-CoV-2 and its interaction with host defence responses need to be understood more in depth.

1.4.1. Immunological features of severe COVID-19

Severe COVID-19 and death have been associated with a dysregulated innate immune response to SARS-CoV-2 infection. This aberrant innate immunity is characterised by an and TNF-α among others. On the other hand, type I and type III IFNs responses were found to be impaired early in the disease course, correlating with the development of severe COVID-19 and propensity to fatal outcome[97]. Severe COVID-19 cases also exhibit an unbalanced production of C-reactive protein, ferritin and D-dimers (serum markers of excessive inflammation) as well as lactate dehydrogenase (cell death indicator). In addition, low and delayed antiviral interferon-responses, overexuberant serum levels of pro-inflammatory cytokines and chemokines, lymphopenia and infiltration of mononuclear cells in infected tissues have also been reported[4, 9, 18-21, 24, 72, 97-103].

Moreover, the patients' exacerbated state of inflammation and antiviral immune response dysregulation was further heightened by the viral interference with modulators of the complement and coagulation systems, prompting clot formation (thrombosis), vascular leakage and intravascular coagulation[104, 105]. Interestingly, the primary contributors to the immunopathology of fatal COVID-19 and its clinical manifestations are not only epithelial cells at the primary site of infection (mainly lung), but also in the liver, gastrointestinal tract or even central nervous system, as well as infected endothelial cells[106, 107].

Focusing on the dysregulation of innate immune responses, infected lung epithelial cells have been found to be the first responders to SARS-CoV-2 infection, as they trigger inflammatory responses by producing the earliest waves of chemokines and cytokines[74, 97, 108, 109]. Specifically, patients afflicted by severe COVID-19 exhibit elevated serum levels of circulating IL-8/CXCL8, CCL2 and CCL8[18, 19, 97, 98], which remain present in the organism beyond viral clearance. CCL2 and CCL8 are recruiters of monocyte-derived macrophages which are found in high numbers in lungs of severe patients[110], whereas CXCL2 and CXCL8 (IL-8) are neutrophile recruiters[19]. An excessive recruitment of neutrophils to the site of infection in response to elevated chemokine secretion entails a higher risk of collateral damage worsening the patient's outcome.

Although a precise signature of inflammatory markers that could serve as a diagnostic tool for poor COVID-19 prognosis does not exist due to patient-to-patient variability, raised levels IL-6 and TNF-α have been identified as a common occurrence[18, 19, 97, 101, 111]. Together with the aforementioned chemokines, these cytokines are induced via inflammatory pathways such as the NF-κB pathway as a result of the hyperinflammatory response to SARS-CoV-2[109]. Secreted IL-6 and TNF represent a proinflammatory complex that reduces monocyte maturation and prompts a cytokine storm with deleterious pulmonary and systemic implications [112-116]. Among the pulmonary effects triggered by IL-6 we can emphasize the weakening of the pulmonary epithelium via vascular endothelial cadherin internalisation. This is due to IL-6's contribution to the rise in vascular endothelial growth factor production and entails the accumulation of alveolar and interstitial fluid compromising gas exchange[14, 117, 118]. All these events can be exceptionally damaging to the lungs, as they disrupt pulmonary surfactant and cause the infected alveolar epithelium to lose resorptive activity. Ultimately, this leads to an

overall increase in alveolar surface tension followed by its collapse as a consequence of an intensified proinflammatory cytokine release, further aggravating lung injury[14, 119, 120]. In parallel, the systemic effects derived from the cytokine storm induced by SARS-CoV-2 have been grouped in what has been termed as "viral sepsis syndrome". This syndrome includes hypotension, myocardial injury and shock, which result from the multiorgan failure common in severe COVID-19 patients[121]. Strikingly, it has been observed that COVID-19 severity and mortality are closely connected to elevated levels of circulating IL-6 and TNF-α. This, together with the expression of cellular markers associated with the activation of proinflammatory monocytes, constitutes a putative diagnostic marker to predict the prognosis of SARS-CoV-2 infected patients[97, 109]. Indeed, circulating levels of IL-6 as well as C-reactive protein (CRP) have been found to be highly predictive of the requirement for invasive mechanical ventilation[122].

Another noteworthy and characteristic feature parallel to the COVID-19 inflammatory signature is the temporally dysregulation of type I and type III interferon responses, which has been proven to be detrimental to all parts of the immune response to infection. Patients that experience mild or moderate COVID-19 develop normal early type I and type III IFN responses to SARS-CoV-2 infection that decrease with viral clearance and recovery from the disease[1]. In a study that compared blood plasma IFN levels relative to healthy controls, all COVID-19 patients were found to have a high presence of IFN-α, whereas only severe cases showed an increase in type III IFN levels[1, 71, 108]. This signals the importance of type III IFN dysregulation in the immunopathology of COVID-19. Furthermore, it has been observed in numerous cases that elevated levels of these IFNs and robust early expression of ISG in patients infected with SARS-CoV-2 were hallmarks of disease severity, correlating with duration of hospitalisation and mortality[1, 71, 108]. Interestingly, there is evidence that the cGAS-STING pathway is implicated in driving excessive type I IFN responses in late-stage COVID[123]. Conversely, these findings have been contradicted by other studies that reported delayed or insufficient IFN responses in severe COVID-19 cases[1, 108, 124]. This lack of effective type I and type III IFN induction together with the robust production of chemokines and inflammation mediators allows SARS-CoV-2 to replicate to higher titres, further exacerbating the inflammatory response[108, 109]. Remarkably, this decrease

in IFN response did not entail a downregulation of ISGs, since MX1 and OAS1 were found to be highly expressed in critically ill patients[108].

Taken together, this data illustrates the differences in the IFN response among COVID-19 patient populations. Remarkably, a couple of mechanisms that explain the decrease of the IFN response is the presence of serum autoantibodies against type I IFN or the incidence of genetic defects in IFN signalling pathways in some patients with poor COVID-19 prognosis[1]. Notwithstanding, additional research should be conducted in order to fully decipher the reasons for this interpatient variability[108]. All these findings support the pathological role of IFN responses in the context of SARS-CoV-2 infection, which remains elusive and is yet to be completely defined.

1.4.2. Immunomodulatory features of SARS-CoV-2 proteins

Pathogens have evolved to interfere with host defence mechanisms. Many of them encode specific proteins that participate in immune evasion strategies. It has been demonstrated that viral proteins carry out immunomodulatory actions during different steps of their life cycle (from viral uptake to replication, budding, etc.)[125]. Some of the most common immunomodulatory mechanisms of viruses consist in hindering the PRR signalling pathways, as is the case for SARS-CoV, MERS-CoV and SARS-CoV-2[126]. These mechanisms include the evasion of PRRs recognition of viral RNA, inhibition of PRRs-mediated signalling cascades, viral proteases-mediated cleavage, modulation of ubiquitination and deubiquitination and host translation shutoff[127]. However, some immune evasion strategies of SARS-CoV-2 have not been completely unveiled. One of the best ways to decipher the immune evasive and dysregulation strategies of SARS-CoV-2 is through the study of its proteins. Proteomics has benefited the discovery of host interaction partners of SARS-CoV-2 proteins as well as their sub-localisation in infected cells by providing protein interaction maps[128, 129]. Also, a number of studies have identified the possible antagonistic effects of some of these viral proteins that contribute to the progression of COVID-19[129, 130]. Specifically, some overexpression and in vitro screening studies, although inconsistent, have suggested that at least N, M, NSP1, NSP3, NSP11, NSP12, NSP13, NSP14, NSP15, ORF3, ORF6, ORF8, ORF9b and ORF10 viral proteins could interfere in innate immune responses such as IFN induction[24-26, 131]. This was verified by a combination of functional and proteomics-based interaction studies in human embryonic kidney (HEK) 293T cells that

highlighted the ability of SARS-CoV-2 proteins ORF3a, ORF6 and ORF9 to exert IFN-antagonistic effects[24, 25, 131]. Furthermore, these latter studies proposed that NSP1, NSP5, NSP13, NSP14 and NSP15 contribute to the hyperinflammatory response characteristic of severe COVID-19 cases[26, 128, 129, 131-133]. Interestingly, some SARS-CoV-2 proteins interfere with PRR detection pathways such as the RIG-I/MDA5 pathway, which is crucial in the detection and response to SARS-CoV-2 infection[127]. All these findings help illustrate how valuable the understanding SARS-CoV-2 protein immunomodulatory functions is in the fight against COVID-19. Many knowledge gaps in the immune evasion mechanisms of SARS-CoV-2 are yet to be filled, since many studies have been conducted in not so relevant cell models like HEK293T cells. Moreover, the interference of individual SARS-CoV-2 proteins on the host cell immune pathways in relevant cell models ought to be investigated in more detail. A number SARS-CoV-2 proteins including ORF3a, ORF6 and ORF9b have been deemed as promising for their potential immunomodulatory effects and are candidates that might be worth a closer look in future research.

1.4.2.1. SARS-CoV-2 ORF3a features

SARS-CoV-2 viroporin ORF3a shares 85.1% similarity and displays immune evasive functions comparable to its predecessor SARS-CoV ORF3a[131]. Several key roles as an innate immune deregulator have been proposed for SARS-CoV-2 ORF3a. One of the most characteristic features of SARS-CoV-2 ORF3a that have been observed is its ability to activate the NOD-, LRR- and pyrin domain-containing protein 3 (NLRP3) inflammasome, the most promiscuous of known inflammasomes[1, 2, 9, 134, 135]. Following NLRP3 activation, caspase 1 is activated allowing for the cleavage of IL-1β and IL-18 into their active forms. Activated NLRP3 also initiates pyroptosis, an extremely inflammatory type of cell death[136]. NLRP3 activation is triggered by the formation of a K^+ channel by ORF3a, since it is an ion channel-inducing viroporin. This K^+ channel creates a K^+ efflux in the host cell that encourages the interaction between NLRP3 and the NIMA-related kinase NEK7, which leads to the recruitment of the apoptosis-associated speck-like protein containing a CARD (ASC) and pro-caspase 1[135]. This completes the NLRP3 inflammasome activation, which induces the production of IL-1β, a highly inflammatory cytokine.

As previously mentioned, it has been proven that SARS-CoV-2 ORF3a prevents the induction of type I and type III IFNs by inhibiting the expression of IRF3 and NF-kB, as shown in luciferase reporter assays. Moreover, ORF3a has demonstrated to hinder the secretion of IFN-β and the transcription of ISGs by avoiding the binding of ISGF3 to its promoter site ISRE[137]. Given the high conservation with SARS-CoV ORF3a, alternative supplementary layers of IFN antagonization by SARS-CoV-2 ORF3a might include the following: upregulation of IFNAR1 ubiquitination followed by lysosomal-mediated degradation, suppression of STAT1 phosphorylation (**Figure 3**) and the inducement of fibrinogen secretion, which predisposes the patients to systemic inflammation and even thrombosis[2, 138-141]. Last, SARS-CoV-2 ORF3a has been found to mainly localised at late endosomes, where it hampers the fusion of lysosomes and autophagosomes, blocking autophagy[137, 142]. Nonetheless, all these mechanisms need to be further verified and characterised.

1.4.2.2. SARS-CoV-2 ORF6 features

Even though various studies have indicated that SARS-CoV-2 ORF6 is a potent type I IFN antagonist[24-26, 113, 128, 129, 131, 143, 144], it has also been reported to be less effective than its relative SARS-CoV ORF6 in the inhibition of the innate immune response[28]. This loss in immune evasion efficacy could be compensated by other SARS-CoV-2 specific proteins that might amplify the effects of SARS-CoV-2 ORF6[130]. SARS-CoV-2 ORF6 is best known for its antagonistic effects against the induction and downstream actions of IFN via the impairment of transcription factor trafficking across the cell's nuclear membrane (**Figure 3**). These effects are targeted against transcription factors such as IRF3, ISGF3, which are crucial for the correct development of the IFN immune response[26, 113, 130, 131]. In detail, it has been proposed that ORF6 interacts directly with nuclear import complexes nucleoporin 98 – ribonucleic acid export 1 (NUP98-RAE1) and NUP96-RAE1. By binding NUP98-RAE1, ORF6 is able to hijack the nuclear pore complex, blocking the translocation of STAT1 from the cytosol to the nucleus of the cell[1, 113, 130]. In this manner, the type I IFN signalling cascade is effectively interrupted[113]. Furthermore, luciferase reporter assays have shown that the expression of IFN-β in HEK293T cells is downregulated by SARS-CoV-2 ORF6. This downregulation is hypothesised to occur via ORF6 proximity interaction with MAVS, as some proteomics studies have revealed[128].

1.4.2.3. SARS-CoV-2 ORF9b features

As in the case of SARS-CoV-2 ORF6, SARS-CoV-2 ORF9b has also been found to prevent the induction of IFN by limiting the RIG-I/MDA5-MAVS-IRF3 axis[129, 143]. In detail, the primary means of interference of SARS-CoV-2 ORF9b with the innate immune response of the host cell is via its interaction with translocase of outer membrane 70 (TOM70), as verified by co-immunoprecipitation assays[130]. TOM70 is a mitochondrial import receptor subunit that mediates the activation of IRF3. This mediation occurs upon SARS-CoV-2 infection by the interaction of TOM70 with MAVS, which is responsible for the recruitment of TBK1/IRF3 to the mitochondria and the subsequent phosphorylation of IRF3[145]. The co-localisation of ORF9b and TOM70 at the mitochondria has been demonstrated by confocal microscopy[143]. Thus, by interacting with TOM70, SARS-CoV-2 ORF9b hinders IRF3 activation and suppresses type I and type III IFN expression (**Figure 3**).

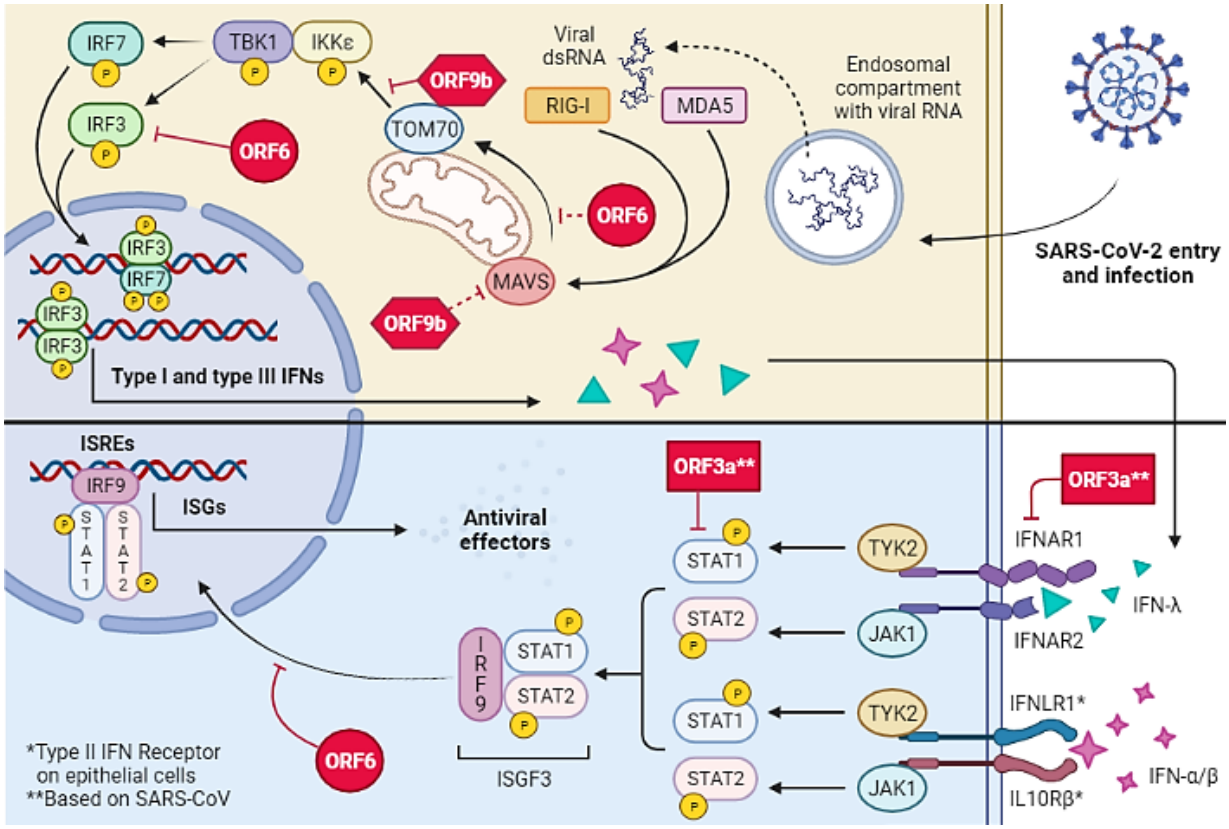

Figure 3. Outline of SARS-CoV-2 ORF3a, ORF6 and ORF9b antagonistic functions on type I and III IFN production and signalling pathways. *Dashed arrows indicate hypothetical mechanisms. Figure adapted from Mirjam Dürkoop, 2021 [85] and created with BioRender.*

Additionally, ORF9b has also been linked to the inhibition of the cGAS - stimulator of Interferon Genes (cGAS-STING) signalling pathway (a cytosolic DNA sensor), as evidenced by recent mechanistic analysis using co-immunoprecipitation[130]. Moreover, luciferase reporter assays have also shown that SARS-CoV-2 ORF9b downregulates the expression of IFN-β in HEK293T cells[143, 145], further exemplifying its IFN antagonistic effects.

Therefore, SARS-CoV-2 ORF3a, ORF6 and ORF9b are most known for impairing IFN responses in the infected host cell by interfering with both the RIG-I/MDA5-MAVS-IRF3 axis and the IFN signalling cascade. Notwithstanding, most of their roles are still being debated and are yet to be elucidated in depth. Although a number of these studies have been conducted on lung epithelial cell lines and immune cells, most of them have used less relevant cell lines such as HEK293T, HeLa and Huh7 cells and have focused on type I IFN responses, which are not as specific to epithelial cells as type III IFN responses. There is a need for more comprehensive research on better epithelial cell models such as A549 and Calu-3 cells to better reproduce the immune responses upon SARS-CoV-2 infection and study the immunomodulatory effects of ORF3a, ORF6 and ORF9b proteins.

2. Aims and Objectives

The overall aim of this Master Thesis Project is to contribute to the understanding of the interactions between the host cell and SARS-CoV-2 proteins and how these proteins can modulate inflammatory immune responses and contribute to COVID-19 pathology, helping to identify possible therapeutic targets in the long term. For this, the immunomodulatory effects of SARS-CoV-2 proteins on inflammatory signaling from the antiviral RIG-I/MDA5 pathway should be studied in human lung epithelial cells.

As it has previously been described, lung epithelial cells are the first target of SARS-CoV-2 and constitute the gateway that allows the entrance of the virus into the organism. Since the lungs also represent the main replication site for SARS-CoV-2, there is great interest in establishing reliable lung epithelial cell models to discover the mechanisms of SARS-CoV-2 infection and devise strategies that can improve the treatment for COVID-19. In this project, we are particularly interested in cytosolic sensors of viral nucleic acid structures, in particular RIG-I/MDA5. Hence, utilising previously developed A549 human lung epithelial cell lines that are able to express SARS-CoV-2 ORF3a, ORF6 and ORF9b proteins upon incubation with doxycycline, we intend to study the possible interference of these proteins with the host cell innate immune pathways that lead to the initiation of pro-inflammatory cytokine responses via RIG-I/MDA5 stimulation. While extensive research on SARS-CoV-2 biology and COVID-19 immunopathology has been conducted in the past two years, most of these studies have been performed on cell types that are inadequate at mimicking the responses of lung epithelial cells to infection. Furthermore, the immunomodulation of type III IFNs by SARS-CoV-2 proteins has not yet been explored in much detail, even though these IFNs are known for playing a critical role in the protection lung epithelial cells from viral infections.

The specific objectives derived from the main aim of this project are the following:

- Perform dose-response/titration experiments at different timepoints in A549 wild-type cells in order to refine and establish optimised protocols for RIG-I/MDA5 stimulation in human lung epithelial cells.
- Assess doxycycline-induced expression of the SARS-CoV-2 proteins in A549 cells transduced with plasmids for ORF3a, ORF6 and ORF9b expression.

- Use the optimized stimulation protocols to assess the effects of SARS-CoV-2 proteins ORF3a, ORF6 and ORF9b on RIG-I/MDA5 pathway-induced cytokine production in human lung epithelial cells. Effects on RIG-I/MDA5-mediated gene and protein expression on the production of chemokines, pro-inflammatory cytokines and type III IFN production as well as on cell death should be studied.

3. Materials and Methods

3.1. Cell culture

3.1.1. Cell lines and culture conditions

In this study, human lung epithelial A549 cells (CCL-185) were obtained from the American Type Culture Collection (ATCC) through Professor Denis Kainov'lab at IKOM/NTNU. A549 cells originate from the tumoral lung tissue of a 58-year-old Caucasian male with non-small cell lung carcinoma. In order to study the antagonistic functions of SARS-CoV-2 against innate immune responses, these A549 cells were modified in a previous master thesis project[85] by lentiviral vector transduction of pLVX-TetOne-Puro plasmids (ceded by Nevan Krogan's laboratory) that conditionally express the SARS-CoV-2 proteins ORF3a, ORF6 and ORF9b upon incubation with tetracyclines. All SARS-CoV-2 viral proteins featured a Strep-II tag on them (transgenes) to be easily identified in western blot assays. Importantly, the viral proteins coding genes expression was controlled by a tetracycline-inducible expression system comprising both Tet-On and Tet-Off Systems, where the transgenes were only expressed in the presence of tetracyclines such as doxycycline. A549 cells were grown in Dulbecco's modified eagle medium (DMEM) (12-604F; BioNordika) supplemented with 10% heat inactivated foetal bovine serum (FBS) (10270; Life Technologies), 2 mM L-glutamine (G7513; Sigma Aldrich) and an additional antibiotic combination of 100 U penicillin and 0.1 mg/mL streptomycin (P0781; Sigma Aldrich) only when maintaining the cells, not when performing experiments on them. This cell culture media recipe will be termed as complete culture media or CCM for the rest of the thesis. All cell lines were assessed free of mycoplasma contamination by Anne Marstad (CEMIR/NTNU).

3.1.2. General cell culture procedures

Cryopreservation of cells

Cells reaching 70-80% confluency were detached and pelleted by centrifugation at 1200 rpm for 5 minutes before being carefully resuspended in freezing medium and added to pre-labelled cryovials. Freezing media contains DMEM supplemented with 20% FBS and 10% dimethyl sulfoxide (DMSO, Sigma-Aldrich). The cells were frozen using a freezing container (Nalgene® Mr. Frosty) filled with isopropyl

alcohol allowing a crucial cooling rate of 1°C/min. The cells were then disposed at -80°C for short term storage or in liquid nitrogen for long term storage.

Thawing of cells

The cell vial was rapidly thawed in a 37°C water bath. 70% ethanol was used to decontaminate the vial and the cell suspension was added to 9 mL of prewarmed complete culture media into a 15 mL centrifuge tube. The cell suspension was centrifuged at 1200 rpm for 5 minutes at room temperature (RT). The cells were resuspended and seeded in 12 ml of CCM in a T75 flask.

Passaging cells

Adherent A549 cells were inspected regularly in the light microscope and grown until 70-80% confluency. A549 were passaged every 2-3 days at a ratio of 1:4 – 1:8. Cell media was changed every 2-3 days and the frequency of sub-culturing was adapted over time. In order to passage adherent cells from a T75 flask, CCM was discarded and 5 mL pre-warmed Dulbecco's Phosphate Buffered Saline (DPBS, D8537; Sigma Aldrich) were added to the flask to wash the cells. Subsequently, 1 mL of 0.25% Trypsin/EDTA (LonzaTM) was added to detach the cells from the flask surface. Cells were incubated until complete detachment was visible at the microscope. To stop the trypsinization process, 5 mL of pre-warmed CCM was added, and the cell suspension transferred into a 15-mL centrifuge tube. The cells were pelleted by centrifugation at 1200 rpm for 5 minutes at room temperature and resuspended in 5 ml of CCM. Depending on the split ratio, the appropriate volume of cell suspension was added to a new cell culture flask. Lastly, fresh pre-warmed supplemented DMEM was added until up to 12 ml.

Assessment of cell number and viability

Before seeding for an experiment, cell number and viability were assessed using Trypan blue exclusion test. The test stains the cells with trypan blue dye allowing to distinguish those who are viable from those who are dead, since the trypan blue dye only permeates and enters dead cells, whose membrane is disrupted. As indicated by the manufacturer, 10 µl of filtered trypan blue were mixed with 10 µl of cell suspension and 10 µl of the resulting mixture were pipetted onto EVE™ cell counting slides (Cat# EVS-050, NanoEntek America, Inc.) and cell number and

viability were assessed with the EVE™ Automated Cell Counter (Cat#EVE-MC, NanoEntek America, Inc.).

3.2. RIG-I/MDA5 stimulation assays

A549 cells were seeded in a 6-, 24- or 96-well-plate at a concentration of 0.04 x 10^6 cells/ml (2 mL per well in 6-well-plates, 500 µL per well in 24-well-plates and 100 µL per well in 96-well-plates) and incubated for 24 hours prior to stimulation. Media containing doxycycline (0.5 µg/ml, #D3072; Sigma-Aldrich) was used in order to induce viral protein expression in cell lines A549 ORF3a, ORF6 and ORF9b. Subsequently, the cells were incubated for 24 hours. For RIG-I/MDA5 stimulation, different concentrations of polyinosinic:polycytidylic acid (poly(I:C), #VPIC-42-01; Invivogen) (0,25 – 10 µg/ml) were delivered to the cytosol of cells using the transfection reagent Lipofectamine RNAiMAX (#13778-075; Invitrogen). As a control, cells were also treated with poly(I:C) alone and RNAiMAX alone. Presumably, when poly(I:C) is transfected alone, it interacts with the TLR3 receptors on the cell surface, resulting in endosomal uptake and TLR3 stimulation. However, when poly(I:C) treatment is supplemented with RNAiMAX, this reagent allows the delivery of poly(I:C) to the cytosol, where itn interacts with and stimulates RIG-I/MDA5. In detail, poly(I:C) was incubated in twice the volume of Lipofectamine RNAiMAX for 10 to 15 minutes and then added to the cells. Cells were incubated for 24 to 48 hours at 37°C before the supernatants and cell lysates were harvested for downstream analysis and stored at -20°C.

3.3. Western Blot Analysis

3.3.1. Basic principle

Western blot analysis is a commonly used technique to detect and analyse proteins from cell lysates. Cells are lysed using a lysis buffer containing proteinase inhibitor before cell lysates are subjected to gel electrophoresis, e.g. sodium dodecyl sulphate polyacrylamide gel electrophoresis (SDS-PAGE). Prior to gel electrophoresis, sample preparation is completed by adding Dithiothreitol (DTT), a redox reagent that breaks down protein disulphide bonds, and Lithium Dodecyl Sulfate (LDS), a loading buffer that contains tracking dyes and prepares the proteins for denaturation. Then, the mixture is heated at 85°C for 10 minutes,

which results in denatured polypeptides, which allows for their separation in the acrylamide gel by means of an electric current. Importantly, the concentration of acrylamide in the gel and its gradient is crucial to determine the resolution of the gel electrophoresis: proteins with high molecular weight require a lower acrylamide concentration whereas proteins with low molecular weight require a higher acrylamide concentration to be separated and distinguished. After migration, polypeptides are transferred from the gel on to a nitrocellulose (NC) or polyvinylidene difluoride (PVDF) membrane by electroblotting in order to enable their immunodetection. Electroblotting employs an electric current to move the negatively charged proteins towards a positively charged anode where the membrane is placed. Afterwards, to visualise and analyse the proteins of interest, the membrane is incubated with a blocking solution, to cover unspecific binding sites in the membrane, followed by a primary antibody, which recognises the protein of interest and binds to it with high specificity. This is followed by an incubation with a secondary antibody, which binds the (often unlabelled) primary antibody and enhances the readout signal. The secondary is conjugated to an enzyme that emits a fluorescent or chemical signal upon the addition of a substrate that allows protein of interest to be detected. The primary antibody can be polyclonal or monoclonal and is produced in a different type of animal than the secondary antibody, which is chosen depending on the species of animal in which the primary antibody was raised. In this study, the target protein was detected by chemiluminescence resulting from the oxidation of the substrate luminol by a horseradish peroxidase (HRP) conjugated to the secondary antibody. Oxidized luminol emits light at a maximum wavelength of 431 nm and is detected in an imaging system.

3.3.2. Standard procedure

Firstly, A549 cells stimulated for 24 hours with poly(I:C) (**section 3.2.**) in 6-well-plates were washed with pre-warmed PBS before being lysed by adding Radioimmunoprecipitation Assay (RIPA) lysis buffer (**Supplementary Table 1**) supplemented with protease inhibitors, incubated under agitation for 15 min at 4°C and scraped. The cell lysates were collected into prelabelled 1.5 ml tubes, centrifugated for 20 min at 10000 rpm and 4°C and either used directly or stored at -20°C. The centrifugation step is necessary to separate the protein-containing supernatant from the cell debris pellet. The samples were then prepared for SDS-

PAGE by adding 7.5 µL NuPAGE® LDS Sample Buffer (4X) (#NP0007; Invitrogen) mixed with 0.1 M dithiothreitol (DTT) (1:100) (#R0861; Thermo Scientific) to 30 µL of each sample and heating at 85°C for 10 minutes. After the incubation, the samples were briefly centrifuged to gather all the condensed solution in the bottom of the tubes and 25 µL of each of them was loaded into a well of NuPAGE® 4-12% Bis-Tris Gel (#WG1402BOX; Invitrogen) in 1X NuPAGE® MES SDS Running buffer (#NP0002; Invitrogen). 5 µL of SeeBlue™ Plus2 Pre-stained Protein Standard (#LC5925; Invitrogen) and 0.5 µL of the MagicMarkTM XP Western Blot Protein Standard (#LC5602; Invitrogen) were loaded as well to monitor protein migration and determine the size of the proteins after visualization of the blotted membrane, respectively. The electrophoresis was run for 30 minutes at 100 V followed by 90 minutes at 150 V, being monitored occasionally. iBlot® 2 NC Regular Stacks (#IB23001; Invitrogen) were employed to transfer the proteins from the gel to a nitrocellulose membrane. The protein transfer was carried out in the iBlot® 2 Gel Transfer Device (#IB21001; Invitrogen) for 9 minutes at 20 V and the membrane followed several steps of washing and incubation as detailed further, all under agitation at 65 rpm and at room temperature except if mentioned differently. A wash consists in incubating the membrane 3 times for 5 min in tris-buffered saline with tween 20 (TBS-T) (0.05 M Tris-HCl pH 7,5, 0.15M NaCl, 0.1% Tween-20) or TBS-T/5% BSA if the next step contains BSA. After a first wash in TBS-T, the membrane was incubated for 1 hour in TBS-T/5% BSA at RT to block unspecific binding sites and prevent a misleading readout, followed by the incubation with the primary mouse Anti-Strep-II antibody (#NBP2-43735, Novus Bio; dilution 1:5000 in TBS-T/5% BSA) overnight at 4°C. After wash, the secondary goat-anti-mouse Ig/HRP antibody (#P047, Dako Denmark A/S; dilution 1:5000 in TBS-T/5% BSA) was added to the membrane and incubated for 1 hour. After wash, the membrane was covered with 4 mL of SuperSignal West Femto Chemiluminescent Substrate (#35096; Thermo Fisher Scientific) for 2-3 minutes, sandwiched in between two transparent plastic films and visualized with the chemiluminescent channel of the Odyssey® Fc Imaging System (LI-COR Biosciences) and the Image Studio V5.2 software at an exposure time of 30 sec to 2 min. In order to assess the GAPDH loading control, the membrane was stripped by adding a mild stripping buffer (1.5% glycine/1% Tween/0.1% SDS, pH 2.2) to the membrane for 10 minutes after a wash in TBS-T. This step allows the incubation with antibodies against other proteins (e.g. GAPDH). After stripping, the membrane was washed

three times in TBS-T for 5 minutes before incubation for 1 hour in TBS-T/5% BSA at RT. Then, the membrane was incubated with mouse anti-GAPDH antibody (#2118, Abcam; dilution 1:5000 in 10 mL TBS-T/5% BSA) under agitation for 1 hour at 4°C. The subsequent steps and visualisation of GAPDH were as described above, using the same type of secondary antibody (goat-anti-mouse Ig/HRP antibody, 1:5000).

3.4. Enzyme-linked Immunosorbent Assay (ELISA)

3.4.1. Basic principle

Enzyme-Linked ImmunoSorbent Assay (ELISA) is based on highly specific interactions between antigens and antibodies to detect and quantify the concentration of peptides, proteins, hormones, or antibodies in a solution. In particular, sandwich ELISA features capture and detection antibodies, both binding specifically to different epitopes of the antigen of interest. In detail, a microtiter plastic plate is first coated with the capture antibody specific to the protein of interest and then incubated in BSA in order to block non-specific binding sites on the plate surface. After a washing step, the sample (for example cell culture supernatant, serum or plasma) is added to the assay plate and the antigen of interest contained in the sample is bound by the capture antibody, immobilising it on the plate surface. Next, the wells are thoroughly washed to ensure all unspecific antigens are removed prior to the addition of the detection antibody, which specifically binds a different epitope of the antigen. Importantly, the detection antibody is either directly conjugated to an enzyme or to biotin, a water-soluble B complex vitamin that specifically binds to streptavidin, a bacterial protein. In this case, the addition of a streptavidin-conjugated enzyme such as horseradish peroxidase (HRP) allows for the binding of this enzyme to the detection antibody. Further, an HRP substrate such as tetramethylbenzidine (TMB) or 2,2'-azino-di-[3-ethylbenzthiazoline-6-sulfonic acid] (ABTS), is added to the plate and its oxidization by HRP results in a change of colour proportional to the number of antigens present in the well. Finally, ELISA stop solution (H_2SO_4) is added to halt the enzymatic reaction turning the solution colour from blue to yellow. Absorbance is immediately measured in a microplate spectrometer reader (BioRad). The concentration of antigen can eventually be determined by means of a standard curve.

3.4.2. Standard procedure

A549 cells were stimulated for 24 or 48 hours with poly(I:C) in 24-well-plates (**section 3.2.**). Cytokine analysis by ELISA was performed from the cell culture supernatants diluted 1:2 using DuoSet antibody sets for IL-6 (#DY206; R&D), IL-8 (#DY208; R&D) and IFN-λ1/3 (IL-29/IL-28β) (#DY1598B; R&D). The standard procedure was followed based on the description from the manufacturer. The assay was performed with half the volumes suggested by R&D Systems in 96-well half-area plates (#3690, Corning®). In-house experiments have previously shown that this set-up produces the same signal strength. The ELISA plate is always sealed with an adherent plastic film before incubation time to avoid contaminating the plate. The volumes of reagents of this protocol are given for a well of a half-well 96-well-plate. In depth, the plate was coated with 50 µL of the capture antibody solution (diluted in PBS as specified by the manufacturer) by an overnight incubation at RT. Subsequently, the plate was washed thrice with 150 µL of wash buffer (PBS/0.1% Tween-20) employing the automated Tecan plate washer. Then, 150 µL of blocking buffer (PBS/1% BSA, termed "reagent diluent" by the manufacturer) were added to block unspecific binding sites, incubating for 2 hours at room temperature. After blocking, the ELISA plate was washed again thrice as explained above. In a separate replica plate, a 2-fold serial dilution of standards in reagent diluent was prepared for each cytokine standard, starting with the highest concentration as recommended by the manufacturer. In addition, cell culture supernatant samples were diluted 1:2 in reagent diluent on the replica plate (30 µl sample + 30 µl reagent diluent, suitable dilution that was determined in preliminary assays). Using a multichannel pipette, 50 µL of standards and samples dilutions were transferred to the ELISA plate and left incubating overnight at RT. Afterwards, the plate was washed thrice again and 50 µL of the detection antibody (diluted in reagent diluent as specified by the manufacturer) were added to the samples to incubate the plate for 2 hours at RT.

Next, the plate was washed thrice once more and each well was incubated with 50 µL of Streptavidin-HRP conjugate (40-fold dilution in reagent diluent) for 20 minutes in the dark at room temperature. After washing the plate five times, 50 µL of TMB substrate solution (1+1 dilution of Reagents A and B, #421101, BioLegend) was added and incubated for 20 minutes in the dark at room temperature. The reaction was stopped by adding 25 µL Stop Solution (1N H_2SO_4).

Lastly, absorbance was measured using a microplate spectrometer reader (BioRad) with parameters set to 450 nanometres (nm) with 570 nm of wavelength correction.

Cytokine concentration was automatically calculated based on the standard curve after subtraction of the background given by the blank sample. The standard curve was generated using BestCurfit software. The experiment was performed in technical duplicates and the data was analysed and visualized in GraphPad Prism Software Version 8.2.0.

3.5. RNA extraction, Reverse Transcription (RT) and quantitative Polymerase Chain Reaction (qPCR) analysis of mRNA levels using TaqMan technology/assays

3.5.1. Basic principle

RT-qPCR is a technique for nucleic acid molecule quantification in biological and environmental samples in real time. It requires extracting RNA from cell lysates before it can be reverse transcribed to cDNA, which is then used for qPCR, where specific genes targets are amplified using fluorescence as reporting system.

First, RNA is extracted by obtaining cell lysates, binding the RNA to a solid phase of silica under certain pH and ionic conditions, washing non-RNA molecules in a series of centrifugation cycles and eluting the purified RNA in an aqueous solution. Importantly, DNase treatment with deoxyribonuclease I is used along the process to degrade genomic DNA present in the samples that could result in false positive signals in the RT-PCR readout. Next, purified RNA is reverse transcribed to cDNA in a thermal cycler, producing as much quantity of cDNA as there was originally RNA. This is to create a stable template on which qPCR can be performed, since RNA is very susceptible to temperature changes. Afterwards, qPCR is performed for specific targets in the cDNA template as well as for a housekeeping or reference gene that is ideally carefully chosen to have the same expression levels in all the samples regardless of their treatment conditions. Either TaqMan® hydrolysis oligonucleotide probes or SYBR Green I dye predesigned by the provider can be used in this method, following the general qPCR chemistry assays.

The TaqMan principle relies on the *Thermus aquaticus* (*Taq)* DNA polymerase with 5' endonuclease activity that cleaves an oligonucleotide probe (Taqman probe) bound to a region in the target gene that lies in between the forward and revers PCR primers. This Taqman probe contains a fluorophore and a quencher in its 5' and 3' end, respectively. When the TaqDNA polymerase cleaves the fluorophore at the 5' end, it is released from the quencher's proximity and emits a fluorescent signal that can be measured and is proportional to the number of amplified target molecules in each PCR cycle. Importantly, the forward and reverse PCR primers as well as the Taqman probe confer three levels of specificity in the qPCR.

The target cDNA amplification reaction is plotted showing 3 phases: the baseline, the exponential phase and the plateau. In the plot, the x-axis represents the number of PCR cycles, whereas the y-axis represents the increment of fluorescence, whose changes are not detectable and remain at background levels until enough amplified product is accumulated. Entering the exponential phase, the PCR product amount doubles with each cycle but, as reagents are consumed, the reaction course is limited and slows until entering the plateau phase (**Figure 4**). The fluorescence threshold is set the same for all samples to the exponential phase above the background signal and before the plateau, and will give the cycle threshold (CT) value for each sample. This allows to relatively quantify the original amount of the target of interest mRNA that was present in the sample knowing the exponential function that describes the reaction progress. Lower C_T values indicate a larger amount of target in the sample, as fewer amplification cycles are needed to accumulate enough reaction product to provide an above-background fluorescence signal. Inversely, higher C_T values indicate a smaller amount of target in the sample, as more amplification cycles are needed to detect an above-background fluorescence signal.

In order to perform the relative quantification (RQ) of the target cDNA correctly, the $2^{-\Delta\Delta Ct}$ method is used, which includes two normalisation steps. A first normalisation step allows to control for technical variations in the input of the template correcting the data by normalisation to a housekeeping gene, which is constitutively expressed in the studied system. A second normalisation step compares the expression of the target genes in the test samples to the expression of the same genes in the control samples. This allows to relatively quantify the amount of target cDNA in the samples.

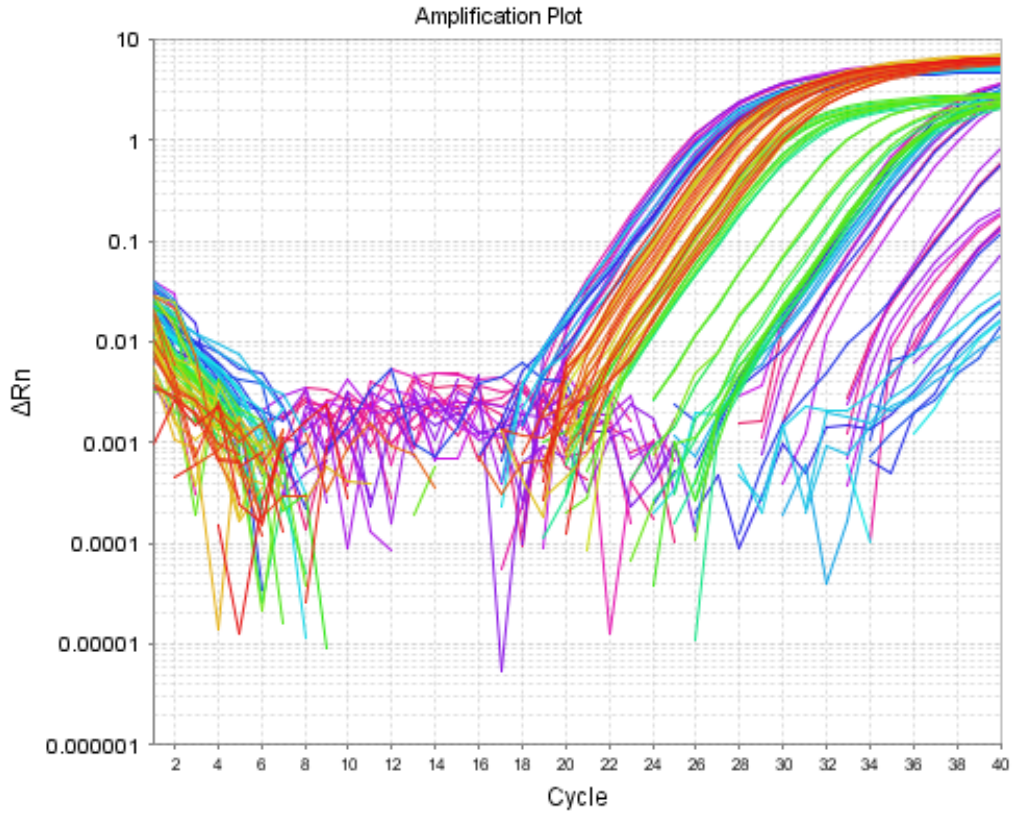

Figure 4. Amplification plot of a qPCR experiment. *ΔRn indicates the fluorescence normalization between the reporter dye signal and the background signal (Applied Biosystems™ ROX™ Dye). Figure generated by StepOnePlus Real-Time PCR System software.*

3.5.2. Standard procedure

Human lung epithelial A549 cells stimulated for 24 hours with poly(I:C) in 24-well-plates (**section 3.2.**). were washed with cold PBS and lysed in RLT buffer containing 1% β-mercaptoethanol. Qiagens' QIAcube was employed to semi-automatically extract the total RNA from the samples. RNA isolation was performed according to the manufacturer's protocol including a DNase I digestion step (RNase-free DNase set) to degrade traces of genomic DNA. ND-1000 spectrophotometer (NanoDrop) was used to quantify the total RNA concentration after extraction. An $OD_{260/280}$ ratio of approximately 2 was confirmed for the samples included in the study, indicating an optimal RNA purification with low contamination. Nucleic acids have an absorbance maximum at 260 nm, whereas proteins have an absorbance maximum at 280 nm (due to tryptophan and tyrosine amino acids). Abnormal 260/280 ratios indicate sample contamination by guanidine, phenol or other reagent used in RNA extraction as well as high protein concentrations. Higher 260/280 ratios indicate a basic pH in the sample whereas

lower 260/280 ratios indicate an acidic pH in the sample. Next, reverse transcription was performed employing High-Capacity RNA-to-cDNA kit to synthesise cDNA from normalised amounts of RNA according to manufacturer's recommendations (Applied Biosystems). Depending on the measured concentration of RNA, qPCR reactions were performed with 10 to 25 ng of cDNA input for each different experiment in a total volume of 20 µl per reaction, PerfeCta qPCR FastMix, (with UNG and ROX, Quanta Biosciences) and TaqMan Gene Expression Assays (Applied Biosystems): TBP (Hs00427620_m1), *IL-6* (Hs00985639_m1), *IFNL1* (Hs00601677_g1), *IFNL3* (Hs04193047_gH). TBP was chosen as the housekeeping gene since its expression had previously been assessed in recent projects[85] as the most stable across the different treatment conditions in comparison to other potential reference gene candidates. StepOnePlus Real-Time PCR System was used to amplify the targeted genes TBP, *IL-6*, *IFNL1* and *IFNL3*, and its in-built software was employed for easy data analysis. Relative quantities of gene expression were calculated using the comparative $2^{-\Delta\Delta Ct}$ method, taking TBP reference gene expression as endogenous control.

3.6. Cytotoxicity/Cell viability assays

3.6.1. Basic principle

Cell viability assays allow to relatively quantify the amount of viable cells in a cell culture. Both the Lactate Dehydrogenase (LDH) and the MTS cell viability assays are based on colorimetric methods. The LDH assay measures LDH activity in the supernatant of plasma membrane-damaged or dead cells, whereas the MTS assay measures the metabolic activity of viable cells in cytotoxicity assays or in proliferation.

Cell death typically entails the damage and rupture of the plasma membrane, which results in the release of cytoplasmic enzymes in the cell culture supernatant, such as the lactate dehydrogenase (LDH). In detail, LDH enzymatic activity catalyses the conversion of lactic acid to pyruvic acid whilst transforming NAD+ into NADH/H+. This product is subsequently used by a catalyst, diaphorase, to reduce a tetrazolium salt, iodonitrotetrazolium (INT), to a red water-soluble

formazan dye with an absorbance maximum at 490 nm. The number of dead cells is directly proportional to the amount of dye produced.

As in the traditional [3-(4,5-dimethylthiazol-2-yl)-2,5-diphenyltetrazolium-bromide] (MTT) assay or in the LDH assay previously described, the MTS assay measures the relative quantity of a formazan product that has an absorbance maximum at 490 nm. The assay incorporates a stable solution of [3-(4,5-dimethylthiazol-2-yl)-5-(3-carboxymethoxyphenyl)-2-(4-sulfophenyl)-2H-tetrazolium], an MTS tetrazolium compound, and an electron coupling reagent (phenazine ethosulfate; PES). Once the MTS tetrazolium solution is added to cells in the culture, viable and metabolically active cells reduce the compound forming a soluble, coloured formazan product. Active NAD(P)H-dependent dehydrogenase enzymes in metabolically active cells are responsible for carrying out the reaction. The number of viable and metabolically active cells in culture is thus directly proportional to the quantity of formazan produced.

3.6.2. Lactate Dehydrogenase (LDH) assay standard procedure

LDH Cytotoxicity Detection Kit (#PT3947-1; Clontech Inc.) was used according to the manufacturer's protocol to perform the LDH assay. LDH Reaction Mixture was prepared immediately before use by mixing 3.5 mL Dye Solution with 77.8 µL Catalyst (1:45 dilution), adding 40 µL of the resulting mixture to each well and incubating for 20-30 minutes at room temperature, avoiding exposure to direct light. Absorbance was measured in a microplate reader (BioRad) at 490 nm, taking 655 nm as a reference wavelength to subtract any background noise due to nonspecific absorbance such as fingerprints, excess cell debris, or others. After subtraction of the background given by the measurement of the absorbance of cell media mixed with reaction mixture, the final measurements were adjusted for the dilution factor of the sample supernatants. Transfected samples were assessed in technical duplicates. Finally, the data was analysed and visualized using GraphPad Prism Software Version 8.2.0.

3.6.3. MTS Assay standard procedure

CellTiter 96® Aqueous One Solution Cell Proliferation Assay (#G3581; Promega) was used to perform the MTS assay according to the manufacturer's protocol. An untreated control, a mock control (only transfection reagent) and a negative control (medium only) were included, being assessed from single wells. 20 µL One

Solution Reagent was added to each well in a 96-well plate containing 100 µL of CCM. Subsequently, the cells were incubated for 1 hour at 37°C (5% CO_2). Immediately after, a microplate spectrometer reader (Bio-Rad) was used to measure the absorbance at 490 nm. In order to subtract background noise, the absorbance was measured at a reference wavelength of 655 nm was also measured. The background absorbance from the negative control was subtracted from all sample measurements. Last, the data was finally analysed and visualized using GraphPad Prism Software Version 8.2.0.

4. Results

4.1. Preliminary stimulation of wild-type A549 cells by poly(I:C) transfection

Many of the studies that have investigated how SARS-CoV-2 viral proteins interfere with inflammatory signalling pathways are done in cell lines such as HEK293T, which are easy to transduce but do not constitute directly relevant cell models for COVID-19 research since they are not lung epithelial cells and not the primary target of SARS-CoV-2. To elucubrate more significant results in this project, we aimed at investigating the effects of SARS-CoV-2 proteins on innate immune responses by employing epithelial cells from human lung. Among the different lung epithelial cell lines available, we picked Calu-3 and A549 cells for being well-established cell lines that had already been transduced with genes coding for different SARS-CoV-2 proteins of interest in a previous master thesis project. After testing both cell lines in the laboratory and getting acquainted with their culturing methods, Calu-3 proved to be difficult to work with (**not shown**) for a number of reasons that will be discussed later (**section 5.1.**). Therefore, we selected the A549 lung adenocarcinoma cell line for our experiments. The phenotype of this cell line is similar to lung epithelial cells targeted by SARS-CoV-2, which makes it particularly suitable for research on SARS-CoV-2 lung infection. As mentioned, three different A549 cell lines transduced with pLVX-TetOne-Puro plasmids containing the individual SARS-CoV2 proteins of interest had already been created in a previous master thesis project (**section 3.1.1.**). These cell lines overexpress SARS-CoV2 ORF3a, ORF6 or ORF9b upon stimulation with tetracyclines and were used to study the effects of SARS-CoV-2 viral proteins on inflammatory responses and innate immune system signalling pathways in lung epithelial cells in more detail.

The first aim of the project was to study the production of inflammatory cytokines in A549 lung epithelial wild-type cells in response to PRR stimulation. The previous master thesis project had tested the stimulation of several PRRs with different synthetic ligands. However, cytokine responses were only observed from few receptors, the most prominent of which was RIG-I/MDA5, whose signalling pathway is involved in the production of IL-1β, IL-6, IL-8, type I and type III IFNs and TNF-α among other cytokines. These results were quite interesting, given that

RIG-I/MDA5 plays a key role in the cytosolic sensing of SARS-CoV-2. Thus, we took this as the starting point for more detailed analyses on the modulatory effects of SARS-CoV-2 proteins on RIG-I/MDA5-induced immune responses in this project.

In a first set of preliminary experiments, inflammatory cytokine production was assessed in wild-type A549 human lung epithelial cells in response to stimulation with different concentrations of poly(I:C). In depth, poly(I:C) is a synthetic dsRNA structure that mimics viral RNA and stimulates the RIG-I/MDA5 pathway in cells, emulating the initial steps of infection. In these experiments, poly(I:C) was used as a proxy for a viral RNA product that can elicit inflammatory responses when sensed by the innate immune system of the host cell. While endocytosed "pure" poly(I:C) stimulates mainly inflammatory responses via TLR3, cytosolically-delivered poly(I:C) stimulates inflammatory responses via the RIG-I/MDA5 pathway. In order for poly(I:C) to be delivered in the cytosol of the cell, it must be combined with a transfection reagent, in this case RNAiMAX. Wild-type A549 cells were treated with increasing concentrations of pure poly(I:C) (TLR3 stimulation) or poly(I:C) in combination with RNAiMAX (RIG-I/MDA5 stimulation) and the production of inflammatory cytokines by these cells was assessed at 24 and 48-hour timepoints. Specifically, we focused on analysing the production of NF-κB and IRF-regulated cytokines that might be induced in infected epithelial cells and play a role in the host response against SARS-CoV-2. These cytokines were IL-6, IL-8 and type III IFNs (IFN-λ1 and IFN-λ3), which have been found to be strongly upregulated in severe COVID-19 cases.

ELISA for IL-6 and RT-qPCR for *IL-6*, *IFNL1* and *IFNL3* (the designated terms for IFN-λ1 and IFN-λ3 mRNAs, respectively) were carried out from cell culture supernatants and lysates 24 and 48 hours after poly(I:C) stimulation. Concomitantly, A549 WT cell viability was analysed by LDH and MTS assays and compared with cytokine production in response to different concentrations of poly(I:C). The aim of these experiments was to find an optimal dose of cytosolic poly(I:C) that triggers a strong RIG-I/MDA5-mediated inflammatory cytokine response without significantly affecting cell viability (as observed in previous experiments with higher doses of poly(I:C) treatment). In addition, these initial experiments allowed the optimisation of methodological procedures and the assessment of their reliability for this and future experimental setups.

4.1.1. RIG-I/MDA-5 stimulation induces IL-6, IFN-λ1 and IFN-λ3 inflammatory cytokine responses in A549 wild-type cells

The first stimulation experiment in this project aimed to determine the preferred range of viral ligand concentrations to be used in future setups. For this purpose, a small-scale experiment including only wild-type A549 cells was performed. Cells were treated with different concentrations (0.5 to 10 µg/ml) of poly(I:C) with RNAiMAX as TR mixed in a 1:2 ratio and incubated for 24 and 48 hours. At these timepoints, supernatants were harvested for analysis. As a control, increasing concentrations of poly(I:C) alone were added to cells, which should not enter the cytosol and thus are not expected to activate the RIG-I/MDA5 signalling pathway. Both at 24 and at 48 hours, a strong induction of IL-6 production was observed in response to cytosolic delivery of poly(I:C) with RNAiMAX, but not in response to poly(I:C) alone (**Figure 5A, B**). This indicates that cytosolic delivery of poly(I:C) stimulates production of IL-6 via the cytosolic sensor RIG-I/MDA5, but not via the endosomal TLR3 pathway in A549 cells. The use of a transfection reagent (RNAiMAX) seems indispensable for the activation of the RIG-I/MDA5 pathway by poly(I:C) and induction of subsequent cytokine secretion.

The highest concentration of secreted IL-6 was observed with lowest dose of transfected poly(I:C), indicating that 0.5 µg/ml of poly(I:C) plus RNAiMAX is sufficient to induce inflammatory cytokine production from A549 cells via RIG-I/MDA5. Measurement of IL-6 secretion by ELISA after each indicated timepoint showed an overall steady decrease of IL-6 concentration in the cell supernatants with higher concentrations of poly(I:C) plus RNAiMAX treatment. This reduction in IL-6 production with increased doses of poly(I:C) may indicate that the treatment of A549 cells with increased doses of poly(I:C) or TR affect cell health or cell viability. In particular, the highest production of IL-6 was observed with 0.5 µg/ml and 1 µg/ml of transfected poly(I:C) treatment at 24 and 48 hours respectively. Moreover, higher concentrations of IL-6 are observed in 48-hour supernatants than in 24-hour supernatants, which is probably due to an accumulation of IL-6 in the supernatant over time (**Figure 5C***)*.

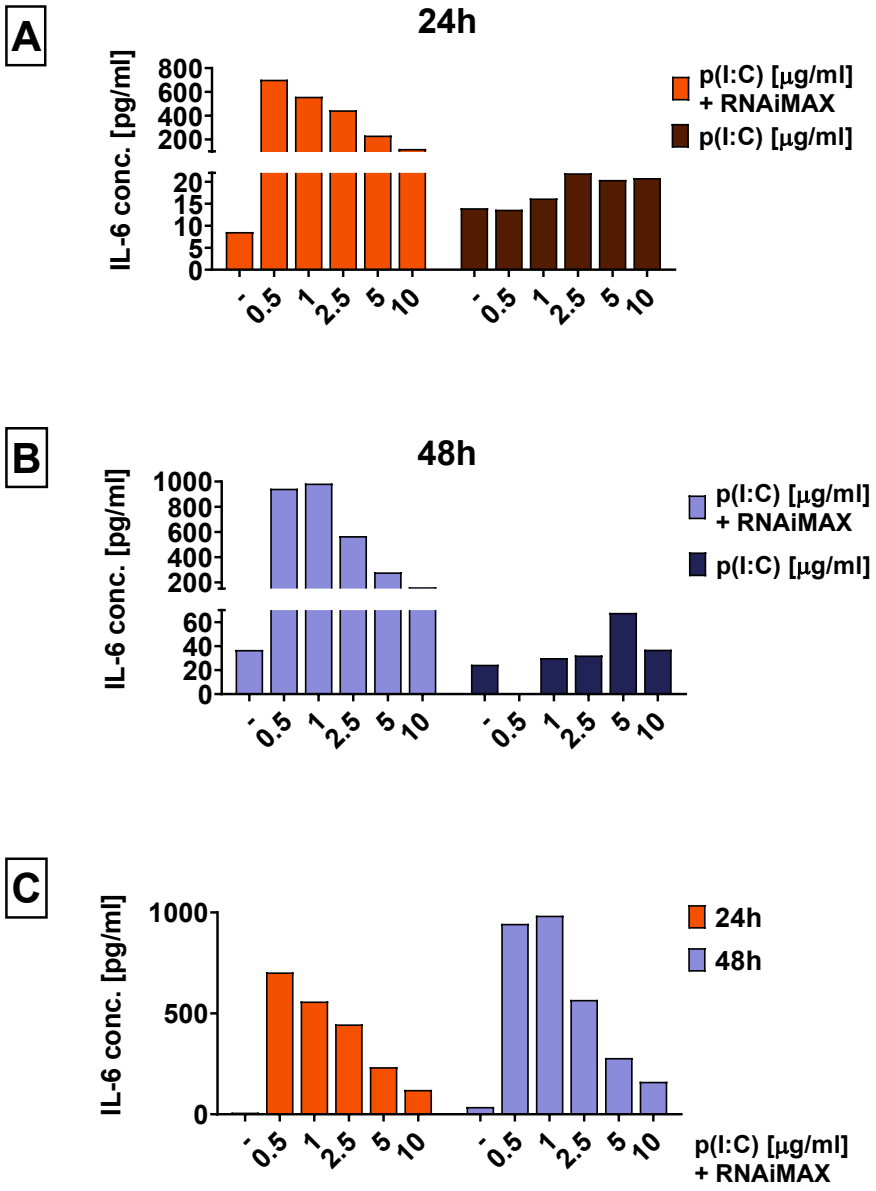

Figure 5. IL-6 secretion in response to RIG-I/MDA5 stimulation at 24 and 48-hour timepoints. *A549 wild-type cells were seeded the day before stimulation with poly(I:C) + lipofectamine RNAiMAX or poly(I:C) alone without TR. Untreated controls were incubated with CCM. After incubation for 24 (**A**) and 48 hours (**B**), cell supernatants were collected and IL-6 production measured by DuoSet ELISA (R&D). Absorbance was measured at 450nm and 570nm and then subtracted. Results show mean from technical duplicates.* ***C.*** *Comparison of IL-6 production from A549 cells after 24 and 48 hours in response to poly(I:C) + RNAiMAX treatment (comparison of results from (A) and (B)).* ** *p≤0.01.*

In addition to cytokine analysis from supernatants by ELISA, A549 WT cells were lysed after removal of the supernatant for RNA extraction. mRNA expression levels of *IL-6*, *IFNL1* and *IFNL3* were analysed by RT-qPCR analysis in A549 cells 24 hours after RIG-I/MDA5 stimulation with increasing concentrations of poly(I:C) + RNAiMAX (also referred to as transfected poly(I:C)). Results were normalised to

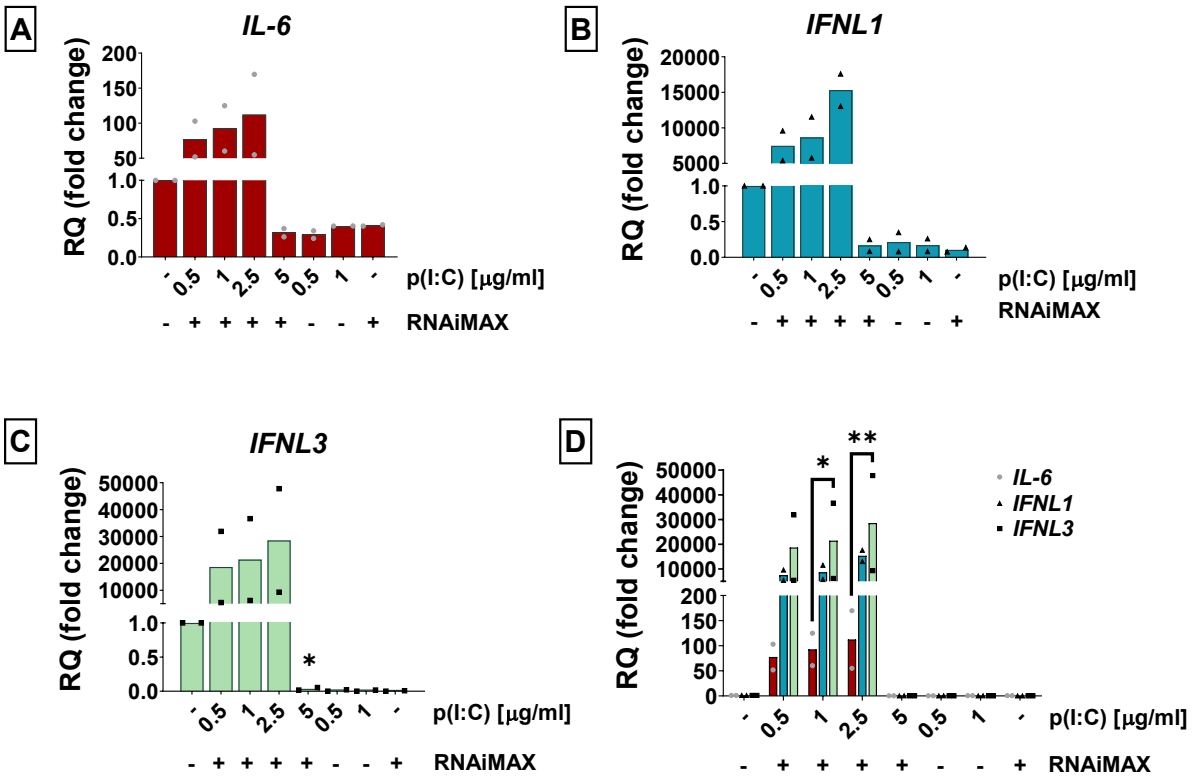

Figure 6. IL-6, IFNL1 and IFNL3 gene expression in wild-type A549 cells after 24-hour stimulation with RIG-I/MDA5 stimulation. *A549 wild-type cells were seeded the day before stimulation with poly(I:C) + lipofectamine RNAiMAX or poly(I:C) alone without TR. Stimulation with RNAiMAX alone (twice the volume used for stimulation with poly(I:C) 1 µg/ml) was included as an experimental control. Untreated controls were incubated with CCM. Cells were lysed after being stimulated for 24 hours. RNA was extracted from the lysates and IL-6 (**A**), IFNL1 (**B**) and IFNL3 (C) mRNA expression was assessed by RT-qPCR. RQ values were calculated relative to TBP housekeeping gene expression. Results show mean from 2 independent experiments. (D) IL-6, IFNL1 and IFNL3 gene expression results from A-C were combined. Differences in treatment response across cytokines were assessed by two-way ANOVA with Tukey correction (**D**). * p≤0.05, ** p≤0.01.*

mRNA expression of the housekeeping gene (TBP). Cells were stimulated with 0.5, 1 and 2.5 µg/ml poly(I:C) for 24 hours, compared to cells that were unstimulated and stimulated with pure poly(I:C) or RNAiMAX alone (twice the volume used for stimulation with the highest concentration of poly(I:C), 0 µg/ml poly(I:C)). We found and overall visible increase in the expression of *IL-6*, *IFNL1* and *IFNL3* was observed at 0.5, 1 and 2.5 µg/ml concentrations of transfected poly(I:C) (**Figure 6A, B, C**). This indicates that RIG-I/MDA5-specific poly(I:C) viral ligand activates the expression of pro-inflammatory cytokines and type-III IFNs when transduced into the cell. In contrast to ELISA findings for secreted IL-6 protein, increased levels of *IL-6* mRNA were found for increasing doses of poly(I:C) + RNAiMAX up to 2.5 (**Figure 5A and 6A**). However, it is worth noting that at a 5 µg/ml concentration of transfected poly(I:C) abrogated mRNA expression of cytokines

completely (**Figure 6A, B, C**), which might be attributed to the detrimental effects of an excessive dosage of poly(I:C) and RNAiMAX to the survival of A549 cells. Likewise, mRNA expression levels of these three cytokines were reduced or non-existent for poly(I:C) or RNAiMAX alone controls (**Figure 6A, B, C**). In addition, when mRNA levels of *IL-6*, *IFNL1* and *IFNL3* were compared 24 hours after RIG-I/MDA5 stimulation, *IFNL3* expression was significantly higher compared to *IL-6* expression when cells were stimulated with 1 or 2.5 µg/ml of poly(I:C) + RNAiMAX (**Figure 6D**).

Given the high response to RIG-I/MDA5 stimulation with low doses of transfected poly(I:C), these results encouraged us to expand the range of poly(I:C) + RNAiMAX treatment to even lower concentrations in order to optimise future experimental setups. In addition, we decided to perform LDH and MTS assays to test if the highest doses of transfected poly(I:C) affect cell health and viability.

4.1.2. Higher concentrations of poly(I:C) decrease cell viability in wild-type A549 cells

Cell viability assays were conducted with A549 wild-type cells. The aim was to determine to what extent the concentration of poly(I:C) + RNAiMAX treatment might be responsible for an increase in cell death and could thereby explain the reduced cytokine levels after stimulation with higher poly(I:C) + RNAiMAX doses (**section 4.1.1.**). Together, the results from these dose-response analysis on cytokine production and cell viability will allow to select the optimal range of poly(I:C) treatment concentrations for future experimental setups that would guarantee the highest possible response to RIG-I/MDA5 stimulation as well as the highest possible cell viability.

In order to choose a suitable and reliable method for analysis of cell viability and to obtain a trustworthy set of results, two different methods of cell viability analysis were performed and compared: an LDH assay (**section 3.6.2.**), measuring the LDH release from dying or already dead cells, and the MTS assay (**section 3.6.3.**), measuring the metabolic activity in viable cells. Carrying out both these assays would also allow to determine which of them would eventually be preferred in future experiments for being more reliable for these experimental conditions.

A549 WT cells were stimulated with increasing doses of poly(I:C) + RNAiMAX and cell viability was assessed 24 and 48 hours post-stimulation by measuring LDH release in cell supernatants or by adding MTS reagent to the cell culture and measuring the presence of formazan product indicative of the metabolic activity of cells. While metabolic activity in the MTS assay directly corresponds to cell viability, the amount of released LDH is inversely proportional to cell viability. The LDH and MTS assays yielded comparable results at the 24-hour timepoint with increased cell death in response to increased doses of transfected poly(I:C) (**Figure 7A, C**). RNAiMAX alone or untransfected poly(I:C) did not affect cell viability. The MTS assay for the 48-hour timepoint showed results that were quite similar to the 24-hour timepoint (**Figure 7D**). However, the 48-hour LDH assay measurements (**Figure 7B**) showed a brusque rise in the relative amount of released LDH at the lowest concentration of poly(I:C) + RNAiMAX treatment with little and irregular variations for the rest of the tested concentrations that did not correlate with the concentration of poly(I:C) used. Strangely, a high release of

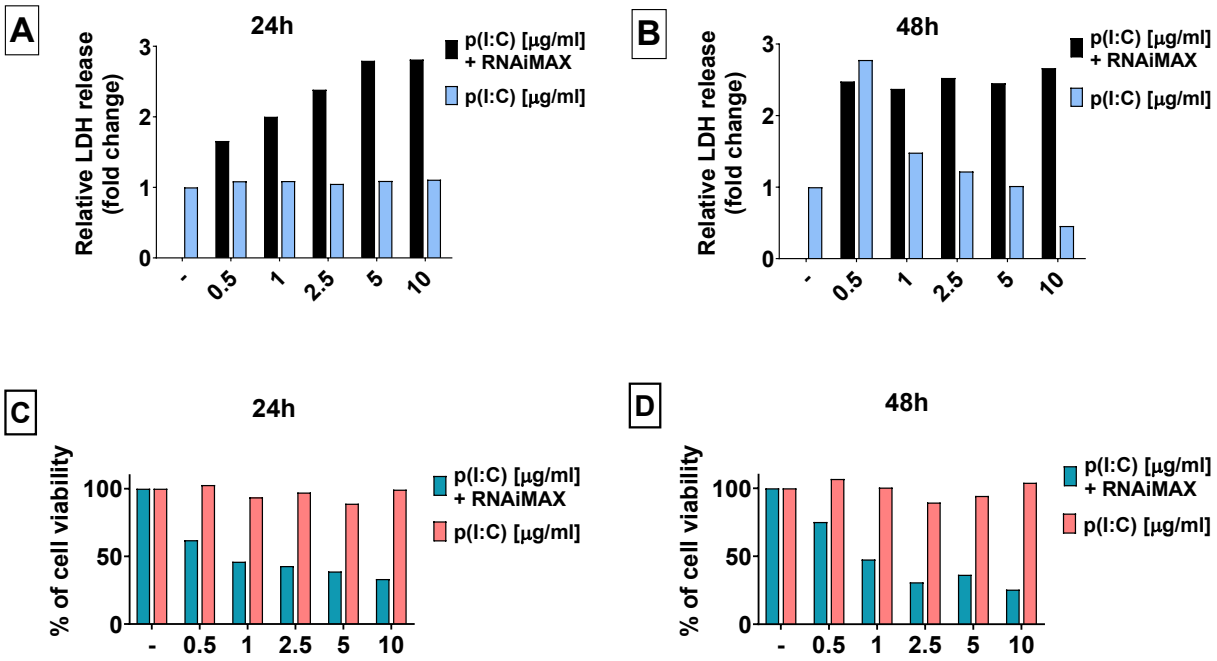

Figure 7. RIG-I/MDA5 stimulation in wild-type A549 cells reduces cell viability and induces cell death. A & B. *LDH release into culture supernatants from wild-type A549 cells untreated or stimulated with poly(I:C) alone or poly(I:C) + lipofectamine RNAiMAX after incubation for 24 (**A**) and 48 hours (**B**). Absorbance was quantified in technical duplicates at 490 nm and 655 nm for background and then subtracted. Results were normalised to the untreated control and show data from one experiment. **C & D.** MTS cell viability MTS assay of wild-type A549 cells untreated or stimulated with poly(I:C) alone or poly(I:C) + lipofectamine RNAiMAX after incubation for 24 (**C**) and 48 hours (**D**). Quantification of absorbance at 490 nm. Results were normalised to the untreated control and show data from one experiment without duplicates.*

LDH was detected at the lowest concentration of treatment with poly(I:C) alone, decaying progressively as the concentration increased. Thus, this first set of cell viability results seemed to favour the MTS assay over the LDH assay in terms of reproducibility at different timepoints and the straightforwardness of the method.

In these initial experiments with A549 wild-type human lung epithelial cells, we could show that the stimulation of the RIG-I/MDA5 signalling pathway with transfected poly(I:C) induces the production of inflammatory cytokines such as IL-6 and type III IFNs in A549 cells (24 and 48 hours post-stimulation). We observed that very low concentrations of poly(I:C) + RNAiMAX treatment were sufficient to induce cytokine production. Furthermore, we detected a reduced cytokine secretion at higher doses of transfected poly(I:C), as well as reduced cytokine mRNA levels at very high doses of transfected poly(I:C). In addition, treatment with increasing concentrations of poly(I:C) + RNAiMAX induced cell death in A549 cells. Based on these results it was decided to focus further experiments on A549 stimulation with 1 µg/ml or lower concentrations of poly(I:C) + RNAiMAX, which were found to induce inflammatory signalling without causing excessive cell death. MTS assay was chosen as the more reliable cell viability assay. These optimised conditions should subsequently be applied to A549 cells overexpressing SARS-CoV-2 viral proteins that might interfere with the RIG-I/MDA5 inflammatory signalling pathway.

4.2. Validation of SARS-CoV-2 ORF3a, ORF6 and ORF9b protein expression in lentiviral-transduced A549 cell lines

In a previous master thesis project[85], three A549 cell lines that conditionally express SARS-CoV-2 ORF3a, ORF6 and ORF9b proteins were generated. The A549 cell lines were lentivirally transduced with pLVX-TetOne-Puro plasmids coding for these SARS-CoV-2 proteins. Transduction and verification of ORF3a, ORF6 and ORF9 viral protein expression was part of this previous master thesis project, as well as some purely exploratory and very preliminarytesting of the inflammatory effects of stimulation with different PRR ligands. However, the effects of RIG-I/MDA5 stimulation had not been extensively studied in these cell lines yet and was thus a main aim for this new master thesis project. We started out by testing if and to what level SARS-CoV-2 proteins ORF3a, ORF6 and ORF9 are expressed

in the A549 cells. Importantly, the genes coding for these viral proteins are under the control of a tetracycline-inducible expression system (Tet-On and Tet-Off Systems), which means they are only expressed when tetracyclines such as doxycycline are present in the cell culture. Moreover, the genes that code for the SARS-CoV-2 proteins of interest in the pLVX-TetOne-Puro plasmids are followed by a sequence coding for a Strep-II tag in order for the resulting proteins to be easily detected by the same specific antibody in WB assays.

In order to decipher to what extent the differences detected between treated and untreated samples within each cell line and across all different cell lines could be attributed to the immunomodulatory effects of SARS-CoV-2 ORF3a, ORF6 and ORF9b, a WB was performed. For this, all of the studied A549 cell lines were incubated without or with doxycycline (0.5 µg/ml) for 24 hours prior to being stimulated with different concentrations of transfected poly(I:C) or no poly(I:C) treatment at all for another 24 hours. After this stimulation step, cells were lysed in RIPA buffer (**Supplementary Table 1**) and lysates were analysed by WB using anti-Strep-II antibodies to detect all SARS-CoV-2 proteins simultaneously. This made it possible to compare the expression of ORF3a, ORF6 and ORF9b proteins at the post-translational level in the A549 cell lines transduced with pLVX-TetOne-Puro plasmids expressing these SARS-CoV-2 proteins. The wild-type A549 cell line was also included in the WB as a negative control, as it should not give out any luminol signal.

As it can be observed in **Figure 8**, the WB showed detectable signals for ORF3a, ORF6 and ORF9b when their respective cell lines had been incubated with doxycycline for 24 hours. The strongest luminol signals were detected for ORF3a, followed by ORF9b, the signal for ORF6 was barely perceptible. All SARS-CoV-2 proteins were detected at their expected level of molecular weight (**Supplementary Table 2**). Results thus indicate a very high expression of ORF3a and high levels of ORF9b in transduced A549 cells after doxycycline induction, but an extremely low expression of ORF6 protein. These differences in SARS-CoV-2 protein expression levels might be caused by the different transduction efficiency of pLVX-TetOne-Puro plasmids and have to be kept in mind when exploring inflammatory responses in these cells in further experiments. Strikingly, higher concentrations of transfected poly(I:C) in combination with RNAiMAX had an effect

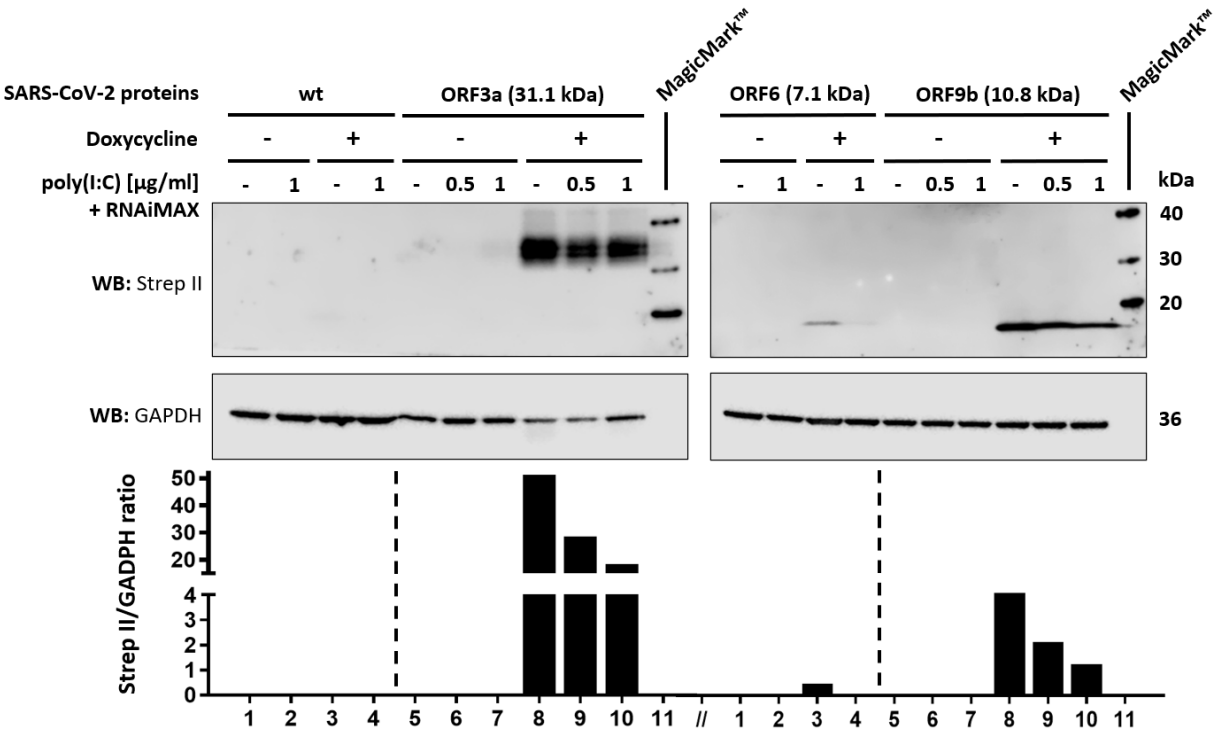

Figure 8. SARS-CoV-2 protein expression in A549 after induction of protein expression with doxycycline. *Samples were collected from WT and ORF3a, ORF6 and ORF9b-transduced A549 lung epithelial cells after induction with 0.5 µg/mL doxycycline for 24 hours. Cells were stimulated with 0.5 or 1 µg/mL of p(I:C), using RNAiMAX as lipofectant. After separation on SDS-PAGE, SARS-CoV-2 viral proteins tagged with Strep-II were detected using mouse anti-Strep-II monoclonal antibody during Western blot. GAPDH was used to normalize the proteins expression.*

on the abundance of the SARS-CoV-2 proteins, reducing its presence in the treated samples, which also has to be kept in mind for further experiments as the expression of some of the studied SARS-CoV-2 proteins might be diminished by poly(I:C) transfection, making it less likely to observe any statistically significant differences in the samples studied.

4.3. Stimulation of wild-type and SARS-CoV-2 ORF3a expressing A549 cells by poly(I:C) transfection

After confirming doxycycline-induced SARS-CoV-2 protein expression in ORF-transduced A549 cell lines, the possible effect of SARS CoV-2 proteins on RIG-I/MDA5 inflammatory responses was studied in A549 lung epithelial cells. Transfected poly(I:C) was used to induce RIG-I/MDA5 signalling. The starting point for these experiments were the optimised stimulation conditions determined in **section 4.1.** with the A549 wild-type cells. A first set of experiments was

conducted with A549 WT cells and the ORF3a-expressing A549 cell line for which the highest levels of SARS-CoV-2 protein expression were found (**section 4.2.**, WB). Based on our first set of experiments (**section 4.1.**), low concentrations of transfected poly(I:C) were explored, starting with concentrations from 0.05 µg/ml. The aim of these titrations was to refine the experimental set up in order to achieve a better compromise between cell viability and RIG-I/MDA5 response. The new experimental setup excluded the highest concentration of transfected poly(I:C) previously used (i.e. 10 µg/ml) as well as 2.5 µg/ml and expanded the range of lower concentrations to include 0.05, 0.1 and 0.25 µg/ml, stimulating both A549 and ORF3a A549 cells for 24 hours and 48 hours.

4.3.1. Cell viability assays of A549 WT and A549 ORF3a do not exhibit statistically significant differences

In order to assess the health and viability of the selected A549 cell lines in response to poly(I:C) treatment, cell viability MTS assays were conducted. The objective of these cell viability assays was to verify if a further reduction in the dosage of transfected poly(I:C) administered to the wild-type and SARS-CoV-2 ORF3a expressing A549 cells could also guarantee a further reduction in cell death. In addition, LDH assays were performed in parallel to confirm the cell viability results obtained with the MTS assay (**Supplementary Figure 1**). This time, both the 24 and the 48-hour timepoints showed comparable and coherent results for both the LDH and the MTS assays.

The MTS cell viability assay at 24 and 48 hours post-stimulation confirms the previously observed tendency of increasing cell death in response to increasing doses of poly(I:C) + RNAiMAX treatment (**Figure 9A, B**). Moreover, no significant differences in cell viability between A549 WT and ORF3a cells at 24 and 48-hour timepoints were found at the different concentrations of transfected poly(I:C). This indicates that ORF3a does not affect cell viability in response to RIG-I/MDA5 stimulation. On the other hand, the additional LDH assay performed on the same samples hints at a higher degree of cell death in A549 WT cells in comparison to A549 ORF3a cells. This observation is statistically significant at 48 hours post-stimulation. However, the LDH assay displayed an overall higher measurement variability than the MTS assay, further exemplifying the lack of trustworthiness of its results. These disparity in the LDH data would have to be further investigated

in order to be fully understood. Therefore, we decided to continue performing only MTS assays in future stimulation assays after having reaffirmed their reliability for these experimental conditions.

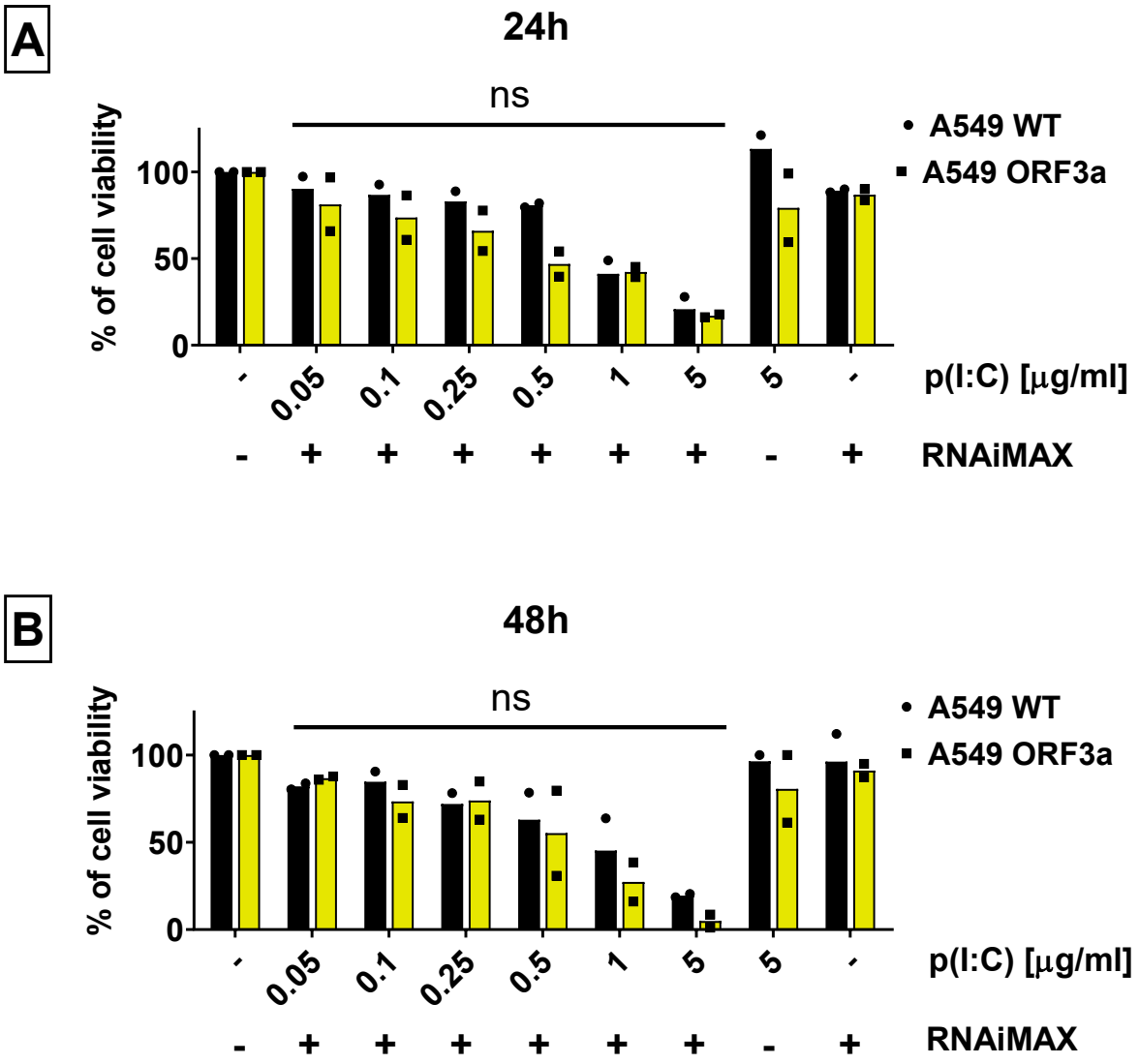

Figure 9. Comparable effects of RIG-I/MDA5 stimulation on cell viability of wild-type and SARS-CoV-2 ORF3a expressing A549 cell lines. *Cell viability (MTS) assay of wild-type and ORF3a-transduced A549 cells untreated or stimulated poly(I:C) + lipofectamine RNAiMAX after incubation for 24 (**A**) and 48 (**B**) hours. Cells were seeded the day before stimulation with poly(I:C) + lipofectamine RNAiMAX. Stimulation with poly(I:C) or RNAiMAX alone (twice the volume used for stimulation with the highest poly(I:C) concentration) was included as an experimental control. Untreated controls were incubated with CCM. Doxycycline (0.5 µg/ml) was added to the CCM of A549 ORF3a-transduced cell line. Quantification of absorbance at 490 nm. Results were normalised to the untreated control and plotted as a percentage and show means of technical duplicates from two independent experiments. Differences in treatment response in both cell lines were assessed by two-way ANOVA with Tukey correction. Ns p>0.05.*

4.3.2. ORF3a reduces pro-inflammatory IL-6 secretion from A549 lung epithelial cells in response to RIG-I/MDA5 stimulation

The previous cell viability MTS assays were paired with ELISA experiments. Secretion of IL-6 protein into the supernatant was analysed by ELISAs after 24 and 48 hours (**Figure 10A, B**). As in the initial experiments, A549 WT cells displayed an overall rise in IL-6 secretion levels when concentration of transfected poly(I:C) increased. The highest IL-6 production was observed for 1 µg/ml of poly(I:C) + RNAiMAX at 24 and 48 hours. Compared to WT A549 cells, ORF3a-expressing A549 cells secreted reduced levels of IL-6 into cell supernatants. In addition, IL-6 responses in A549 ORF3a cells were found almost unchanged in response to all concentrations of transfected poly(I:C) (0.05 to 5 µg/ml) used for stimulation at 24 hours. However, after 48 hours, a more dose-dependent effect of IL-6 secretion was observed in ORF3a A549 cells, where the highest response to transfected poly(I:C) treatment is visible at 0.5 µg/ml. Of note, wild-type A549 cells were visibly more responsive to transfected poly(I:C) in comparison to their counterpart cell line expressing ORF3a, as observed in the higher levels of secreted IL-6 and their variation across different treatment concentrations.

These first experiments including ORF3a-expressing A549 cells indicate that SARS-CoV-2 protein ORF3a might interfere with the RIG-I/MDA5 signalling pathway by inhibiting production and secretion of pro-inflammatory cytokine IL-6. Overall, the newer range of lower poly(I:C) concentrations seem to induce an IL-6 response comparable to the highest poly(I:C) concentrations. Experiments seem to yield favourable results and the chosen concentrations used for RIG-I/MDA5 stimulation are enough to perceive differences between the cell lines. Nevertheless, further experiments and statistical analysis are necessary in order to confirm this first assumption. In these, the other cell lines expressing ORF6 and 9b will also be included to further explore the possible immunomodulatory effects of these other relevant SARS-CoV-2 proteins.

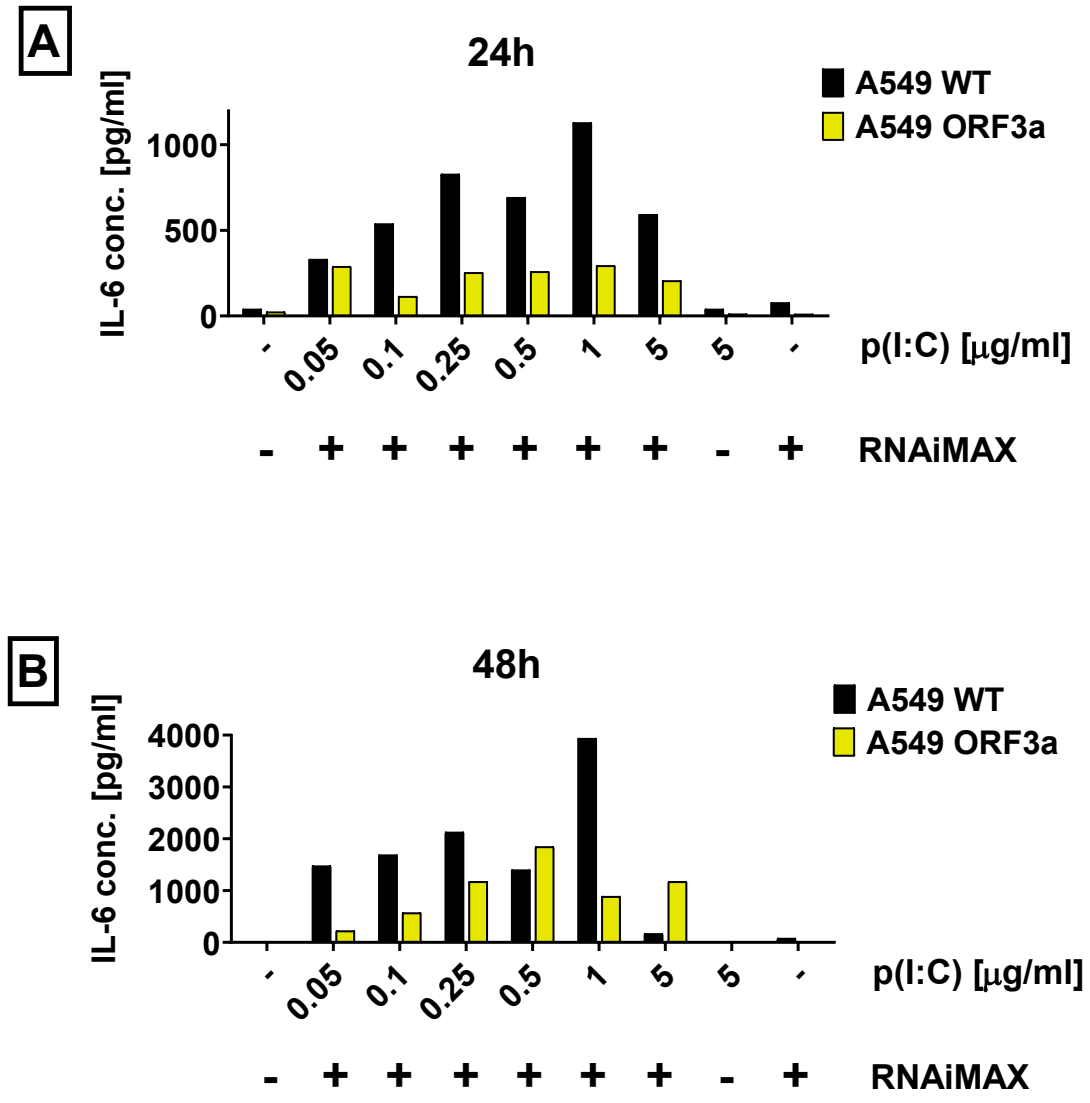

Figure 10. Reduced IL-6 secretion from SARS-CoV-2 ORF3a-expressing A549 compared to A549 wild-type human lung epithelial cells in response to RIG-I/MDA5 stimulation. *Cells were seeded the day before stimulation with poly(I:C) + lipofectamine RNAiMAX. Stimulation with poly(I:C) or RNAiMAX alone (twice the volume used for stimulation with the highest poly(I:C) concentration) was included as an experimental control. Untreated controls were incubated with CCM. Doxycycline (0.5 µg/ml) was added to the CCM of A549 ORF3a-transduced cell line. After incubation for 24 (**A**) and 48 hours (**B**), cell supernatants were collected. Analysis of IL-6 secretion levels was performed by DuoSet ELISA (R&D) in technical duplicates. Absorbance was measured at 450 nm and 570 nm and then subtracted. Controls were incubated with CCM. Mean from two independent experiments.*

4.3.3. Pro-inflammatory cytokine and type III IFN expression in A549 wild-type and ORF3a cells visibly peak at a concentration of 1 µg/ml of poly(I:C) + RNAiMAX treatment

Following the ELISA results obtained for IL-6 secretion in RIG-I/MDA5-stimulated A549 wild-type and ORF3a cells, RNA was extracted from these cell lines and RT-

qPCR was performed upon poly(I:C) and RNAiMAX treatment for 24 hours. The aim of this experiment consisted in confirming the upregulation of IL-6 secretion at the transcriptional level. In addition to *IL-6*, gene expression levels of *IFNL1* and *IFNL3* was also analysed, as these type III IFNs represent key actors in the innate immune response against SARS-CoV-2 infection. As shown in **Figure 11**, all these targets were found to be visibly upregulated at the transcriptional level in A549 WT cells, showing higher levels of mRNA transcripts with increasing concentrations of poly(I:C) + RNAiMAX before reaching a concentration of 5 µg/ml of transfected poly(I:C), at which the expression levels drastically drop. This is most certainly due to excessive cell death caused by the high dosage of poly(I:C) treatment. Especially, *IFNL1* expression was considerably higher than *IL-6* and *IFNL3* across almost all transfected poly(I:C) concentrations. Interestingly, out of all tested concentrations of poly(I:C) + RNAiMAX, 1 µg/ml proved to be the most "immunogenic", achieving the highest RQ values for all three targets. This might the highest dose of transfected poly(I:C) that does not yet induce too much cell death.

In contrast to the observed reduced levels of secreted IL-6 measured by ELISA (**section 4.2.1.**), *IL-6* mRNA levels were found to be much higher in ORF3a-expressing A549 cells compared to A549 WT cells in response to increasing doses of transfected poly(I:C), suggesting the ability of ORF3a to induce the transcription of pro-inflammatory cytokines. Furthermore, *IL-6* and *IFNL1* were visibly found to be more highly expressed in A549 ORF3a than in A549 wild-type cells, whereas *IFNL3* was slightly more upregulated in A549 wild-type than in A549 ORF3a. Although more independent experiments ought to be conducted and analysed by statistical methods, this might be a first insight into how SARS-CoV-2 might manipulate the inflammatory response in lung epithelial cells to its own advantage in order to ensure a successful infection of the host cell. All in all, this series of experiments allowed us to further restrict the range of concentrations used in the stimulation of the RIG-I/MDA5 pathway to 0.25, 0.5 and 1 µg/ml, which were deemed to be the best compromise between cell viability and the innate immune response to the infection.

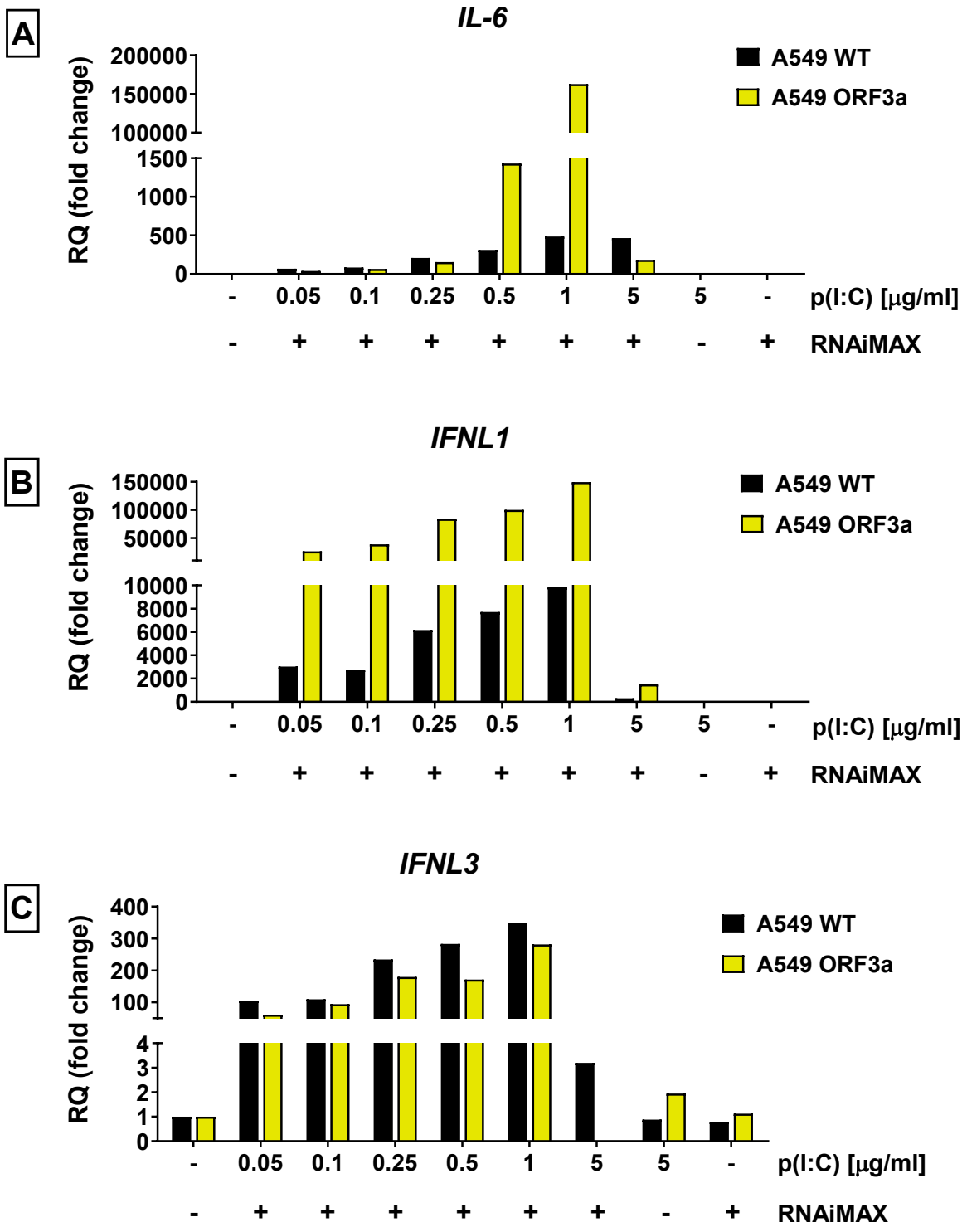

Figure 11. IL-6, IFNL1 and IFNL3 gene expression upon 24-hour RIG-I/MDA5 stimulation of wild-type and SARS-CoV-2 ORF3a expressing A549 cell lines. *Cells were seeded the day before stimulation with poly(I:C) + lipofectamine RNAiMAX. Stimulation with poly(I:C) or RNAiMAX alone (twice the volume used for stimulation with the highest poly(I:C) concentration) was included as an experimental control. Untreated controls were incubated with CCM. Doxycycline (0.5 µg/ml) was added to the CCM of A549 ORF3a-transduced cell line. Cells were lysed after being stimulated for 24 hours. RNA was extracted from the lysates and IL-6 (**A**), IFNL1 (**B**) and IFNL3 (**C**) mRNA expression was assessed by RT-qPCR in technical duplicates. RQ calculated relative to TBP gene expression. Ct=40 was set for undetermined samples. Results from one experiment.*

4.4. Stimulation of wild-type and SARS-CoV-2 ORF3a, ORF6 and ORF9b expressing A549 cells by poly(I:C) transfection

After having titrated a wide range of transfected poly(I:C) concentrations in A549 wild-type and ORF3a cell lines and settled for the three most promising, the experimental setup appeared to be optimised enough for being expanded. Thus, additional A549 ORF6 and ORF9b cell lines were included in a newer series of ELISA, cell viability and RT-qPCR experiments. In these experiments including all ORF-expressing A549 cell lines, ELISAs were extended to protein secretion analysis of type III IFNs (IFN-λ1/3) as well as the chemokine IL-8. These cytokines are relevant in immune response against SARS-CoV-2, as they are also regulated via the RIG-I/MDA5 and NF-κB/IRF pathways. These experiments aim at providing a more comprehensive and holistic view on the key actors that participate in the innate immune antiviral response to SARS-CoV-2 infection.

In these set of experiments, wild-type and ORF3a, ORF6 and ORF9b transduced A549 cell lines were cultured in doxycycline-containing media for a day prior to being treated with poly(I:C) and RNAiMAX. This earlier incubation period was necessary to allow the tetracycline-inducible lentiviral vectors to express the SARS-CoV-2 proteins of interest. This was followed by RIG-I/MDA5 stimulation by poly(I:C) treatment in combination with TR for 24 and 48 hours. Cell viability was assessed by MTS assay 24 hours post-stimulation. Secretion of IL-6, type III IFNs and IL-8 in A549 wild-type, ORF3a, ORF6 and ORF9b cell supernatants was analysed at 24 and 48-hour timepoints by ELISA. In addition, RNA was extracted for RT-qPCR experiments 24 hours after poly(I:C) transfection. Last, a specific set of experiments was conducted in which cytokine production was assessed in A549 ORF3a, ORF6 and ORF9b cells that had been incubated in the absence of doxycycline, impeding the induction of SARS-CoV-2 protein expression in these cell lines. This was done as a mean of comparison of the variations between ORF-transduced and WT A549 cell lines, which should behave similarly in these experimental conditions.

4.4.1. SARS-CoV-2 proteins do not affect cell viability in A549 cell lines 24 and 48 hours after poly(I:C) + RNAiMAX treatment

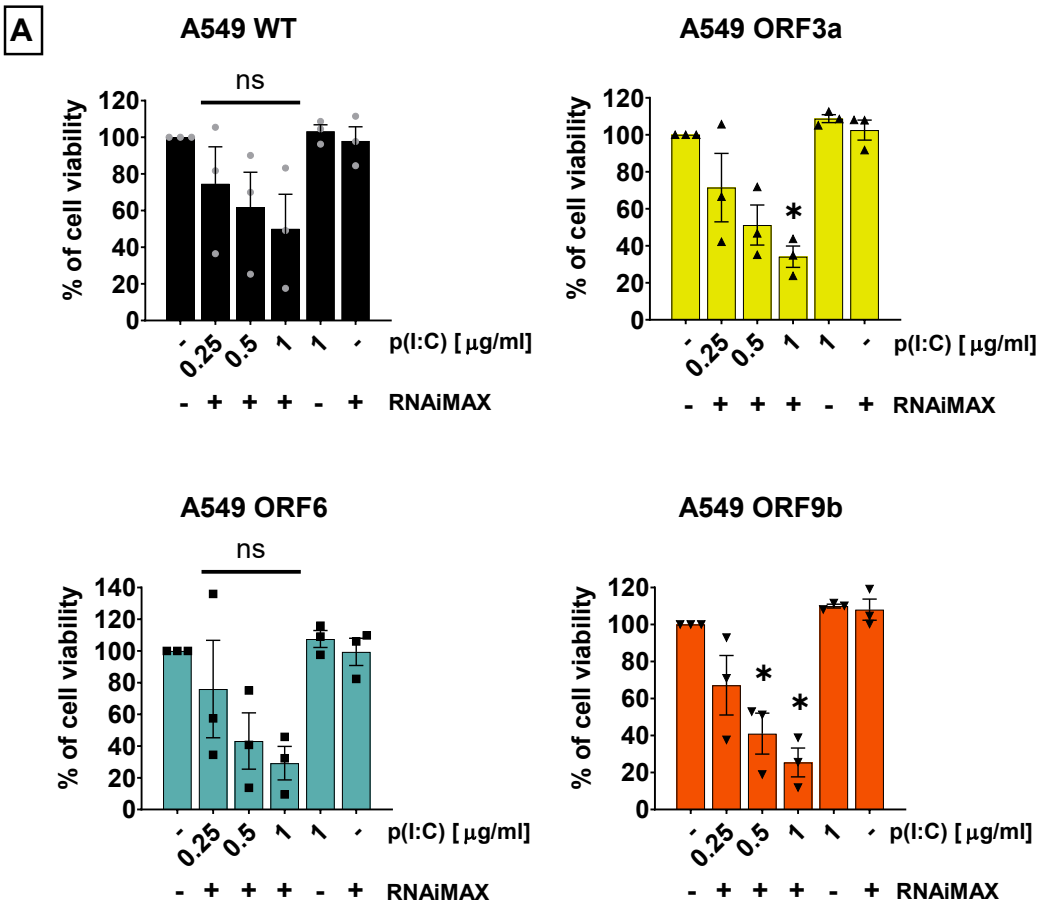
A
A549 WT
A549 ORF3a
A549 ORF6
A549 ORF9b
ns
% of cell viability
p(I:C) [µg/ml]
RNAiMAX
0.25
0.5
1
*

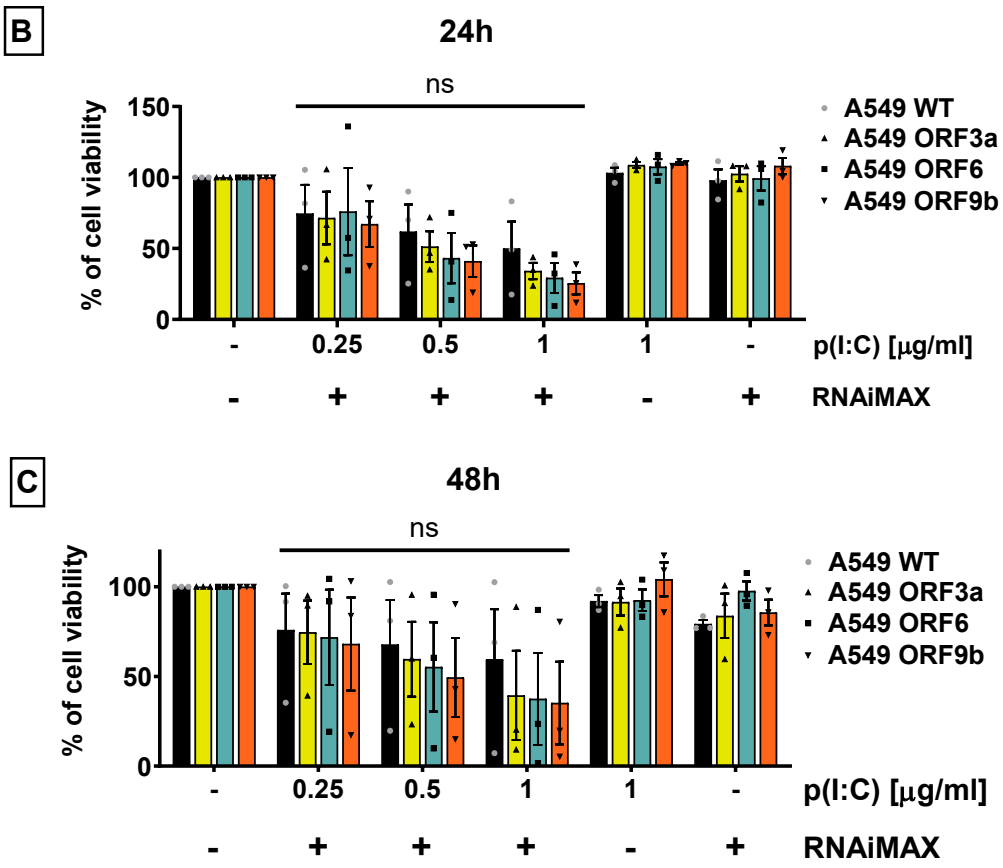
B
24h
ns
% of cell viability
A549 WT
A549 ORF3a
A549 ORF6
A549 ORF9b
p(I:C) [µg/ml]
RNAiMAX
0.25
0.5
1

C
48h
ns
% of cell viability
A549 WT
A549 ORF3a
A549 ORF6
A549 ORF9b
p(I:C) [µg/ml]
RNAiMAX
0.25
0.5
1

Figure 12. Cell viability of wild-type and SARS-CoV-2 ORF3a, ORF6 and ORF9b expressing A549 cell lines in response to 24-hour RIG-I/MDA5 stimulation. *Cell viability (MTS) assay of wild-type and ORF3a, ORF6 and ORF9b-transduced A549 cells untreated or stimulated with poly(I:C) + lipofectamine RNAiMAX after incubation for 24 and 48 hours. Cells were seeded the day before stimulation with poly(I:C) + lipofectamine RNAiMAX. Stimulation with poly(I:C) or RNAiMAX alone (twice the volume used for stimulation with the highest poly(I:C) concentration) was included as an experimental control. Untreated controls were incubated with CCM. Doxycycline (0.5 µg/ml) was added to the CCM of A549 ORF3a, ORF6 and ORF9b-transduced cell line media. Quantification of absorbance at 490 nm. Results were normalised to the untreated control and plotted as a percentage and show means from three independent experiments. One-way ANOVA with Dunnett correction was performed for A549 WT, ORF3a, ORF6 and ORF9b cell lines comparing treated to untreated (**A**). Differences in treatment response across cell lines at 24- (**B**) and 48-hour (**C**) timepoints were assessed by two-way ANOVA with Tukey correction. ns $p>0.05$, * $p\leq0.05$.*

Cell viability in cells treated with poly(I:C) + RNAiMAX was assessed by MTS assays 24 and 48 hours after stimulation of the RIG-I/MDA5 pathway (**Figure 12**). As it had been observed in the previous sets of experiments, all tested cell lines showed a decrease in cell viability with higher concentrations of transfected poly(I:C) at 24 hours (**Figure 12A**). In depth cell viability changes were not found to be statistically significant between untreated and poly(I:C)-transfected A549 wild-type and ORF6 cells. However, they did show visible differences following the trends of their counterpart A549 ORF3a and ORF9b cell lines, which did show statistically significant changes. This further proves the lethal effects of transfected poly(I:C) with regard to cell viability. On the other hand, the comparison of cell death across all tested cell lines showed no significant differences for 0.25, 0.5 and 1 µg/ml of poly(I:C) + RNAiMAX at 24 and 48-hour timepoints (**Figure 12B and C**). This suggests that the cell viability of all selected cell lines would be affected by poly(I:C) in a similar manner for each individual concentration of transfected poly(I:C). The reason for the lack of significant differences in these results is clearly due to the extremely different measurements observed in the MTS assay, which are too variable to produce any concise results. Again, performing additional independent experiments would reduce variability and increase measurement reliability potentially rendering statististically significant results. On the whole, these series of results allowed us to confirm the selection of the 24-hour timepoint as the most relevant for future experiments given its overall higher reliability.

4.4.2. Effects of SARS-CoV-2 ORF3a, ORF6, ORF9b on RIG-I/MDA5-induced IL-6 cytokine production in A549 human lung epithelial cells

The effects of SARS-CoV-2 ORF3a, ORF6 and ORF9b proteins on the production of IL-6 in response to RIG-I/MDA5 stimulation of A549 cells was assessed in cell lysates at the mRNA level as well as in cell supernatants at the protein level.

4.4.2.1. ORF3a, ORF6 and ORF9b do not significantly affect IL-6 protein secretion in A549 cells in response to activation of the RIG-I/MDA5 pathway

IL-6 secretion was analysed in the cell supernatants of A549 wild-type, ORF3a, ORF6 and ORF9b cells at 24- and 48-hour timepoints after poly(I:C) + RNAiMAX treatment by ELISA. IL-6 secretion was compared 24 hours post-stimulation within each cell line (**Figure 13A**) as well as between different cell lines for all concentrations of transfected poly(I:C) (**Figure 13B**).

At 24 hours, IL-6 secretion was not significantly different in any of the SARS-CoV-2 protein-expressing cell lines when compared to the A549 WT cell line for any concentration of transfected poly(I:C) (**Figure 13B**). This observation was also true at 48 hours, where no significant differences were reported either (**Figure 13C**). However, IL-6 secretion did show statistically significant differences between A546 ORF6 and A549 ORF9b when these cells had been transfected with 0.5 µg/ml of poly(I:C) concentration for 24 hours (**Figure 13B**). In detail, A549 ORF9b cell supernatants presented significantly higher IL-6 secretion levels than A549 ORF6, although this effect was lost at the 48-hour timepoint (**Figure 13C**) and neither of these cells showcased significant differences to the wild-type A549 cell line. This would make it possible to affirm that the ability of SARS-CoV-2 proteins ORF6 and ORF9b to induce pro-inflammatory cytokine secretion (i.e. IL-6) in the context of COVID-19 is highly variable. In this case, at first sight ORF9b would be the SARS-CoV-2 protein that would trigger IL-6 production more strongly, whereas ORF6 would induce IL-6 production less efficiently.

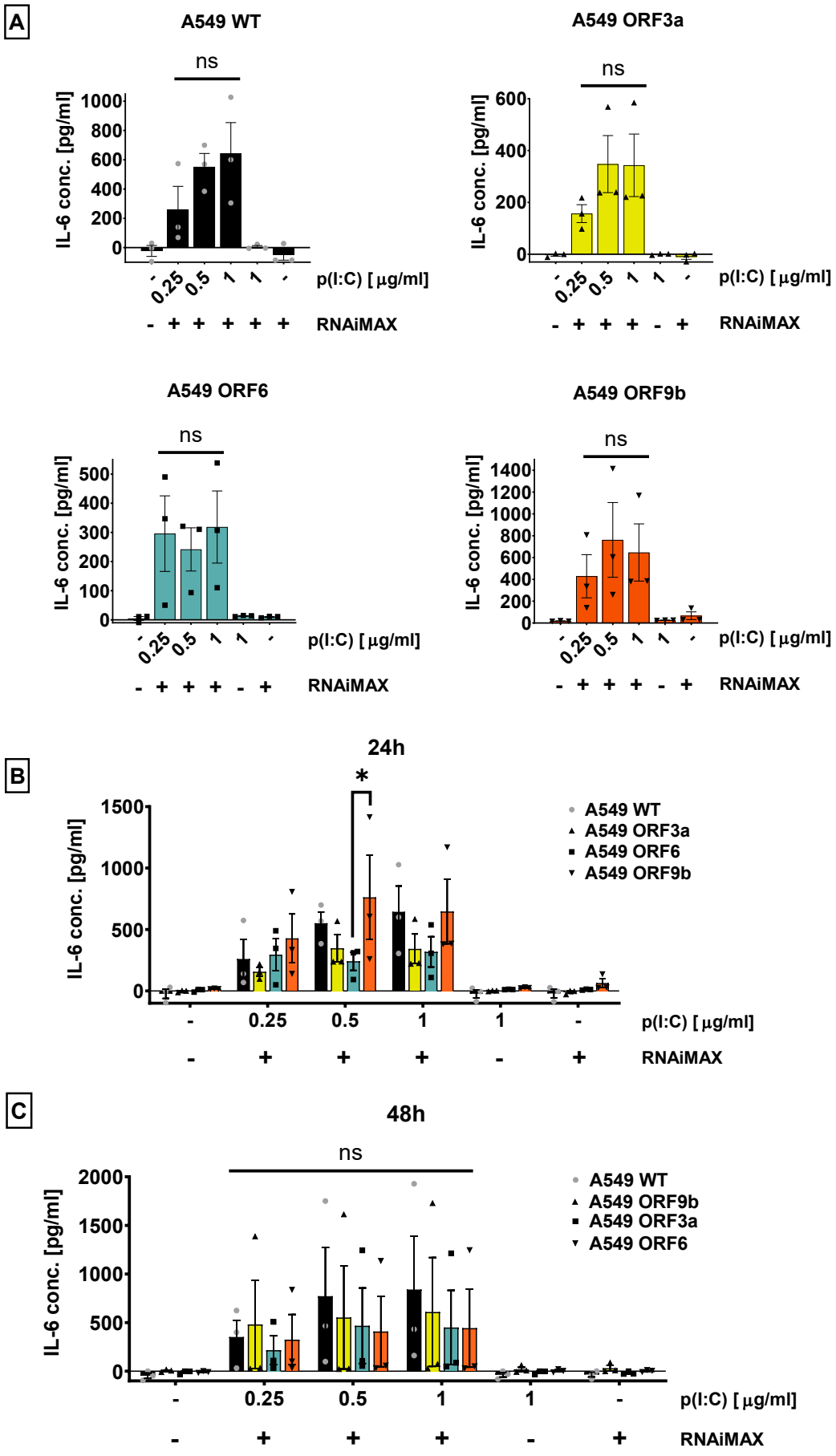
A
A549 WT
ns
IL-6 conc. [pg/ml]
1000
800
600
400
200
0
p(I:C) [µg/ml]
- 0.25 0.5 1 1 -
RNAiMAX
- + + + + +
A549 ORF3a
ns
IL-6 conc. [pg/ml]
600
400
200
0
p(I:C) [µg/ml]
- 0.25 0.5 1 1 -
RNAiMAX
- + + + - +
A549 ORF6
ns
IL-6 conc. [pg/ml]
500
400
300
200
100
0
p(I:C) [µg/ml]
- 0.25 0.5 1 1 -
RNAiMAX
- + + + - +
A549 ORF9b
ns
IL-6 conc. [pg/ml]
1400
1200
1000
800
600
400
200
0
p(I:C) [µg/ml]
- 0.25 0.5 1 1 -
RNAiMAX
- + + + - +
B
24h
*
IL-6 conc. [pg/ml]
1500
1000
500
0
A549 WT
A549 ORF3a
A549 ORF6
A549 ORF9b
- 0.25 0.5 1 1 -
p(I:C) [µg/ml]
- + + + - +
RNAiMAX
C
48h
ns
IL-6 conc. [pg/ml]
2000
1500
1000
500
0
A549 WT
A549 ORF9b
A549 ORF3a
A549 ORF6
- 0.25 0.5 1 1 -
p(I:C) [µg/ml]
- + + + - +
RNAiMAX

Figure 13. IL-6 secretion of wild-type and SARS-CoV-2 ORF3a, ORF6 and ORF9b expressing A549 cell lines in response to 24-hour RIG-I/MDA5 stimulation. *Cells were seeded the day before stimulation with poly(I:C) + lipofectamine RNAiMAX. Stimulation with poly(I:C) or RNAiMAX alone (twice the volume used for stimulation with the highest poly(I:C) concentration) was included as an experimental control. Untreated controls were incubated with CCM. Doxycycline (0.5 µg/ml) was added to A549 ORF3a, ORF6 and ORF9b-transduced cell line media. After incubation for 24 hours, cell supernatants were collected. Analysis of IL-6 secretion levels was performed by DuoSet ELISA (R&D) in technical duplicates. Absorbance was measured at 450nm and 570nm and then subtracted. Controls were incubated with CCM. Mean from three independent experiments. One-way ANOVA with Dunnett correction was performed for A549 WT, ORF3a, ORF6 and ORF9b cell lines comparing treated to untreated (**A**). Differences in treatment response across cell lines at 24- (**B**) and 48-hour (**C**) timepoints were assessed by two-way ANOVA with Tukey correction. ns p>0.05, * p≤0.05.*

Strickingly, individual values for this ELISA experiment revealed great disparities for the treated samples, which explains the lack of statistical significance. More stringent independent experiments of these ELISA experiments would be needed in order to be able to reverse this lack of statistical significance. Altogether, these ELISA results for IL-6 secretion encouraged us to continue analysing the presence of cytokines only in those samples that had been stimulated with transfected poly(I:C) for 24 hours, since they were deemed as more promising in the devise of possible statistical differences across data groups.

4.4.2.2. SARS-CoV-2 ORF3a, ORF6 and ORF9b proteins upregulate RIG-I/MDA5-induced *IL-6* mRNA production at the transcriptional level

IL-6 mRNA levels were analysed by RT-qPCR to verify its production at the transcriptional level. After all selected A549 cell lines had been stimulated for 24 hours, cells were lysed and their RNA was extracted, followed by reverse transcription and quantitative PCR. Only samples that were treated with 0.5 µg/ml were selected to be analysed, since this concentration of transfected poly(I:C) was deemed as an optimal compromise between a cytokine response and a limited cell death. Results were analysed with the $\Delta\Delta C_t$ comparative method and they only presented statistically significant differences to their untreated controls in A549 wild-type and ORF3a expressing cell lines, while the change in *IL-6* transcriptional expression remained non-significant in A549 ORF6 and ORF9b cell lines (**not shown**). However, the expression of *IL-6* in A549 ORF6 and ORF9b increases at least 100-fold for every measurement taken, which could as well be interpreted as a relevant induction of pro-inflammatory cytokine expression in these cell lines.

Remarkably, all SARS-CoV-2 protein-transduced cell lines treated with transfected poly(I:C) presented statistically higher induction of *IL-6* with when compared to treated A549 wild-type cell lines, being A549 ORF3a the cell line to exhibit the highest difference followed by A549 ORF9b and A549 ORF6 (**Figure 14**). Therefore, these RT-qPCR results demonstrate the strong pro-inflammatory effects of ORF3a, ORF6 and ORF9b viral proteins in the context of SARS-CoV-2 infected lung epithelial cells.

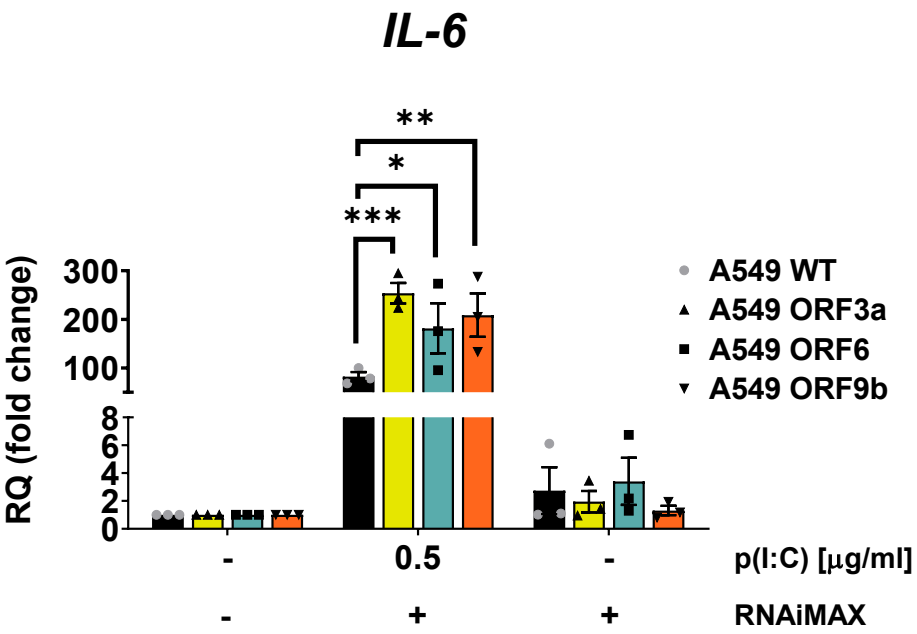

Figure 14. IL-6 gene expression from wild-type and SARS-CoV-2 ORF3a, ORF6 and ORF9b expressing A549 cell lines in response to 24-hour RIG-I/MDA5 stimulation. *Cells were seeded the day before stimulation with poly(I:C) + lipofectamine RNAiMAX. Stimulation with poly(I:C) or RNAiMAX alone (twice the volume used for stimulation with the highest poly(I:C) concentration) was included as an experimental control. Untreated controls were incubated with CCM. Doxycycline (0.5 µg/ml) was added to the CCM of A549 ORF3a, ORF6 and ORF9b-transduced cell line media. Cells were lysed after being stimulated for 24 hours. RNA was extracted from the lysates and IL-6, IFNL1 and IFNL3 mRNA expression was assessed by RT-qPCR in technical duplicates. RQ calculated relative to TBP gene expression. Ct=40 was set for undetermined samples. Results show means from three independent experiments. Differences in treatment response in the expression of IL-6 cell lines were assessed by two-way ANOVA with Tukey correction. ns p>0.05, * p≤0.05, ** p≤0.01, *** p≤0.001.*

4.4.3. Effects of SARS-CoV-2 ORF3a, ORF6 and ORF9b on RIG-I/MDA5 induced IFN-λ1/3 cytokine production in A549 human lung epithelial cells

Having studying IL-6 expression and secretion after poly(I:C) stimulation for 24 and 48 hours, we decided to follow these experiments up by exploring the expression and secretion of type III IFNs in all selected A549 in the same

experimental setup used for IL-6. It is worth mentioning that while the ELISA antibodies recognised both the secretion of IFN-λ1 and IFN-λ3 together as one (IFN-λ1/3), the RT-qPCR primers did distinguish between *IFNL1* (IFN-λ1, IL-29) and *IFNL3* (IFN-λ3, IL-28β). Because IFN-λ2 and IFN-λ3 present 96% of sequence homology, both these cytokines are highly related in their structure and carry out several overlapping functions. Therefore, we thought that the analysis of IFN-λ2 wouldn't provide any relevant additional information and we decided to not prioritise it in this series of experiments.

4.4.3.1. No significant effects of SARS-CoV-2 ORF3a, ORF6 and ORF9b on RIG-I/MDA5-induced IFN-λ1/3 protein secretion in A549 human lung epithelial cells

As detected by ELISA, IFN-λ1/3 secretion was visibly upregulated to similar levels for all concentrations of transfected poly(I:C) in all selected cell lines (**Figure 15**). However, all recorded measurements showed great variability once more, which accounts for the lack of statistical significance when comparing any of the treatment concentrations to the untreated control (**Figure 15A, B, C, D**). A slight time difference in the collection of cell supernatants after RIG-I/MDA5 stimulation for 24 hours could explain this elevated measurement variability. Likewise, when comparing across cell lines for each different treatment concentration, no statistically significant differences were found, even though every cell line seemed to visibly increase the levels of IFN-λ1/3 in their respective cell supernatants (**Figure 15E**). Therefore, these results are inconclusive and require more precise measurements with lower variability to provide any significant information on IFN-λ1/3 secretion in the context of lung epithelial cells infected with SARS-CoV-2.

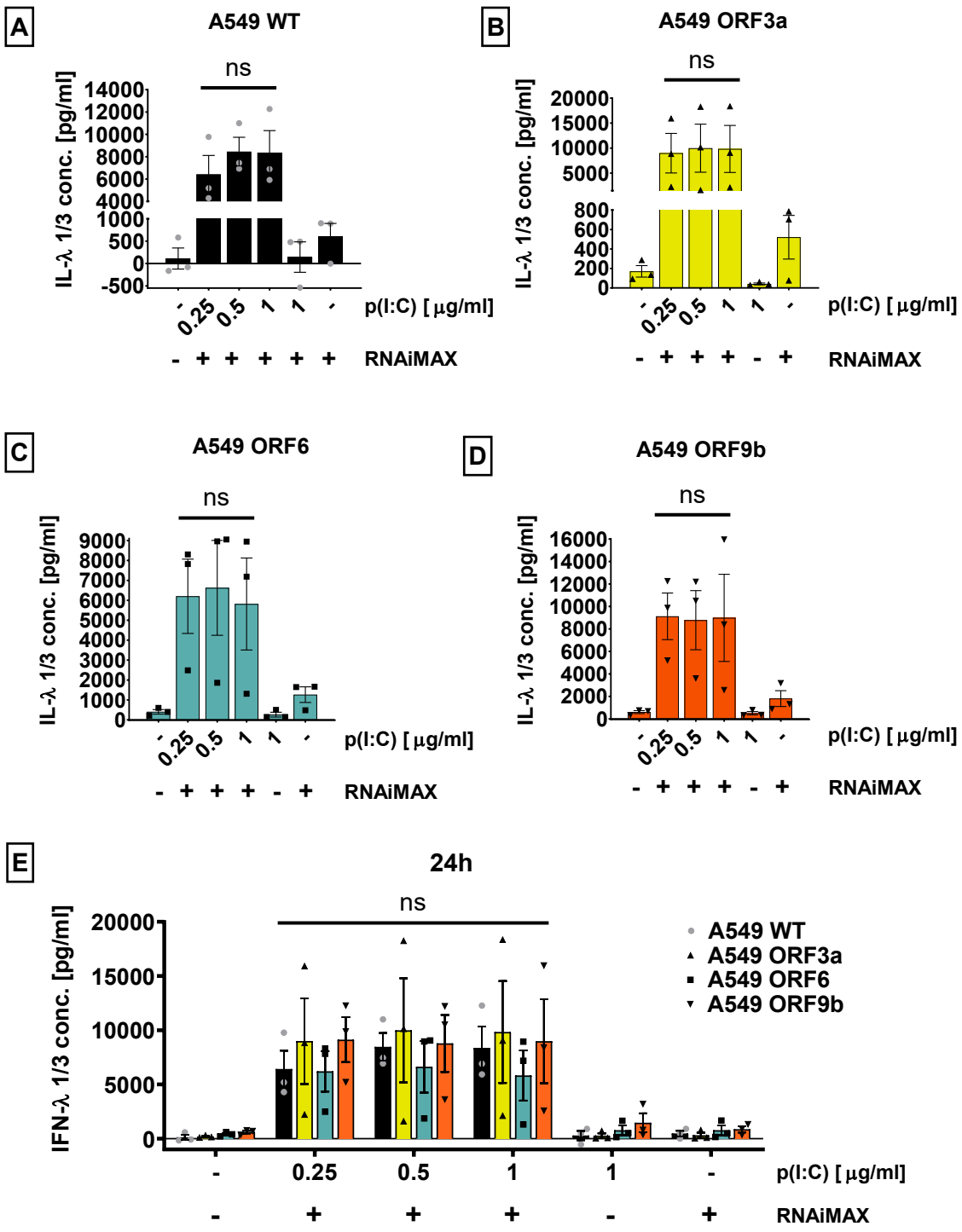

Figure 15. IFN-λ1/3 secretion of wild-type and SARS-CoV-2 ORF3a, ORF6 and ORF9b expressing A549 cell lines in response to 24-hour RIG-I/MDA5 stimulation. *Cells were seeded the day before stimulation with poly(I:C) + lipofectamine RNAiMAX. Stimulation with poly(I:C) or RNAiMAX alone (twice the volume used for stimulation with the highest poly(I:C) concentration) was included as an experimental control. Untreated controls were incubated with CCM. Doxycycline (0.5 μg/ml) was added to A549 ORF3a, ORF6 and ORF9b-transduced cell line media. After incubation for 24 hours, cell supernatants were collected. Analysis of IFN-λ1/3 secretion levels was performed by DuoSet ELISA (R&D) in technical duplicates. Absorbance was measured at 450nm and 570nm and then subtracted. Controls were incubated with CCM. Mean from three independent experiments. One-way ANOVA with Dunnett correction was performed for A549 WT (**A**), ORF3a (**B**), ORF6 (**C**) and ORF9b (**D**) cell lines comparing treated to untreated. Differences in treatment response across cell lines were assessed by two-way ANOVA with Tukey correction (**E**). ns p>0.05.*

4.4.3.2. No significant effects of SARS CoV-2 ORF3a, ORF6 and ORF9b on RIG-I/MDA5 induced IFN-λ1/3 mRNA expression in A549 human lung epithelial cells

Because of the inconclusiveness of these results, a series of RT-qPCR experiments for *IFNL1* and *IFNL3* mRNA expression was performed in order to assess whether type III IFNs would be induced at the transcriptional level with statistically significant differences. Nonetheless, RT-qPCR results proved to be almost as

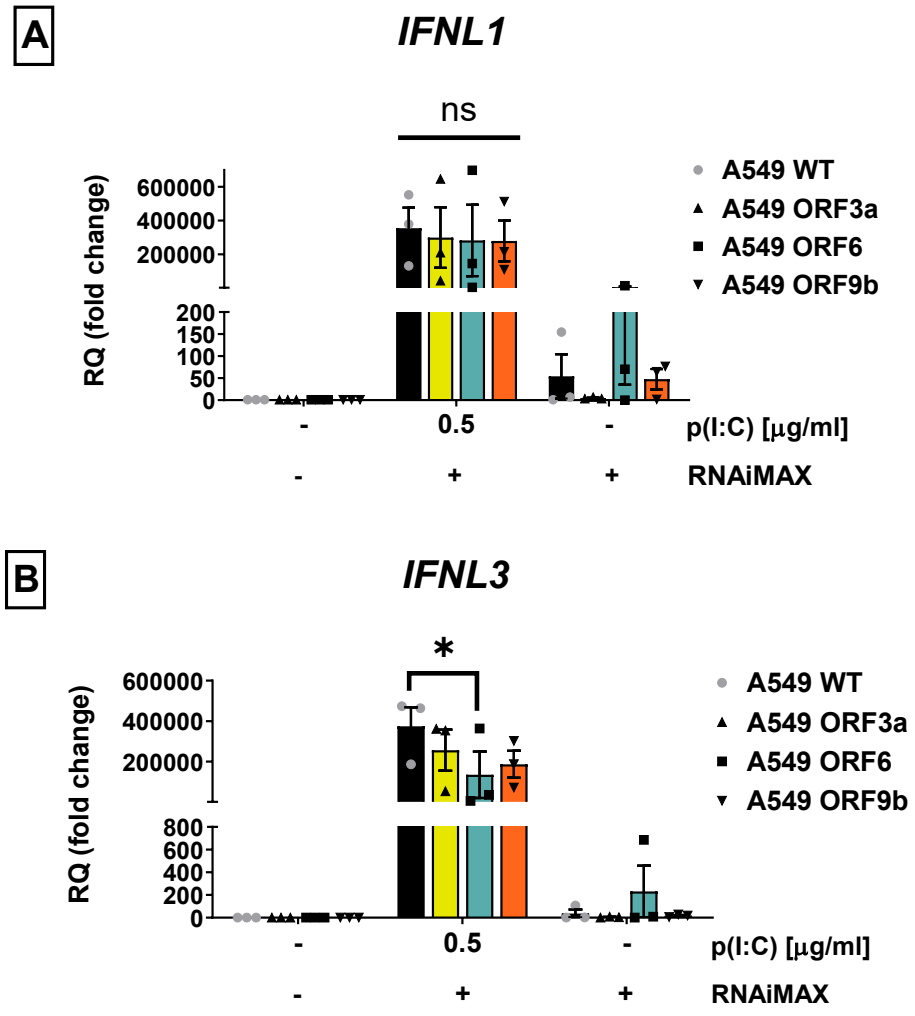

Figure 16. IFNL1 and IFNL3 gene expression from wild-type and SARS-CoV-2 ORF3a, ORF6 and ORF9b expressing A549 cell lines in response to 24-hour RIG-I/MDA5 stimulation. *Cells were seeded the day before stimulation with poly(I:C) + lipofectamine RNAiMAX. Stimulation with poly(I:C) or RNAiMAX alone (twice the volume used for stimulation with the highest poly(I:C) concentration) was included as an experimental control. Untreated controls were incubated with CCM. Doxycycline (0.5 µg/ml) was added to A549 ORF3a, ORF6 and ORF9b-transduced cell line media. Cells were lysed after being stimulated for 24 hours. RNA was extracted from the lysates and IFNL1 (**A**) and IFNL3 (**B**) mRNA expression was assessed by RT-qPCR in technical duplicates. RQ calculated relative to TBP gene expression. Ct=40 was set for undetermined samples. Results show means from three independent experiments. Differences in treatment response across cell lines were assessed by two-way ANOVA with Tukey correction. ns p>0.05, * p≤0.05.*

uncertain as the previous ELISA results. Although visibly higher, *IFNL1* mRNA levels were not significantly higher in any of the tested A549 cell lines after being transfected with poly(I:C) for 24 hours when compared to their untreated controls (**not shown**). There were also no statistically significant differences between A549 cell lines transfected with 0.5 µg/ml of poly(I:C) (**Figure 16A**). Parallelly, *IFNL3* mRNA expression levels for each of the selected A549 cell lines were visibly upregulated upon poly(I:C) transfection for 24 hours, although none of these increments proved to have any statistical significance (**not shown**). The only statistically significant difference was observed in the comparison across A549 cell lines treated with 0.5 µg/ml of poly(I:C), where A549 ORF6 showcased a significantly lower transcriptional induction of *IFNL3* compared to A549 WT (**Figure 16B**). This might speak to the immunomodulatory abilities of ORF6, which seems to be capable of reducing the IFN-λ3 response over the course of SARS-CoV-2 infection. Altogether, these additional analysis of the expression of *IFNL1* and *IFNL3* at the transcriptional level by RT-qPCR almost did not disclose any relevant contrast to what had been detected in previous ELISAs for these type III IFNs and more independent experiments would be needed in both types of methods to reach more conclusive results.

Taken together, these results demonstrate that type III IFNs are induced upon RIG-I/MDA5 stimulation in A549 cells and that neither ORF3a, ORF6 nor ORF9b show statistically significant changes in mRNA transcription or in protein secretion of these cytokines.

4.4.4. Effects of SARS CoV-2 ORF3a, ORF6 and ORF9b on RIG-I/MDA5-induced IL-8 chemokine production in A549 human lung epithelial cells

The last cytokine that was considered for our ELISA experiments was IL-8, an important chemokine in the recruitment of innate immune cells such as neutrophiles to the site of infection. IL-8 expression is induced by NF-κB via RIG-I/MDA5 signalling pathway. Therefore, IL-8 presumably holds a key role in the clearance of SARS-CoV-2 infected cells limiting the spread of the virus. The results of the ELISA for IL-8 turned out to be more enlightening than for the previous type-III IFNs, presenting more precise measurements. This was evident in the

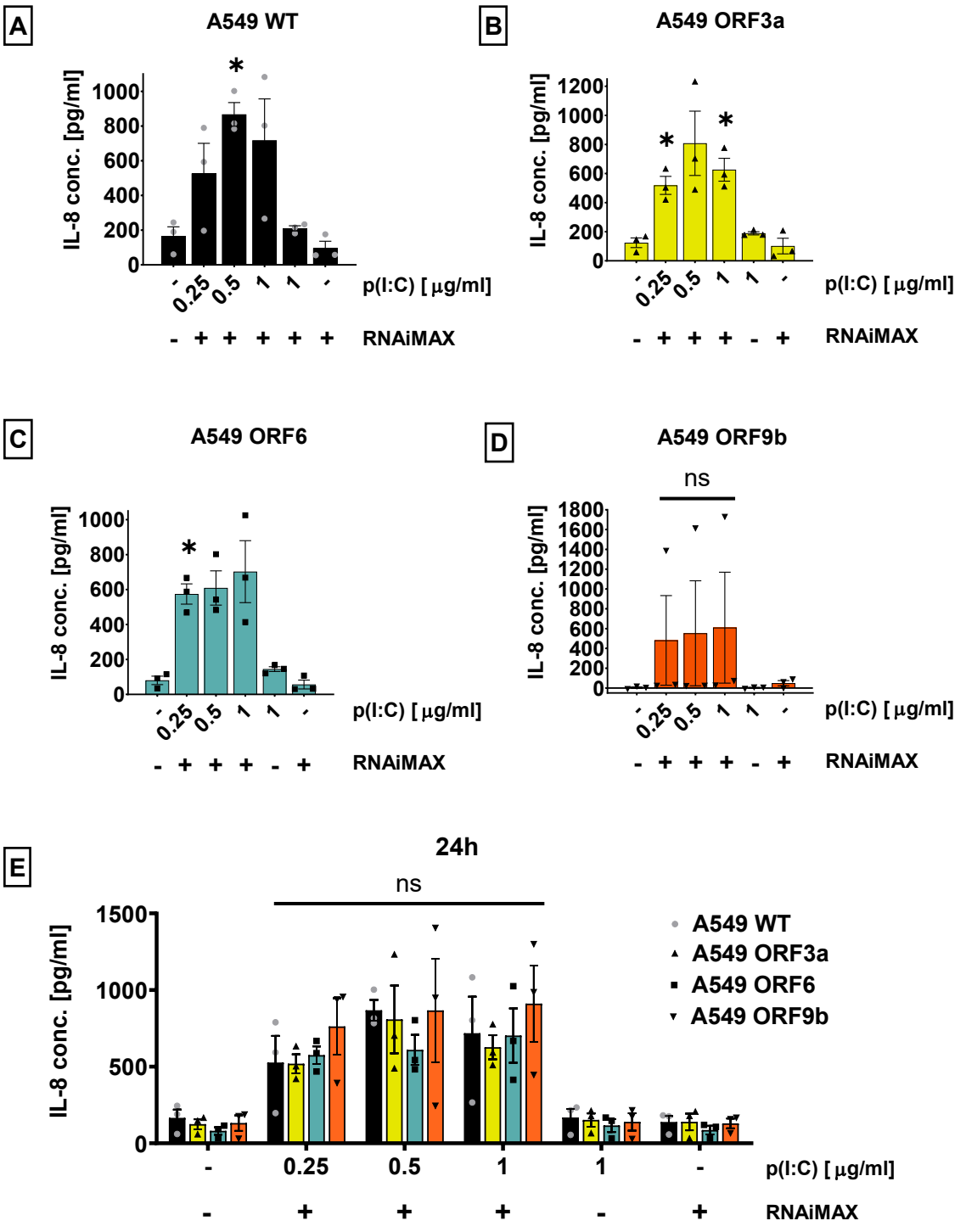

Figure 17. IL-8 secretion of wild-type and SARS-CoV-2 ORF3a, ORF6 and ORF9b expressing A549 cell lines in response to 24-hour RIG-I/MDA5 stimulation. *Cells were seeded the day before stimulation with poly(I:C) + lipofectamine RNAiMAX. Stimulation with poly(I:C) or RNAiMAX alone (twice the volume used for stimulation with the highest poly(I:C) concentration) was included as an experimental control. Untreated controls were incubated with CCM. Doxycycline (0.5 µg/ml) was added to A549 ORF3a, ORF6 and ORF9b-transduced cell line media. After incubation for 24 hours, cell supernatants were collected. Analysis of IL-8 secretion levels was performed by DuoSet ELISA (R&D) in technical duplicates. Absorbance was measured at 450nm and 570nm and then subtracted. Controls were incubated with CCM. Mean from three independent experiments. One-way ANOVA with Dunnett correction was performed for A549 WT (**A**), ORF3a (**B**), ORF6 (**C**) and ORF9b (**D**) cell lines comparing treated to untreated. Differences in treatment response across cell lines were assessed by two-way ANOVA with Tukey correction (**E**). ns p>0.05, * p≤0.05.*

higher production of IL-8 in wild-type and ORF3a and ORF6-expressing A549 cell lines upon stimulation with poly(I:C) in combination with RNAiMAX (**Figure 17A, B, C**). In detail, IL-8 secretion was statistically upregulated in the cell supernatants of A549 WT at 0.5 μg/ml, of A549 ORF3a at 0.25 and 1 μg/ml, and of A549 ORF6 at 0.25 μg/ml of transfected poly(I:C) treatment. In the case of the ORF9b, no statistically significant differences were observed between the treated samples and the untreated control due to high measurement variability (**Figure 17D**). At the same time, the presence of IL-8 in the cell supernatants was assessed across the different A549 cell lines for each different treatment concentration. Again, for this set of ELISA experiments none of the A549 cell lines proved to secrete significantly higher or lower amounts of IL-8 than any of the rest (**Figure 17E**). All in all, these ELISA results display more conclusive results than the previous ELISAs performed for IFN-λ1/3.

4.5. Expression and secretion of pro-inflammatory cytokines in A549 cell lines incubated in the absence of doxycycline

The previous WB experiments (**section 4.2.**) confirmed that the SARS-CoV-2 proteins of interest are expressed in A549 cell lines after induction with doxycycline. However, ORF3a, ORF6 and ORF9b were present in different levels, being ORF3a the most predominantly expressed SARS-CoV-2 protein followed by ORF9b and ORF6. In addition, treatment with poly(I:C) + RNAiMAX also seemed to diminish the expression levels of these SARS-CoV-2 proteins. Knowing this, a series of experiments was performed in order to compare the cell viability and cytokine response between A549 cell lines that had been previously incubated with or without doxycycline prior to stimulation of the RIG-I/MDA5 signalling pathway. These experiments would allow us to discern whether the effects observed in the previous series of assays are due to SARS-CoV-2 protein induction by doxycycline treatment or unrelated factors unique to each of the different cell lines. Theoretically, ORF3a, ORF6 and ORF9b-transduced A549 cell lines should behave similarly to the wild-type A549 cell line since none of these SARS-CoV-2 proteins are expressed when these cell lines have not been incubated with doxycycline. Thus, we set out to repeat ELISAs, MTS assays and RT-qPCR experiments with the

same treatment concentrations chosen for the previous ones to verify whether this assumption was correct.

4.5.1. Cell viability in A549 cell lines in the absence of doxycycline

In conjunction with the previous series of ELISAs, the cell viability of all A549 cell lines was analysed by MTS assay after being incubated in doxycycline-free media and transfected with the selected poly(I:C) concentrations for 24 hours. The results obtained revealed a decay in cell viability comparable to that observed in the previous experimental setups that included doxycycline in the CCM, where higher concentrations of transfected poly(I:C) entailed higher cell death. At the same time, all A549 cell lines showcased visibly similar relative amounts of viable cells for each individual poly(I:C) concentration (**Figure 18**). This observation speaks to the fact that the viability of all cell lines is affected in the same way by poly(I:C) treatment when the ORF proteins are not being expressed. Therefore, in the absence of doxycycline, wild-type and ORF-transduced A549 cell lines do behave equally with respect to their viability.

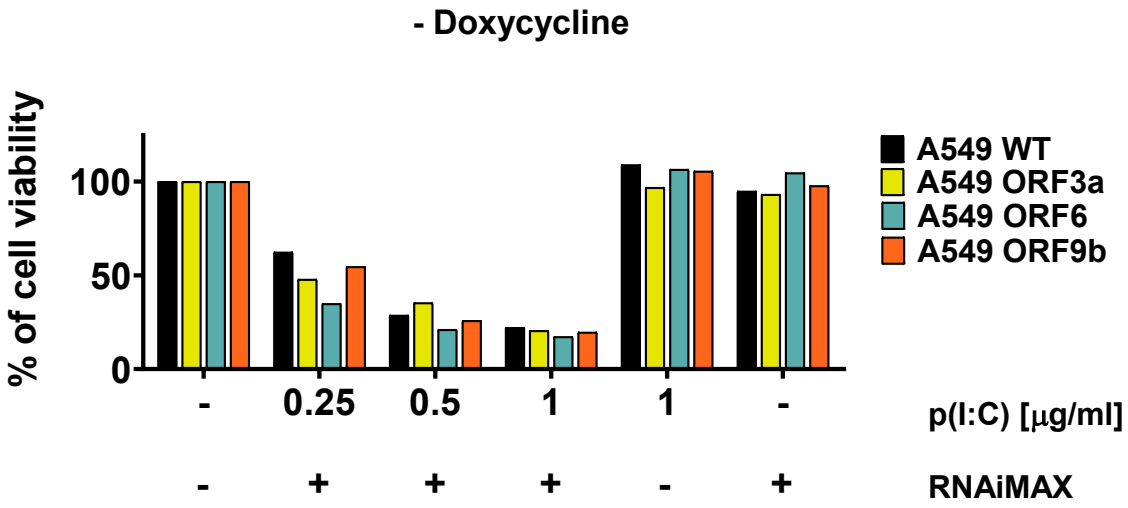

Figure 18. Cell viability of doxycycline-untreated wild-type and SARS-CoV-2 ORF3a, ORF6 and ORF9b expressing A549 cell lines in response to 24-hour RIG-I/MDA5 stimulation. *Cell viability (MTS) assay of wild-type and ORF3a, ORF6 and ORF9b-transduced A549 cells untreated or stimulated with poly(I:C) + lipofectamine RNAiMAX after incubation for 24 hours. Cells were seeded the day before stimulation with poly(I:C) + lipofectamine RNAiMAX. Stimulation with poly(I:C) or RNAiMAX alone (twice the volume used for stimulation with the highest poly(I:C) concentration) was included as an experimental control. Untreated controls were incubated with CCM. Quantification of absorbance at 490 nm. Results were normalised to the untreated control and plotted as a percentage and represent data from one experiment.*

4.5.2. Secretion of IL-6, IFN-λ1/3 and IL-8 in the absence of doxycycline

ELISA results obtained after RIG-I/MDA5 stimulation in all selected A549 cell lines incubated in the absence of doxycycline exhibited visibly higher levels for each of the different pro-inflammatory cytokines studied which respect to their untreated control. Interestingly, IL-6 and IFNL1 secretion revealed no statistically significant differences when comparing the different selected A549 cell lines to each other (**Figure 19A, B**). Although these results are most likely due to the variability of the measurements and the reduced number of independent experiments performed, they could also prove that the pro-inflammatory and antiviral cytokine response of all tested cell lines are similar enough when the expression of ORF3a, ORF6 and ORF9b proteins is not being induced in the transduced A549 cell lines.

On the other hand, multiple comparison of IL-8 secretion among all the cell lines was performed in order to verify if they behaved equally upon RIG-I/MDA5 stimulation (**Figure 19C**). Surprisingly, several statistically significant differences were found between the cell lines. For 0.25 µg/ml and 0.5 µg/ml of transfected poly(I:C), A549 ORF9b was significantly upregulated in comparison to A549 WT. Meanwhile, for 1 µg/ml of transfected poly(I:C), A549 ORF3a and ORF6 showed statistically significant downregulation, whereas A549 ORF9b displayed statistically significant upregulation in relation to A549 WT. Taken together, these results prove the existence of a differential IL-8 response upon poly(I:C) transfection between A549 wild-type and ORF-transduced A549 cells incubated in the absence of doxycycline. This cannot be explained by the presence of residual tetracyclines in the CCM, since the previous WB results detected no residual expression of any ORF-transduced proteins in the doxycycline-untreated samples. This effect might be due to variations in absorbance measurements and the reduced number of independent experiments performed in these conditions. Notably, this should influence the way in which previous IL-8 ELISA results are interpreted, given that the ORF-transduced cell lines are predisposed to vary in relation to the wild-type cell line upon RIG-I/MDA5 stimulation even when the SARS-CoV-2 proteins are not being expressed and this needs to be taken into account.

All in all, there is a trend in which the cell line A549 ORF9b shows higher levels of secreted IL-6, type III IFNs and IL-8 responses than the wild-type A549 WT cell line when SARS-CoV-2 protein expression is not induced. In addition, there are

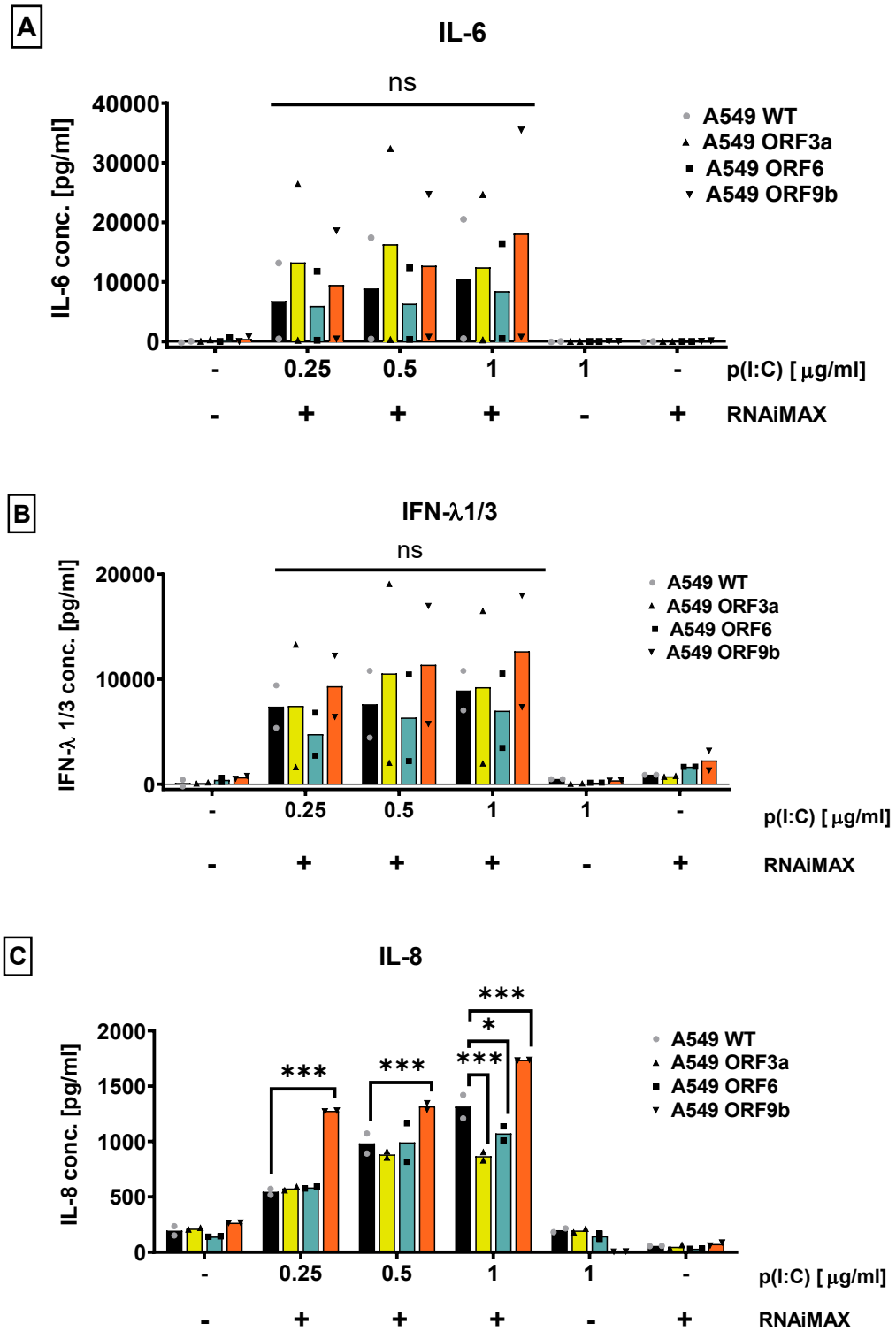

Figure 19. IL-6, IFN-λ1/3 and IL-8 secretion of doxycycline-untreated wild-type and ORF3a, ORF6 and ORF9b expressing A549 cell lines in response to 24-hour RIG-I/MDA5 stimulation. *Cells were seeded the day before stimulation with poly(I:C) + lipofectamine RNAiMAX. Stimulation with poly(I:C) or RNAiMAX alone (twice the volume used for stimulation with the highest poly(I:C) concentration) was included as an experimental control. Untreated controls were incubated with CCM. After incubation for 24 hours, cell supernatants were collected. Analysis of IL-6 (**A**), IFN-λ1/3 (**B**) and IL-8 (**C**) secretion levels was performed by DuoSet ELISA (R&D) in technical duplicates. Absorbance was measured at 450nm and 570nm and then subtracted. Controls were incubated with CCM. Mean from two independent experiments. Differences in treatment response across cell lines were assessed by two-way ANOVA with Tukey correction. ns p>0.05.*

some variations in the cytokine levels between cell lines. This might be due to the reduced number of experiments performed and to individual stimulations. However, there are no significant differences in the levels of secreted cytokines in response to RIG-I/MDA5 stimulation, apart from some results for IL-8 which could not be further investigated.

4.5.3. A549 cell lines express different levels of pro-inflammatory cytokines and type III IFNs in the absence of doxycycline

Lastly, in order to obtain a more holistic view of the pro-inflammatory cytokine and type III IFN production, RT-qPCR was done once more to analyse the expression of *IL-6*, *IFNL1* and *IFNL3* and confirm whether they would be differently up or downregulated at the transcriptional level for each of the selected A549 cell lines. As it can be observed in **Figure 20**, all types of A549 cell lines exhibit considerably higher levels of each of the analysed cytokines in relation to their untreated controls when they undergo poly(I:C) transfection for 24 hours. In addition, when comparing the mRNA expression levels of the selected cytokines to the wild-type A549 cell line, *IL-6* was visibly more induced in ORF3a and ORF6-expressing A549 cell lines, *IFNL1* induction appeared to be higher in A549 ORF6 and lower in A549 ORF3a and ORF9b, and *IFNL3* was downregulated in all of the ORF-expressing A549 cell lines. Nonetheless, overall, the expression data are in the same range for all the cell lines and suggest that there are no considerable differences in the mRNA levels of any of the analysed cytokines in the absence of doxycycline treatment. This is a favourable and expected behaviour for these A549 modified cell lines.

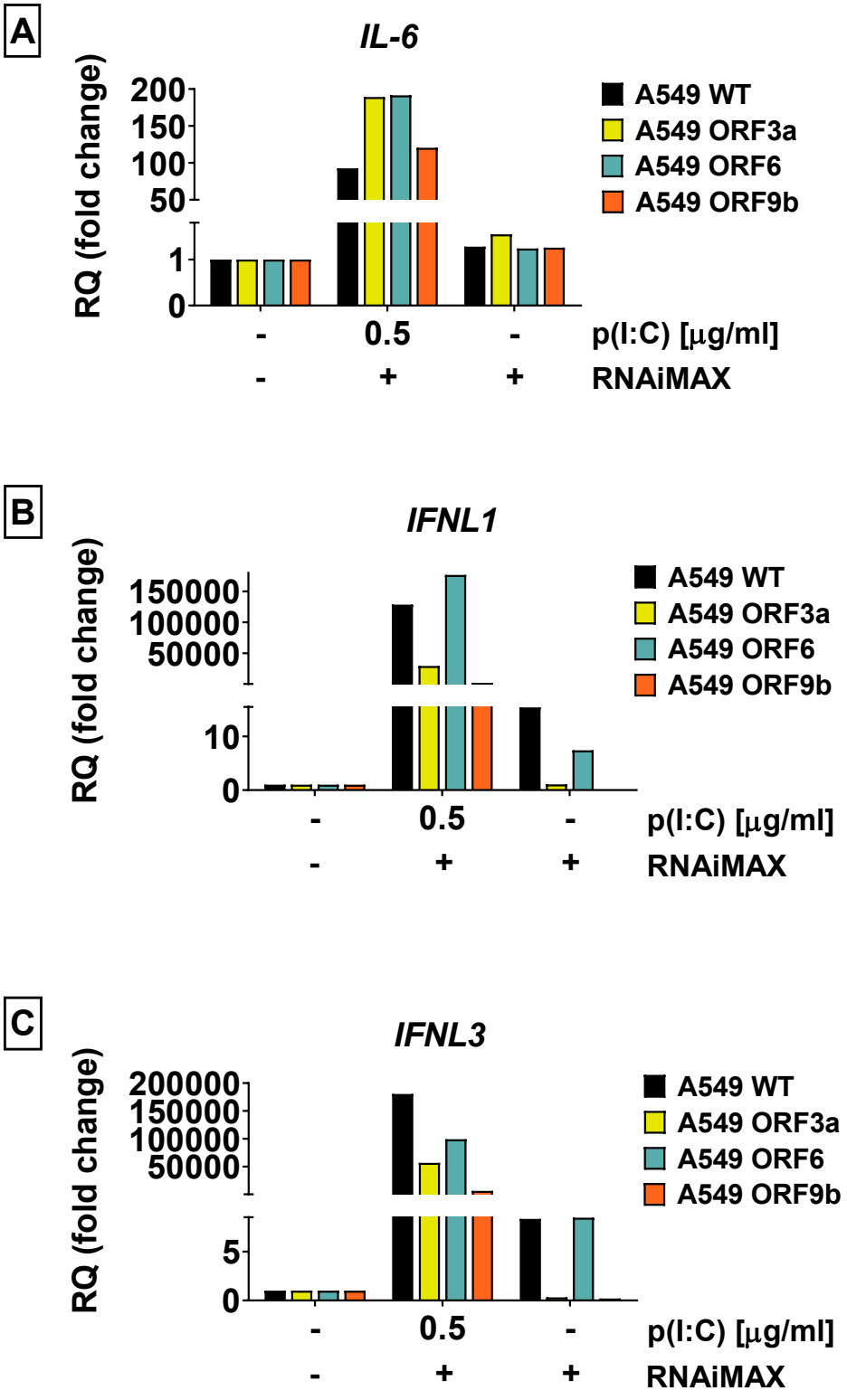

Figure 20. IL-6, IFNL1 and IFNL3 gene expression from doxycycline-untreated wild-type and ORF3a, ORF6 and ORF9b expressing A549 cell lines in response to 24-hour RIG-I/MDA5 stimulation. *Cells were seeded the day before stimulation with poly(I:C) + lipofectamine RNAiMAX. Stimulation with poly(I:C) or RNAiMAX alone (twice the volume used for stimulation with the highest poly(I:C) concentration) was included as an experimental control. Untreated controls were incubated with CCM. Cells were lysed after being stimulated for 24 hours. RNA was extracted from the lysates and IL-6, IL- IFNL1 and IFNL3 mRNA expression was assessed by RT-qPCR in technical duplicates. RQ calculated relative to TBP gene expression. Ct=40 was set for undetermined samples. Results represent data from one experiment.*

5. Discussion

5.1. Human lung epithelial cells secrete inflammatory cytokines and type III IFNs through the RIG-I/MDA5 signalling pathway

Ever since the COVID-19 pandemic started and major research on SARS-CoV-2 begun, most of the studies on the functionality of individual SARS-CoV-2 viral proteins have been performed in cell models that are not the virus' target for primary infection (e.g. HEK293T cells) [24-26, 143]. In fact, fewer experimental setups have chosen lung epithelial cells such as A549[9, 146, 147], which are human alveolar basal epithelial cells derived from a 58-year-old Caucasian male with lung adenocarcinoma (ATCC). Because SARS-CoV-2 has a natural tropism for lung epithelial cells, they constitute an ideal cell type to study innate immune responses in the context of COVID-19. Once infected, lung epithelial cells contribute to the immunomodulation of the antiviral response by the recruitment, activation and inducement of innate immune cells via chemokine, cytokine and IFN production[49, 51, 95]. It is of utmost importance to characterise the nature of these responses in lung epithelial cell models, as they can better mimic the immunogenic response to SARS-CoV-2. For this purpose, we chose A549 lung epithelial cells, which simulate the phenotypes of primary airway epithelial cells (AECs)[148, 149] and have previously proven to be valuable models to study SARS-CoV-2 infection[19, 49, 51].

Notably, Calu-3 lung epithelial cells (derived from human bronchial submucosal epithelial glands[150, 151] have also been employed to study the immunomodulatory effects of SARS-CoV-2 proteins, since they have been found to express high levels of hACE2 receptor[149, 152], which would indicate their condition as a SARS-CoV-2 target and better suitability as a model to study SARS-CoV-2 lung infection. However, the correct culturing and handling of Calu-3 has also proven to be challenging to attain due to the elevated cell death in the passaging process of the cells, which is known to cause stress-released DAMPs[85]. In turn, DAMPS, may activate innate immune pathways prompting inflammatory responses supplementary to stimulation by poly(I:C) transfection, generating unreliable results[153]. In addition, the Calu-3 phenotype is often altered when passage numbers above 12 are reached, which constitutes another handicap for this cell type[154]. Importantly, there is also a need to preserve an epithelial monolayer of

Calu-3 cells in order to ensure cell polarization as well as the creation of a transepithelial electrical resistance (TEER)[148, 151, 154]. Failure to do so would entail the alteration of pro-inflammatory responses as well as the dysregulation of signalling pathways involved in cell repair and differentiation[155]. Conversely, A549 cells are less prone to phenotypic changes and do not require the formation of tight junctions and TEER[154, 156]. Moreover, A549 cells can be and are often transduced with hACE2 to allow a better study of SARS-CoV-2 infection[50, 51]. In addition, this cell type allows for higher passage numbers and its culture conditions are easier to maintain, unlike Calu-3 cells. It has also been proven that A549 cells do not produce inflammatory cytokines before being stimulated, which ensures higher result reliability[85, 156]. Lastly, previous studies conducted by our group demonstrated that, in comparison to Calu-3 cells, A549 cells exhibited more suitable inflammatory and antiviral responses upon poly(I:C) stimulation to study viral interference with innate immune pathways as statistically significant differences in cytokine and type III IFN production in response to RIG-I/MDA5 stimulation on Calu-3 cells have not been observed in these preliminary studies from our team. Moreover, Calu-3 cells exhibited slow growth when our group tried to culture them in a previous master thesis project[85] and they presented a high number of passages, having an undefined age and source. For all these reasons, although Calu-3 cells hold great potential in the reproducibility of SARS-CoV-2 infection, we were compelled to abandon our work with this cell line in this project, as they would have unnecessarily increased its complexity and compromised the trustworthiness of our results. Nevertheless, this cell line might be tested in future research at fresh, low passages, having been transduced again with ORF3a, ORF6 and ORF9b genes.

In detail, we focused on studying the immunomodulatory effects of SARS-CoV-2 viral proteins ORF3a, ORF6 and ORF9b in A549 lung epithelial cells by analysing the cytokine IL-6, chemokine IL-8 and type-III IFN response upon RIG-I/MDA5 stimulation. Specifically, we analysed IFN-λ1 and IFN-λ3, whose immune actions have been extensively characterised in recent years[84, 157]. Given the fact that IFN-λ2 shares 96% sequence homology with IFN-λ3, both these cytokines are highly related in their structure and immunological roles, exerting several overlapping functions[157, 158]. Knowing this, we decided to not prioritise the analysis of IFN-λ2 in this series of experimental setups, as we thought it would not provide any

relevant additional information. Later in the project we tried to order anti-IFN-λ2 antibodies for ELISA experiments, but the provider was out of stock. Thus, we eventually had to postpone the analysis of IFN-λ2 expression and secretion in the tested A549 cell lines for some time in the near future. In addition, we did not study type I IFN responses in this project, since their actions on epithelial cells do not seem to be as relevant as those of type III IFNs. Nonetheless, type I IFN production might also be analysed in the future at the protein and mRNA level in order to have a wider perspective on the profile of cytokines that are altered as part of the innate immune response against SARS-CoV-2.

In order to refine our experimental setup, we first started testing different concentrations of poly(I:C) with and without transfection reagent (Lipofectamine RNAiMAX) in A549 wild-type cells (**section 4.1.**). The choice of RNAiMAX as the TR over other cationic-lipid TRs like Lipofectamine 2000 was due to its perfected design to specifically deliver siRNA and miRNA intracellularly with high efficiency, including poly(I:C) since it is a synthetic dsRNA analogue (ThermoFisher, Invitrogen life technologies). Furthermore, the protocol for the RNAiMAX-mediated transfection of poly(I:C) in A549 and other cells had been perfected by our group in previous studies[85, 159]. The testing of different poly(I:C) concentrations in combination with RNAiMAX allowed us to fine-tune our analysis of immunogenic responses to SARS-CoV-2 infection by selecting the concentrations that proved to stimulate the RIG-I/MDA5 pathway more efficiently while being the least detrimental to cell viability. This poly(I:C) + RNAiMAX titration has not been performed in previous studies in the context of SARS-CoV-2 infection in A549 lung epithelial cells, since only one pre-fixed concentration of poly(I:C) there[9, 85, 160].

In this project we used untransfected poly(I:C) as a control, which is endocytosed and is expected to stimulate TLR3 in endosomes but not the RIG-I/MDA5 pathway in the cytosol. We found that wild-type A549 cells were unresponsive to treatment with poly(I:C) without transfection reagent at either 24 or 48 hours (**Figure 5A, B**), showing no secretion of IL-6 in cell supernatants. This contrasts to other studies[160], where there was a clear rise in IL-6 levels in cell supernatants upon poly(I:C)-mediated TLR3 stimulation. The disparity between these results could be explained by an insufficient quantity of poly(I:C) used to stimulate the TLR3 surface receptor. A higher range of concentrations of poly(I:C) could result in a stronger TLR3 stimulation and IL-6 secretion in cell supernatants. However, for

the purpose of our study, we were interested in demonstrating that the expression and secretion of IL-6, IL-8 and type III IFNs was not being induced by TLR3 signalling from the endosomal membrane, but by the RIG-I/MDA5 axis from the cytosol. Therefore, the highest chosen concentration of poly(I:C) used for the stimulation of A549 cells in the absence of transfection reagent was always kept below the possible threshold for TLR3 stimulation. Indeed, the highest concentration of pure poly(I:C) used in our experiments did not induce either a significant cytokine response or cell death, which guarantees that all the innate immune responses analysed were entirely attributed to the downstream effects of the RIG-I/MDA5 signalling pathway.

In contrast, A549 cells were responsive to transfection of poly(I:C) with RNAiMAX at both timepoints, showing the highest secretion levels of IL-6 at 0.5 and 1 µg/ml of treatment at 24 and 48 hours respectively, which were the lowest concentrations of all transfected poly(I:C) concentrations tested (**Figure 5A, B**). In addition, we observed considerable cell death at higher doses of poly(I:C) + RNAiMAX. Because RNAiMAX alone did not induce such effect, the decrease in cell viability must be attributed to the combination of poly(I:C) with this transfection reagent. This prompted us to lower the range of transfected poly(I:C) concentrations in future experiments to use doses that were able to trigger cytokine response without causing excessive cell death. These ELISA results were confirmed by the analysis of *IL-6* mRNA expression levels, which were also visibly upregulated. In addition, the expression levels of *IFNL1* and *IFNL3* were also analysed by RT-qPCR, showing an even higher induction of the transcription of these type III IFN genes. However, as opposed to their secretion levels, the presence of transcripts for these cytokines peaked at 2.5 µg/ml of transfected poly(I:C) before dropping dramatically at 5 µg/ml of treatment (**Figure 6**), which encouraged us to test the cytokine responses at these higher concentrations in the next round of experiments. On the other hand, these results are in line with the observed viability of the poly(I:C) transfected cells, which inversely correlated with the treatment concentration, showing lower viability when higher concentrations of poly(I:C) were transfected (**Figure 7A, B, D**). Notably, no LDH release was measured in cells treated with poly(I:C) alone, except for the 48-hour timepoint (**Figure 7C**), which showed uncoherent results probably due to technical errors. All in all, these results support the relevance of our titration strategy, pointing out the importance of testing

different treatment concentrations to select those higher immunogenic responses and lower cell death to allow for the fine-tuning of the experimental setup.

5.2 Selection of a reliable read-out to assess cell viability in A549 lung epithelial cell stimulation experiments.

As transfection of A549 cells with poly(I:C) might affect cell health and viability, we sought out to find a suitable, convenient and reliable read-out to assess cell viability in the planned. To accomplish this aim, among the numerous assays at our disposal (trypan blue or propidium iodide staining, ATP measurement, etc.), we narrowed down our choice to LDH and MTS viability assays for their straightforwardness and wide-spread use and initiated the first round of experiments by performing both assays simultaneously in order to decide which one fitted our setup the best. The results obtained revealed that both viability assays were complementary for the most part, being the amount of LDH released into cell supernatants coherent with the absorbance detected in the MTS assay, which is a result of the amount of formazan product generated by viable and metabolically active cells. Notably, LDH and MTS assays conveyed comparable results for wild-type A549 cell viability at 24 hours (**Figure 7**). On the contrary, at 48 hours, the LDH assay presented anomalous measurements possibly explicable by technical errors made while performing the assay. Nonetheless, in subsequent experiments, the results obtained were coherent with the MTS assays. Overall, both assays were found highly reliable for the estimation of cell viability at 24 hours post-stimulation, but the MTS assay yielded more coherent results at 48 hours.

At this point, we selected the MTS assay as the preferred assay for further viability analysis of A549 cells. The main reason that led us to make this choice was the limited volume and availability of cell supernatants for all A549 cell lines tested, since they were cultured in 24-well plates and their use was prioritised to perform ELISAs. Moreover, conducting MTS assays resulted less complicated given the ease of seeding the different cell lines in 96-well plates when the pertinent dilutions had already been made for seeding in 24-well plates for the RIG-I/MDA5 stimulation experiments. Lastly, the MTS assay is cheap and easy to perform as it only requires the addition of a ready-made MTS tetrazolium solution to the cell culture before

measuring the absorbance in the same 96-well plate after incubation for 1 hour, further simplifying the execution of the assay. One of the drawbacks worth mentioning for the MTS assays performed in this project is that the measurements were not taken in technical duplicates given the restricted available space in the 96-well plates. Another caveat that has to be taken into consideration when carrying out MTS assays is that it has been demonstrated that they are not able to distinguish between the effects of cell death and cell cycle inhibition[161]. This is due to the metabolic inactivity of the cells that experience growth inhibition. Furthermore, if specific aspects of the cellular metabolism are altered the MTS assay will also provide unreliable measurements[162]. Nonetheless, for the particular conditions studied in these series of experiments, the selected A549 cells were not expected to be dysregulated at the metabolic level or present any form of cycle inhibition. Hence, the MTS assay still assured a high reliability for the accomplishment of these projects' aims.

Of note, there are several types of cell death, usually characterised by morphological criteria such as cell fragmentation, phagocytosis by neighbouring cells or loss of plasma membrane integrity[163, 164]. Notably, previous studies have reflected the potential use of poly(I:C) in the treatment of cancer, as it induces TLR3-mediated cell apoptosis. Specifically, upon TLR3 activation mediated by poly(I:C), caspase 8 is recruited to the TLR3 receptor via receptor-interacting protein 1 (RIP-1) undergoing autocatalytic activation, which results in apoptosis-induced cell death in cancerous cells, including lung cancer cells such as A549[165-167]. This is relevant to understanding the cell death mechanisms that the treated A549 cells initiate and how they affect the experimental setup. However, even for high doses of poly(I:C) alone (which stimulates TLR3) in our experiments, we did not observe increased cell death in A549 cells (**Figs 4.1**). Remarkably, transfected poly(I:C) has also proven to trigger apoptosis-induced cell death through the activation of MDA5 in cancer cells, releasing type I IFNs and IL-6 in the process[167-169]. Therefore, we assume that the main type of cell death that we observed from poly(I:C) transfection in our A549 cell cultures is apoptosis. Since transfection reagent RNAiMAX alone did not induce increased cell death even in the highest concentration, it might be further assumed that the cell death is caused by the RIG-I/MDA5 activation from cytosolic poly(I:C). Nevertheless, further studies

should be conducted to verify the type of cell death in our experiments and if it is a direct consequence of the activation of the RIG-I/MDA5 pathway.

5.3 Comparison of RIG-I/MDA5 stimulation in wild-type and ORF3a expressing A549 cells.

Following the evidence presented by the first results from the preliminary experiments, we decided to lower the range concentrations of poly(I:C) treatment to verify whether a higher cytokine response to RIG-I/MDA5 stimulation and cell viability could be achieved. Furthermore, we included A549 ORF3a-transduced cells in the experimental setup in order to better optimise the timepoints, treatment concentration and viability in our methods. Only one to two sets of experiments comparing A549 WT to A549 ORF3a innate immune responses were conducted since the optimised protocols were soon extended to the rest of the modified A549 cell lines. The new range of concentrations visibly showed to stimulate IL-6 production more efficiently in A549 wild-type cells and to a lesser extent A549 ORF3a-transduced cells, as detected in cell supernatants (**Figure 10**). This could be an insight into the immunomodulatory effects of the ORF3a SARS-CoV-2 protein, which could interfere with the cell's cytokine-production machinery to allow the virus replication in the cell to remain unnoticed by the immune system, contributing to the spread of the SARS-CoV-2 infection in the organism. In detail, ORF3a would exert its antagonizing effects on the cell's antiviral and anti-inflammatory responses by diminishing pro-inflammatory cytokine production through the downregulation of the NF-κB pathway[137], which is responsible for the induction of IL-6 expression. Interestingly, a study by Yajuan Rui et al. has revealed that there is a possible connection between ORF3a and the NF-κB pathway via STING, an ER-associated cytosolic signalling molecule that senses microbial cyclic dinucleotides or aberrant DNA species and induces the expression of pro-inflammatory cytokines and type I IFNs[170, 171]. Specifically, ORF3a interacts with STING blocking the induction of the NF-κB pathway mediated by this cytosolic sensor[171]. In this manner, the activation of the host cell's innate immune system would become impaired. Notwithstanding, other authors have argued that SARS-CoV-2 ORF3a would contribute to the activation of NF-κB, given that its relative SARS-CoV ORF3a has previously been found to induce the expression of IL-8 and

pro-IL-1β through NF-κB stimulation[9]. Nevertheless, a general consensus is yet to be reached by the scientific community on these immunomodulatory actions of ORF3a.

In addition, stimulation with poly(I:C) alone as an experimental control showed no major visible IL-6 secretion, indicating that the RIG-I/MDA5 axis is the signalling pathway responsible for cytokine secretion in our setup and not other PRRs like TLR3, as other groups have also shown[49, 172, 173]. Nonetheless, this treatment with pure poly(I:C) could in theory be endocytosed and stimulate endosomal TLR3. Additionally, analysis of *IL-6* relative expression by RT-qPCR confirmed the results obtained in the ELISA of IL-6 secretion levels. On the other hand, *IFNL1* and *IFNL3* (IL-29 and IL-28β, respectively) mRNA expression also reflected an increase in the transcription of both these IFNs with higher doses of treatment until reaching 1 μg/ml of transfected poly(I:C), concentration after which the transcription levels dropped, most likely due to excessive cell death. Remarkably, these RT-qPCR results reflect how the host cell responds to the infection by upregulating the production of pro-inflammatory cytokines and type III IFN mRNAs. However, this effect is not followed by a corresponding increase in the secretion of these cytokines, suggesting that ORF3a might interfere in the translation of these transcripts rather than in the signalling from the RIG-I/MDA5 axis. Because these results were only from one experiment that was intended to test assay conditions, we wanted to look further into this effect in experiments including all A549 cell lines. Regarding cell viability assessment, both LDH and MTS assays showed higher cell death as the concentration of transfected poly(I:C) used in stimulation increased (**Supplementary Figure 1 and Figure 9**), being the amount of LDH released coherent with the percentage of cell viability calculated in the MTS assay, pointing to the reliability of both assays. Taken together, these results allowed us to establish a more restricted and effective range of poly(I:C) concentrations to be transfected in the final version of our experimental setup. Moreover, it hinted at the immunomodulatory effects of ORF3a and its importance for successful SARS-CoV-2 infection and dissemination.

5.4 Effect of SARS-CoV-2 ORF3a, ORF6 and ORF9b in the production of cytokines and type III IFNs

After having explored, narrowed down and decided the optimal range of concentrations in the aforementioned preliminary RIG-I/MDA5 stimulation assays, we decided to scale up the experimental setup to include the remaining ORF6 and ORF9b-transduced A549 cell lines. This made it possible to compare all three SARS-CoV-2 protein expressing cell lines at once with the intention of unveiling similar or opposite effects of the viral proteins of interest in the context of SARS-CoV-2 infection in the lungs. These tailored concentrations promised a maximal response to transfected poly(I:C) treatment while keeping a considerably high percentage of cell viability in all sets of experiments.

Overall, we did not observe statistically significant differences in the secretion of IL-6 in the cell supernatants of any of the tested cell lines, neither at 24 hours nor at 48 hours. This is due to the high variations in the absorbance measurements at both timepoints, even though some trend can be perceived (**Figure 13**). In contrast, *IL-6* mRNA expression in all the ORF-expressing cell lines, especially A549 ORF3a, was significantly higher than in A549 WT cells, hinting at the pro-inflammatory immunomodulatory effects of these SARS-CoV-2 proteins. On the other hand, IL-8 secretion significantly increased in ORF3a and ORF6-expressing A549 cell lines 24 after stimulation with 0.25 µg/ml poly(I:C) + RNAiMAX, indicating the impact of these SARS-CoV-2 proteins on the pro-inflammatory response (**Figure 17A, B, C**). It has been demonstrated that SARS-CoV-2 infection of lung epithelial cells prompts high IL-6 and IL-8 production[49, 69]. Likewise, severe COVID-19 patients presented elevated concentrations of IL-6 and IL-8 in their serum samples[18, 19]. These findings are partially coherent with our results for *IL-6* transcripts levels and IL-8 protein levels in poly(I:C)-transfected A549 cells. The fluctuations we observed reflect the ability of ORF proteins to interfere with NF-κB-mediated inflammatory cytokine pathways[39, 54, 57, 58]. Looking at our ELISA and RT-qPCR results combined, we can identify ORF3a and ORF6 as the most prominent candidates in the set of SARS-CoV-2 proteins tested to significantly interfere with the NF-κB pathway. Interestingly, we noticed a similar pattern in the immunomodulation of IL-6 and IL-8 secretion in the different cell lines. The secretion of both these cytokines was visibly lower in cell lines A549 ORF3a and ORF6 in comparison with the A549 wild-type cell line, whereas in the

A549 ORF9b cell line secretion was visibly higher (**Figure 13B and 17E**). Notwithstanding, it must be pointed out that the analysis of IL-8 secretion in the absence of doxycycline exhibited statistically significant differences between the ORF-transduced A549 cell lines and the wild-type cell line, proving that there might be pre-existent differences between the cell lines even if they are not expressing the SARS-CoV-2 proteins of interest. Therefore, this condition brings a certain inconclusiveness to our results obtained in ORF-expressing A549 cells and they need to be interpreted with caution.

Notably, although visibly upregulated, the secretion of IFN-λ1/3 at 24 hours did not exhibit significantly higher levels of IFNs, as presented in **Figure 15**. These results were in accordance with the IFN-λ1 and IFN-λ3 expression levels revealed by RT-qPCR, where there were also no statistically significant differences with the exception of A549 ORF6, which showed a statistically significant downregulation of IFN-λ3 mRNA in comparison to the wild-type cell line. These observations might be caused by the variability between these ELISAs, as they were performed on three sets of independent stimulation experiments in which cell health and density measures might fluctuate hiding actual differences between the studied groups. Several in vivo and in vitro studies on SARS-CoV-2 infection, as well as numerous clinical observations of COVID-19 patients have also described a lack of antiviral IFN production[24, 25, 72, 99]. Interestingly, it has previously been demonstrated that only the nuclear translocation of IRF3 and not NF-κB is affected in the context of SARS-CoV-2 infection[69], which implies that the immunomodulatory functions of SARS-CoV-2 proteins would be primarily oriented towards the hampering of the host cell IFN response (e.g. IFN-λ1/3) and not the production of pro-inflammatory cytokines and chemokines (e.g. IL-6, IL-8). A plausible explanation for this is that type III IFNs are primarily regulated via IRFs while IL-6 is regulated by NF-κB. ORF3a, ORF6 and ORF9b could then exert most of their immunomodulatory effects by obstructing IRF-mediated and not NF-κB-mediated gene expression. Additionally, other studies have suggested that SARS-CoV-2 proteins participate in the maintenance of a precise balance between pro-inflammatory and anti-inflammatory states in the infected host cell that guarantees viral replication and assembly followed by virion spread, as it has been observed for asymptomatic COVID-19 cases[174]. Nonetheless, all the findings reported up to date on the production of type I and type III IFNs in SARS-CoV-2-infected cells are rather

contradicting. Many of the discrepancies observed are due to the cell model employed in the studies. For instance, HEK293T cells transiently transfected with ORF3a, ORF6 and ORF9b exhibited a suppressed type I IFN response,[24, 25, 137], whereas type I and type III IFNs proved to be upregulated in primary human air-liquid airway epithelial cells (HAECs), hACE2-expressing A549 and Calu-3 infected with SARS-CoV-2. However, these IFN responses were not able to restrict viral replication in these lung epithelial cell models[49, 51, 132]. Another important remark to bear in mind when studying the effects of individual SARS-CoV-2 proteins on lung epithelial cells as opposed to the host cell response to infection with the whole SARS-CoV-2 virus is that the actions of these proteins might be synergistic, producing completely different effects on type III IFN antagonism when they are combined in a real in vivo SARS-CoV-2 infection. Taken together, these observations could explain why our experiments cannot reflect a statistically significant type III IFN upregulation. Nonetheless, further experiments will be necessary to verify whether the type III IFN expression in each A549 modified cell lines yields statistically significant differences, as opposed to the current results. The main factor to be changed in future ELISA experiments in order to reduce the variability observed in our measurements would consist in being more precise in the collection of supernatants at the exact timepoint studied. In this round of experiments, the supernatants were often collected with approximately 1 hour difference from the 24-hour timepoint, which could have influenced the levels of the analysed cytokines present in the cell supernatants contributing to the increase in variations in the absorbance measurements. Additional timepoints (6, 12, 18 and/or 30 hours) could also be explored in these experiments to evaluate if they provide more reliable results.

With regard to the cell viability measured in this more complex experimental setup, we verified once more a statistically significant increase in cell death as concentrations of transfected poly(I:C) augmented (**Figure 12**), which stressed the relevance of choosing the right concentrations of treatment in stimulation experiments of this kind. This tendency in cell viability was consistent with the *IL-6*, *IFNL1* and *IFNL3* relative expression levels measured by qPCR, which only showed a significant increase at 0.5 µg/ml and not at the highest concentration of transfected poly(I:C) (**Figure 14 and 16**), at which cell death is so elevated that

it compromises the production of the transcripts for these cytokines in the cell culture.

Last, we conducted a final series of experiments to verify the correct expression of SARS-CoV-2 viral proteins upon doxycycline induction as well as the cytokine expression and antiviral IFN response in the absence of doxycycline treatment, when the SARS-CoV-2 proteins of interest are not expressed in the ORF-transduced cell lines. The WB results revealed a substantially differential expression between ORF3a, ORF6 and ORF9b, being ORF6 the least abundant SARS-CoV-2 protein in the analysed samples. These discrepancies in the quantity of each SARS-CoV-2 protein studied should be considered as an important factor in the analysis of our results, as the different levels of the SARS-CoV-2 proteins of interest could mean that the most expressed may apparently have more immunomodulatory effects than the others. Concomitantly, a reduction in the levels of SARS-CoV-2 proteins was observed in accordance with the concentration of poly(I:C) transfected into the samples (**Figure 8**). This effect cannot be explained by the increase in cell death for higher concentrations of transfected poly(I:C) observed in the previous MTS assays because the intensity of the GAPDH control bands remains relatively constant across treatments and does not seem to correlate at all with the decrease in the ORF proteins expression. The interference of poly(I:C) with the production of ORF proteins could happen either at the transcriptional, post-transcriptional or post-translational level by the interference of poly(I:C) with either one of their respective cell machineries.

6. Conclusion and Future Perspectives

Although an incredible amount of literature on the pathology of COVID-19 has been published over the past two years, we only have a limited understanding of the host innate immune responses against SARS-CoV-2 infection and the immune evasive mechanisms of this virus. It is of utmost importance to fill the knowledge gaps that currently exist in order to elucidate alternative viral treatments that could be more efficient and accepted by the population. The main research conducted on this field has been focused on type I IFN responses in cell models that are not able to mimic lung epithelial cells response to SARS-CoV-2 infection correctly. Thus, the conclusions reached in these studies should be confirmed or improved in better model systems and by addressing relevant cytokines such as type III IFNs.

This project is centred on studying the interactions between SARS-CoV-2 proteins ORF3a, ORF6 and ORF9b with the host immune responses. In particular, we explored the immunomodulatory effects of these individual SARS-CoV-2 proteins on type III IFN, chemokine and pro-inflammatory cytokine responses upon RIG-I/MDA5 induction. One of the main conditions observed in severe cases of COVID-19 is the cytokine release syndrome, where chemokines, type I IFNs and pro-inflammatory cytokines (IL-1β, IL-6, IL-8, and TNF) are hyper-produced on response to NF-κB activation mediated by SARS-CoV-2[175]. Our results were not in accordance with these observations, since overall ORF3a, ORF6 and ORF9b did not significantly modulate protein production of IL-6 and IL-8, even though these proteins induced on the transcriptional level, showing statistically significant differences between the cell lines. Importantly, the lack of IFN-λ1 and IFN-λ3 responses could hint at a possible inhibition of type III IFNs by ORF3a, ORF6 and ORF9b. These results would be in agreement with previous studies that demonstrate that IRF3 translocation is hampered by ORF6 and IRF3 activation is blocked by ORF9b. Interestingly, some groups have proposed the use of IFNs early in the course of SARS-CoV-2 infection to promote an overall antiviral state and prevent clinical severity.

There are several ways in which this line of research could continue in order to fully elucidate the mechanisms by which these and other SARS-CoV-2 proteins interfere with the innate immune host response to COVID-19. First of all, obtaining

more independent experiments would provide a more accurate picture of the statistical significance of some of the cytokines analysed in this project, in particular IL-6 and IL-8. Although most of the experiments were repeated three times, this was not enough to establish statistically significant differences. In addition, further experiments including other members of the type III IFN family such as IFN-λ2 as well as other predominant cytokines in COVID-19 clinical cases (e.g. IL-10, IL-12, IL-17α and IL-18) could aid in the characterisation of the cytokine response to the three SARS-CoV-2 proteins of interest. This could be done by RT-qPCR, ELISA or even multiplex ELISA. This latter option was omitted for this project for being too expensive and for focusing on the major cytokines induced by the RIG-I/MDA5, NF-κB and IRF pathways that are important in the pathology COVID-19. However, multiplex ELISA might be tried in future studies since we did not see remarkable differences for the selected cytokines. Additionally, the study of the immunomodulatory effects of ORF3a, ORF6 and ORF9b on other membrane, endosomes and cytosolic PRRs (e.g. TLRs, RLRs, cGAS-STING) could also be addressed in future studies. On the other hand, the study of alternative SARS-CoV-2 proteins like NSP13 and NSP15, which have been proposed as possible contributors to the immunomodulatory effects of SARS-CoV-2 might reveal novel interactions between the virus and the host cell's immune mechanisms. All these viral-host protein complexes could be explored in depth by knock-out studies as well as mass spectrometry techniques after immunoprecipitation, where the Strep-II tags attached to the SARS-CoV-2 proteins of interest would allow to separate and purify these complexes from the rest of the cellular components. Most importantly, examining the immune response to SARS-CoV-2 infection in different cell lines and how the cellular crosstalk between these is affected would provide a broader perspective on SARS-CoV-2 immune evasive strategies. In late stage severe COVID, production of inflammatory cytokines from other cell types like innate immune cells may be more important than that from epithelial cells. Not much is known about macrophages and dendritic cells as well as how SARS-CoV-2 proteins modulate cytokine responses in these cells. Thus, more detailed studies should be conducted in these cell lines. For instance, it has been discovered that type III IFN receptor IFNLR1 is expressed in alveolar macrophages, making them an attractive cell type for this purpose. In addition, co-cultures of type I and type II alveolar epithelial cells might constitute a better alternative to single-cell cultures to study this crosstalk between SARS-CoV-2-infected lung cells.

Furthermore, primary lung epithelial cells derived from induced pluripotent stem cells (iPSCs) promise to be the most adequate cell model to mimic the immunopathology of COVID-19 in lung epithelial cells. Most of the arguments for this claim are based on the phenotype of iPSC-derived lung epithelial cells, which shares a higher degree of similarities to that of actual lung epithelial cells than cancer cell lines and do not contain tumour-associated mutations. Importantly, the results obtained might also be affected due to the fact that some of the SARS-CoV-2 proteins of interest such as ORF6 were not expressed at satisfactory levels and protein expression decreased with increasing concentrations of poly(I:C) treatment (as shown in **Figure 8**; WB). This unexpected behaviour should be investigated in future experiments and the creation of newer cell lines such as iPSC-derived lung epithelial cells transduced with the same pLVX-TetOne-Puro plasmids coding for these and others SARS-CoV-2 proteins is being currently considered by our group. Last, lung organoids could also be developed from iPSCs to create a more complex experiment set up and obtain a holistic view on the immune mechanisms that characterise SARS-CoV-2 infection in the lung.

Overall, these studies will be expected to contribute to the devise of more efficient antiviral treatments that could resolve COVID-19 in alternative ways, especially in severe cases. These new therapeutic strategies are of great need, given the fact that a segment of the population still remains unvaccinated and that immune-evasive variants are a constant threat to the achievement of herd immunity. Furthermore, we should rely not only on preventive measures against COVID-19, but also on treatments that could improve the outcome of severe cases and lower their risk of mortality. Only this will release the pressure that our society has been under for the last two years.

References

1. Wong, L.-Y. R.; Perlman, S., Immune dysregulation and immunopathology induced by SARS-CoV-2 and related coronaviruses—are we our own worst enemy? *Nature Reviews Immunology* 2022, *22* (1), 47-56.
2. Siu, K. L.; Yuen, K. S.; Castano-Rodriguez, C.; Ye, Z. W.; Yeung, M. L.; Fung, S. Y.; Yuan, S.; Chan, C. P.; Yuen, K. Y.; Enjuanes, L., Severe acute respiratory syndrome Coronavirus ORF3a protein activates the NLRP3 inflammasome by promoting TRAF3-dependent ubiquitination of ASC. *The FASEB Journal* 2019, *33* (8), 8865-8877.
3. Chan, J. F.; Lau, S. K.; To, K. K.; Cheng, V. C.; Woo, P. C.; Yuen, K.-Y., Middle East respiratory syndrome coronavirus: another zoonotic betacoronavirus causing SARS-like disease. *Clin. Microbiol. Rev.* 2015, *28* (2), 465-522.
4. V'kovski, P.; Kratzel, A.; Steiner, S.; Stalder, H.; Thiel, V., Coronavirus biology and replication: implications for SARS-CoV-2. *Nature Reviews Microbiology* 2021, *19* (3), 155-170.
5. Tang, B. S.; Chan, K.-h.; Cheng, V. C.; Woo, P. C.; Lau, S. K.; Lam, C. C.; Chan, T.-l.; Wu, A. K.; Hung, I. F.; Leung, S.-y., Comparative host gene transcription by microarray analysis early after infection of the Huh7 cell line by severe acute respiratory syndrome coronavirus and human coronavirus 229E. *J. Virol.* 2005, *79* (10), 6180-6193.
6. Zhang, A.-R.; Shi, W.-Q.; Liu, K.; Li, X.-L.; Liu, M.-J.; Zhang, W.-H.; Zhao, G.-P.; Chen, J.-J.; Zhang, X.-A.; Miao, D., Epidemiology and evolution of Middle East respiratory syndrome coronavirus, 2012-2020. *Infectious diseases of poverty* 2021, *10* (03), 1-13.
7. WorldHealthOrganization WHO Coronavirus Disease (COVID-19) Dashboard.
8. Vora, S. M.; Lieberman, J.; Wu, H., Inflammasome activation at the crux of severe COVID-19. *Nature Reviews Immunology* 2021, *21* (11), 694-703.
9. Su, C.-M.; Wang, L.; Yoo, D., Activation of NF-κB and induction of proinflammatory cytokine expressions mediated by ORF7a protein of SARS-CoV-2. *Sci. Rep.* 2021, *11* (1), 1-12.
10. Nishiga, M.; Wang, D. W.; Han, Y.; Lewis, D. B.; Wu, J. C., COVID-19 and cardiovascular disease: from basic mechanisms to clinical perspectives. *Nature Reviews Cardiology* 2020, *17* (9), 543-558.
11. Tadic, M.; Cuspidi, C.; Mancia, G.; Dell'Oro, R.; Grassi, G., COVID-19, hypertension and cardiovascular diseases: Should we change the therapy? *Pharmacol. Res.* 2020, *158*, 104906.
12. Han, H. J.; Nwagwu, C.; Anyim, O.; Ekweremadu, C.; Kim, S., COVID-19 and cancer: From basic mechanisms to vaccine development using nanotechnology. *Int. Immunopharmacol.* 2021, *90*, 107247.
13. Yong, S. J., Long COVID or post-COVID-19 syndrome: putative pathophysiology, risk factors, and treatments. *Infect. Dis.* 2021, *53* (10), 737-754.
14. Matthay, M. A.; Zemans, R. L.; Zimmerman, G. A.; Arabi, Y. M.; Beitler, J. R.; Mercat, A.; Herridge, M.; Randolph, A. G.; Calfee, C. S., Acute respiratory distress syndrome. *Nature reviews Disease primers* 2019, *5* (1), 1-22.
15. Petrilli, C. M.; Jones, S. A.; Yang, J.; Rajagopalan, H.; O'Donnell, L.; Chernyak, Y.; Tobin, K. A.; Cerfolio, R. J.; Francois, F.; Horwitz, L. I., Factors associated with hospital admission and critical illness among 5279 people with coronavirus disease 2019 in New York City: prospective cohort study. *BMJ* 2020, *369*.
16. Al-Samkari, H.; Karp Leaf, R. S.; Dzik, W. H.; Carlson, J. C.; Fogerty, A. E.; Waheed, A.; Goodarzi, K.; Bendapudi, P. K.; Bornikova, L.; Gupta, S., COVID-19 and coagulation: bleeding and thrombotic manifestations of SARS-CoV-2 infection. *Blood* 2020, *136* (4), 489-500.

17. Berlin, D. A.; Gulick, R. M.; Martinez, F. J., Severe covid-19. *N. Engl. J. Med.* 2020, *383* (25), 2451-2460.
18. Huang, C.; Wang, Y.; Li, X.; Ren, L.; Zhao, J.; Hu, Y.; Zhang, L.; Fan, G.; Xu, J.; Gu, X., Clinical features of patients infected with 2019 novel coronavirus in Wuhan, China. *The lancet* 2020, *395* (10223), 497-506.
19. Blanco-Melo, D.; Nilsson-Payant, B. E.; Liu, W.-C.; Uhl, S.; Hoagland, D.; Møller, R.; Jordan, T. X.; Oishi, K.; Panis, M.; Sachs, D., Imbalanced host response to SARS-CoV-2 drives development of COVID-19. *Cell* 2020, *181* (5), 1036-1045. e9.
20. Giamarellos-Bourboulis, E. J.; Netea, M. G.; Rovina, N.; Akinosoglou, K.; Antoniadou, A.; Antonakos, N.; Damoraki, G.; Gkavogianni, T.; Adami, M.-E.; Katsaounou, P., Complex immune dysregulation in COVID-19 patients with severe respiratory failure. *Cell Host Microbe* 2020, *27* (6), 992-1000. e3.
21. Junqueira, C.; Crespo, Â.; Ranjbar, S.; Lewandrowski, M.; Ingber, J.; de Lacerda, L. B.; Parry, B.; Ravid, S.; Clark, S.; Ho, F., SARS-CoV-2 infects blood monocytes to activate NLRP3 and AIM2 inflammasomes, pyroptosis and cytokine release. *Research square* 2021.
22. Skowronski, D. M.; Astell, C.; Brunham, R. C.; Low, D. E.; Petric, M.; Roper, R. L.; Talbot, P. J.; Tam, T.; Babiuk, L., Severe acute respiratory syndrome (SARS): a year in review. *Annu. Rev. Med.* 2005, *56*, 357-381.
23. Harrison, A. G.; Lin, T.; Wang, P., Mechanisms of SARS-CoV-2 transmission and pathogenesis. *Trends Immunol.* 2020, *41* (12), 1100-1115.
24. Lei, X.; Dong, X.; Ma, R.; Wang, W.; Xiao, X.; Tian, Z.; Wang, C.; Wang, Y.; Li, L.; Ren, L., Activation and evasion of type I interferon responses by SARS-CoV-2. *Nature communications* 2020, *11* (1), 1-12.
25. Xia, H.; Cao, Z.; Xie, X.; Zhang, X.; Chen, J. Y.-C.; Wang, H.; Menachery, V. D.; Rajsbaum, R.; Shi, P.-Y., Evasion of type I interferon by SARS-CoV-2. *Cell Rep.* 2020, *33* (1), 108234.
26. Yuen, C.-K.; Lam, J.-Y.; Wong, W.-M.; Mak, L.-F.; Wang, X.; Chu, H.; Cai, J.-P.; Jin, D.-Y.; To, K. K.-W.; Chan, J. F.-W., SARS-CoV-2 nsp13, nsp14, nsp15 and orf6 function as potent interferon antagonists. *Emerging microbes & infections* 2020, *9* (1), 1418-1428.
27. Cevik, M.; Kuppalli, K.; Kindrachuk, J.; Peiris, M., Virology, transmission, and pathogenesis of SARS-CoV-2. *BMJ* 2020, *371*.
28. Hoffmann, M.; Kleine-Weber, H.; Schroeder, S.; Krüger, N.; Herrler, T.; Erichsen, S.; Schiergens, T. S.; Herrler, G.; Wu, N.-H.; Nitsche, A., SARS-CoV-2 cell entry depends on ACE2 and TMPRSS2 and is blocked by a clinically proven protease inhibitor. *Cell* 2020, *181* (2), 271-280. e8.
29. Mishra, T.; Sreepadmanabh, M.; Ramdas, P.; Sahu, A. K.; Kumar, A.; Chande, A., SARS CoV-2 nucleoprotein enhances the infectivity of lentiviral spike particles. *Frontiers in cellular and infection microbiology* 2021, *11*.
30. Trougakos, I. P.; Stamatelopoulos, K.; Terpos, E.; Tsitsilonis, O. E.; Aivalioti, E.; Paraskevis, D.; Kastritis, E.; Pavlakis, G. N.; Dimopoulos, M. A., Insights to SARS-CoV-2 life cycle, pathophysiology, and rationalized treatments that target COVID-19 clinical complications. *J. Biomed. Sci.* 2021, *28* (1), 1-18.
31. Poduri, R.; Joshi, G.; Jagadeesh, G., Drugs targeting various stages of the SARS-CoV-2 life cycle: Exploring promising drugs for the treatment of Covid-19. *Cell. Signal.* 2020, *74*, 109721.

32. Vabret, N.; Britton, G. J.; Gruber, C.; Hegde, S.; Kim, J.; Kuksin, M.; Levantovsky, R.; Malle, L.; Moreira, A.; Park, M. D., Immunology of COVID-19: current state of the science. *Immunity* 2020, *52* (6), 910-941.
33. Ziegler, C. G.; Allon, S. J.; Nyquist, S. K.; Mbano, I. M.; Miao, V. N.; Tzouanas, C. N.; Cao, Y.; Yousif, A. S.; Bals, J.; Hauser, B. M., SARS-CoV-2 receptor ACE2 is an interferon-stimulated gene in human airway epithelial cells and is detected in specific cell subsets across tissues. *Cell* 2020, *181* (5), 1016-1035. e19.
34. Ju, X.; Zhu, Y.; Wang, Y.; Li, J.; Zhang, J.; Gong, M.; Ren, W.; Li, S.; Zhong, J.; Zhang, L., A novel cell culture system modeling the SARS-CoV-2 life cycle. *PLoS Pathog.* 2021, *17* (3), e1009439.
35. Cortese, M.; Lee, J.-Y.; Cerikan, B.; Neufeldt, C. J.; Oorschot, V. M.; Köhrer, S.; Hennies, J.; Schieber, N. L.; Ronchi, P.; Mizzon, G., Integrative imaging reveals SARS-CoV-2-induced reshaping of subcellular morphologies. *Cell Host Microbe* 2020, *28* (6), 853-866. e5.
36. Letko, M.; Marzi, A.; Munster, V., Functional assessment of cell entry and receptor usage for SARS-CoV-2 and other lineage B betacoronaviruses. *Nature microbiology* 2020, *5* (4), 562-569.
37. Shah, V. K.; Firmal, P.; Alam, A.; Ganguly, D.; Chattopadhyay, S., Overview of Immune Response During SARS-CoV-2 Infection: Lessons From the Past. *Front. Immunol.* 2020, *11*.
38. Akira, S.; Uematsu, S.; Takeuchi, O., Pathogen recognition and innate immunity. *Cell* 2006, *124* (4), 783-801.
39. Alexopoulou, L.; Holt, A. C.; Medzhitov, R.; Flavell, R. A., Recognition of double-stranded RNA and activation of NF-κB by Toll-like receptor 3. *Nature* 2001, *413* (6857), 732-738.
40. Schoggins, J. W.; Rice, C. M., Interferon-stimulated genes and their antiviral effector functions. *Curr. Opin. Virol.* 2011, *1* (6), 519-525.
41. Totura, A. L.; Whitmore, A.; Agnihothram, S.; Schäfer, A.; Katze, M. G.; Heise, M. T.; Baric, R. S., Toll-like receptor 3 signaling via TRIF contributes to a protective innate immune response to severe acute respiratory syndrome coronavirus infection. *MBio* 2015, *6* (3), e00638-15.
42. Mazaleuskaya, L.; Veltrop, R.; Ikpeze, N.; Martin-Garcia, J.; Navas-Martin, S., Protective role of Toll-like receptor 3-induced type I interferon in murine coronavirus infection of macrophages. *Viruses* 2012, *4* (5), 901-923.
43. Akira, S.; Hoshino, K., Myeloid differentiation factor 88—dependent and—independent pathways in toll-like receptor signaling. *The Journal of infectious diseases* 2003, *187* (Supplement_2), S356-63.
44. Fitzgerald, K. A.; McWhirter, S. M.; Faia, K. L.; Rowe, D. C.; Latz, E.; Golenbock, D. T.; Coyle, A. J.; Liao, S.-M.; Maniatis, T., IKKε and TBK1 are essential components of the IRF3 signaling pathway. *Nat. Immunol.* 2003, *4* (5), 491-496.
45. Zheng, M.; Karki, R.; Williams, E. P.; Yang, D.; Fitzpatrick, E.; Vogel, P.; Jonsson, C. B.; Kanneganti, T.-D., TLR2 senses the SARS-CoV-2 envelope protein to produce inflammatory cytokines. *Nat. Immunol.* 2021, *22* (7), 829-838.
46. Rehwinkel, J.; Gack, M. U., RIG-I-like receptors: their regulation and roles in RNA sensing. *Nature Reviews Immunology* 2020, *20* (9), 537-551.
47. Liwinski, T.; Zheng, D.; Elinav, E., The microbiome and cytosolic innate immune receptors. *Immunol. Rev.* 2020, *297* (1), 207-224.
48. Bruns, A. M.; Horvath, C. M., Antiviral RNA recognition and assembly by RLR family innate immune sensors. *Cytokine Growth Factor Rev.* 2014, *25* (5), 507-512.

49. Thorne, L. G.; Reuschl, A. K.; Zuliani-Alvarez, L.; Whelan, M. V.; Turner, J.; Noursadeghi, M.; Jolly, C.; Towers, G. J., SARS-CoV-2 sensing by RIG-I and MDA5 links epithelial infection to macrophage inflammation. *The EMBO journal* 2021, *40* (15), e107826.
50. Li, Y.; Renner, D. M.; Comar, C. E.; Whelan, J. N.; Reyes, H. M.; Cardenas-Diaz, F. L.; Truitt, R.; Tan, L. H.; Dong, B.; Alysandratos, K. D., SARS-CoV-2 induces double-stranded RNA-mediated innate immune responses in respiratory epithelial-derived cells and cardiomyocytes. *Proceedings of the National Academy of Sciences* 2021, *118* (16).
51. Rebendenne, A.; Chaves Valadão, A. L.; Tauziet, M.; Maarifi, G.; Bonaventure, B.; McKellar, J.; Planès, R.; Nisole, S.; Arnaud-Arnould, M.; Moncorgé, O., SARS-CoV-2 triggers an MDA-5-dependent interferon response which is unable to control replication in lung epithelial cells. *J. Virol.* 2021, *95* (8), e02415-20.
52. Zalinger, Z. B.; Elliott, R.; Rose, K. M.; Weiss, S. R., MDA5 is critical to host defense during infection with murine coronavirus. *J. Virol.* 2015, *89* (24), 12330-12340.
53. Hausmann, S.; Marq, J.-B.; Tapparel, C.; Kolakofsky, D.; Garcin, D., RIG-I and dsRNA-induced IFNβ activation. *PLoS One* 2008, *3* (12), e3965.
54. Seth, R. B.; Sun, L.; Ea, C.-K.; Chen, Z. J., Identification and characterization of MAVS, a mitochondrial antiviral signaling protein that activates NF-κB and IRF3. *Cell* 2005, *122* (5), 669-682.
55. Kawai, T.; Takahashi, K.; Sato, S.; Coban, C.; Kumar, H.; Kato, H.; Ishii, K. J.; Takeuchi, O.; Akira, S., IPS-1, an adaptor triggering RIG-I-and Mda5-mediated type I interferon induction. *Nat. Immunol.* 2005, *6* (10), 981-988.
56. Strähle, L.; Marq, J.-B.; Brini, A.; Hausmann, S.; Kolakofsky, D.; Garcin, D., Activation of the Beta Interferon Promoter by Unnatural Sendai Virus Infection Requires RIG-I and Is Inhibited by Viral C Proteins. *J. Virol.* 2007, *81* (22), 12227-12237.
57. Goubau, D.; Deddouche, S.; e Sousa, C. R., Cytosolic sensing of viruses. *Immunity* 2013, *38* (5), 855-869.
58. Fitzgerald, K. A.; Kagan, J. C., Toll-like Receptors and the Control of Immunity. *Cell* 2020, *180* (6), 1044-1066.
59. Chu, Q.; Gao, Y.; Xu, G.; Wu, C.; Xu, T., Transcriptome comparative analysis revealed poly (I: C) activated RIG-I/MDA5-mediated signaling pathway in miiuy croaker. *Fish Shellfish Immunol.* 2015, *47* (1), 168-174.
60. Wörnle, M.; Sauter, M.; Kastenmüller, K.; Ribeiro, A.; Roeder, M.; Schmid, H.; Krötz, F.; Mussack, T.; Ladurner, R.; Sitter, T., Novel role of toll-like receptor 3, RIG-I and MDA5 in poly (I: C) RNA-induced mesothelial inflammation. *Mol. Cell. Biochem.* 2009, *322* (1), 193-206.
61. Inao, T.; Harashima, N.; Monma, H.; Okano, S.; Itakura, M.; Tanaka, T.; Tajima, Y.; Harada, M., Antitumor effects of cytoplasmic delivery of an innate adjuvant receptor ligand, poly (I: C), on human breast cancer. *Breast Cancer Res. Treat.* 2012, *134* (1), 89-100.
62. Matijević, T.; Pavelić, J., Poly (I: C) treatment influences the expression of calreticulin and profilin-1 in a human HNSCC cell line: a proteomic study. *Tumour Biol.* 2012, *33* (4), 1201-1208.
63. Lu, J.; Zhou, Z.; Sun, B.; Han, B.; Fu, Q.; Han, Y.; Yuan, W.; Xu, Z.; Chen, A., MiR-520d-5p modulates chondrogenesis and chondrocyte metabolism through targeting HDAC1. *Aging* 2020, *12* (18), 18545-18560.
64. Qin, L.; Lin, J.; Xie, X., CircRNA-9119 suppresses poly I: C induced inflammation in Leydig and Sertoli cells via TLR3 and RIG-I signal pathways. *Mol. Med.* 2019, *25* (1), 1-13.

65. Thoma, A.; Lightfoot, A. P., NF-kB and Inflammatory Cytokine Signalling: Role in Skeletal Muscle Atrophy. In *Muscle Atrophy*, Xiao, J., Ed. Springer Singapore: Singapore, 2018; pp 267-279.
66. Kagoya, Y.; Yoshimi, A.; Kataoka, K.; Nakagawa, M.; Kumano, K.; Arai, S.; Kobayashi, H.; Saito, T.; Iwakura, Y.; Kurokawa, M., Positive feedback between NF-κB and TNF-α promotes leukemia-initiating cell capacity. *The Journal of clinical investigation* 2014, *124* (2), 528-542.
67. Rahman, M. M.; McFadden, G., Modulation of NF-κB signalling by microbial pathogens. *Nature reviews. Microbiology* 2011, *9* (4), 291-306.
68. Li, W.; Qiao, J.; You, Q.; Zong, S.; Peng, Q.; Liu, Y.; Hu, S.; Liu, W.; Li, S.; Shu, X., SARS-CoV-2 Nsp5 activates NF-κB pathway by upregulating SUMOylation of MAVS. *Front. Immunol.* 2021, *12*.
69. Neufeldt, C. J.; Cerikan, B.; Cortese, M.; Frankish, J.; Lee, J. Y.; Plociennikowska, A.; Heigwer, F.; Prasad, V.; Joecks, S.; Burkart, S. S.; Zander, D. Y.; Subramanian, B.; Gimi, R.; Padmanabhan, S.; Iyer, R.; Gendarme, M.; El Debs, B.; Halama, N.; Merle, U.; Boutros, M.; Binder, M.; Bartenschlager, R., SARS-CoV-2 infection induces a pro-inflammatory cytokine response through cGAS-STING and NF-κB. *Commun Biol* 2022, *5* (1), 45.
70. Honda, K.; Takaoka, A.; Taniguchi, T., Type I inteferon gene induction by the interferon regulatory factor family of transcription factors. *Immunity* 2006, *25* (3), 349-360.
71. Lucas, C.; Wong, P.; Klein, J.; Castro, T. B.; Silva, J.; Sundaram, M.; Ellingson, M. K.; Mao, T.; Oh, J. E.; Israelow, B., Longitudinal analyses reveal immunological misfiring in severe COVID-19. *Nature* 2020, *584* (7821), 463-469.
72. Hadjadj, J.; Yatim, N.; Barnabei, L.; Corneau, A.; Boussier, J.; Smith, N.; Péré, H.; Charbit, B.; Bondet, V.; Chenevier-Gobeaux, C., Impaired type I interferon activity and inflammatory responses in severe COVID-19 patients. *Science* 2020, *369* (6504), 718-724.
73. Mathew, D.; Giles, J. R.; Baxter, A. E.; Oldridge, D. A.; Greenplate, A. R.; Wu, J. E.; Alanio, C.; Kuri-Cervantes, L.; Pampena, M. B.; D'Andrea, K., Deep immune profiling of COVID-19 patients reveals distinct immunotypes with therapeutic implications. *Science* 2020, *369* (6508), eabc8511.
74. Turner, M. D.; Nedjai, B.; Hurst, T.; Pennington, D. J., Cytokines and chemokines: At the crossroads of cell signalling and inflammatory disease. *Biochimica et Biophysica Acta (BBA)-Molecular Cell Research* 2014, *1843* (11), 2563-2582.
75. Hammond, M.; Lapointe, G. R.; Feucht, P. H.; Hilt, S.; Gallegos, C. A.; Gordon, C. A.; Giedlin, M. A.; Mullenbach, G.; Tekamp-Olson, P., IL-8 induces neutrophil chemotaxis predominantly via type I IL-8 receptors. *The Journal of Immunology* 1995, *155* (3), 1428-1433.
76. Miller, E.; Cohen, A.; Nagao, S.; Griffith, D.; Maunder, R.; Martin, T.; Weiner-Kronish, J.; Sticherling, M.; Christophers, E.; Matthay, M., Elevated levels of NAP-1/interleukin-8 are present in the airspaces of patients with the adult respiratory distress syndrome and are associated with increased mortality. *Am. Rev. Respir. Dis.* 1992, *146* (2), 427-432.
77. Heidemann, J.; Ogawa, H.; Dwinell, M. B.; Rafiee, P.; Maaser, C.; Gockel, H. R.; Otterson, M. F.; Ota, D. M.; Lügering, N.; Domschke, W., Angiogenic effects of interleukin 8 (CXCL8) in human intestinal microvascular endothelial cells are mediated by CXCR2. *J. Biol. Chem.* 2003, *278* (10), 8508-8515.
78. Jucker, M.; Abts, H.; Li, W.; Schindler, R.; Merz, H.; Gunther, A.; Von Kalle, C.; Schaadt, M.; Diamantstein, T.; Feller, A., Expression of interleukin-6 and interleukin-6 receptor in Hodgkin's disease. 1991.

79. Smith, K. A.; Maizels, R. M., IL-6 controls susceptibility to helminth infection by impeding Th2 responsiveness and altering the Treg phenotype in vivo. *Eur. J. Immunol.* 2014, *44* (1), 150-161.
80. Takeda, K.; Kaisho, T.; Yoshida, N.; Takeda, J.; Kishimoto, T.; Akira, S., Stat3 activation is responsible for IL-6-dependent T cell proliferation through preventing apoptosis: generation and characterization of T cell-specific Stat3-deficient mice. *The Journal of Immunology* 1998, *161* (9), 4652-4660.
81. Gauldie, J.; Richards, C.; Northemann, W.; Fey, G.; Baumann, H., IFNβ2/BSF2/IL-6 Is the Monocyte-derived HSF That Regulates Receptor-specific Acute Phase Gene Regulation in Hepatocytes a. *Ann. N. Y. Acad. Sci.* 1989, *557* (1), 46-59.
82. Harrison, D. A., The jak/stat pathway. *Cold Spring Harb. Perspect. Biol.* 2012, *4* (3), a011205.
83. Kishimoto, T., IL-6: from its discovery to clinical applications. *Int. Immunol.* 2010, *22* (5), 347-352.
84. Lazear, H. M.; Schoggins, J. W.; Diamond, M. S., Shared and distinct functions of type I and type III interferons. *Immunity* 2019, *50* (4), 907-923.
85. Dürkoop, M. Studying the immunomodulatory effects of SARS-CoV-2 viral proteins in human lung epithelial cell lines. Norwegian University of Science and Technology, 2021.
86. Okabayashi, T.; Kojima, T.; Masaki, T.; Yokota, S.-i.; Imaizumi, T.; Tsutsumi, H.; Himi, T.; Fujii, N.; Sawada, N., Type-III interferon, not type-I, is the predominant interferon induced by respiratory viruses in nasal epithelial cells. *Virus Res.* 2011, *160* (1), 360-366.
87. Ivashkiv, L. B.; Donlin, L. T., Regulation of type I interferon responses. *Nature Reviews Immunology* 2014, *14* (1), 36-49.
88. Durbin, R. K.; Kotenko, S. V.; Durbin, J. E., Interferon induction and function at the mucosal surface. *Immunol. Rev.* 2013, *255* (1), 25-39.
89. Odendall, C.; Kagan, J. C., The unique regulation and functions of type III interferons in antiviral immunity. *Curr. Opin. Virol.* 2015, *12*, 47-52.
90. Dixit, E.; Boulant, S.; Zhang, Y.; Lee, A. S.; Odendall, C.; Shum, B.; Hacohen, N.; Chen, Z. J.; Whelan, S. P.; Fransen, M., Peroxisomes are signaling platforms for antiviral innate immunity. *Cell* 2010, *141* (4), 668-681.
91. Odendall, C.; Dixit, E.; Stavru, F.; Bierne, H.; Franz, K. M.; Durbin, A. F.; Boulant, S.; Gehrke, L.; Cossart, P.; Kagan, J. C., Diverse intracellular pathogens activate type III interferon expression from peroxisomes. *Nat. Immunol.* 2014, *15* (8), 717-726.
92. Wack, A.; Terczyńska-Dyla, E.; Hartmann, R., Guarding the frontiers: the biology of type III interferons. *Nat. Immunol.* 2015, *16* (8), 802-809.
93. Sheppard, P.; Kindsvogel, W.; Xu, W.; Henderson, K.; Schlutsmeyer, S.; Whitmore, T. E.; Kuestner, R.; Garrigues, U.; Birks, C.; Roraback, J., IL-28, IL-29 and their class II cytokine receptor IL-28R. *Nat. Immunol.* 2003, *4* (1), 63-68.
94. Kotenko, S. V.; Gallagher, G.; Baurin, V. V.; Lewis-Antes, A.; Shen, M.; Shah, N. K.; Langer, J. A.; Sheikh, F.; Dickensheets, H.; Donnelly, R. P., IFN-λs mediate antiviral protection through a distinct class II cytokine receptor complex. *Nat. Immunol.* 2003, *4* (1), 69-77.
95. Qin, C.; Zhou, L.; Hu, Z.; Zhang, S.; Yang, S.; Tao, Y.; Xie, C.; Ma, K.; Shang, K.; Wang, W., Dysregulation of immune response in patients with coronavirus 2019 (COVID-19) in Wuhan, China. *Clin. Infect. Dis.* 2020, *71* (15), 762-768.
96. Suryawanshi, R. K.; Koganti, R.; Agelidis, A.; Patil, C. D.; Shukla, D., Dysregulation of Cell Signaling by SARS-CoV-2. *Trends Microbiol.* 2021, *29* (3), 224-237.

97. Gustine, J. N.; Jones, D., Immunopathology of Hyperinflammation in COVID-19. *The American Journal of Pathology* 2021, *191* (1), 4-17.
98. Reusch, N.; De Domenico, E.; Bonaguro, L.; Schulte-Schrepping, J.; Baßler, K.; Schultze, J. L.; Aschenbrenner, A. C., Neutrophils in COVID-19. *Front. Immunol.* 2021, *12*, 952.
99. Vanderheiden, A.; Ralfs, P.; Chirkova, T.; Upadhyay, A. A.; Zimmerman, M. G.; Bedoya, S.; Aoued, H.; Tharp, G. M.; Pellegrini, K. L.; Manfredi, C., Type I and type III interferons restrict SARS-CoV-2 infection of human airway epithelial cultures. *J. Virol.* 2020, *94* (19), e00985-20.
100. García, L. F., Immune response, inflammation, and the clinical spectrum of COVID-19. *Front. Immunol.* 2020, *11*, 1441.
101. Zhou, F.; Yu, T.; Du, R.; Fan, G.; Liu, Y.; Liu, Z.; Xiang, J.; Wang, Y.; Song, B.; Gu, X., Clinical course and risk factors for mortality of adult inpatients with COVID-19 in Wuhan, China: a retrospective cohort study. *The lancet* 2020, *395* (10229), 1054-1062.
102. Ruan, Q.; Yang, K.; Wang, W.; Jiang, L.; Song, J., Clinical predictors of mortality due to COVID-19 based on an analysis of data of 150 patients from Wuhan, China. *Intensive Care Med.* 2020, *46* (5), 846-848.
103. Merad, M.; Martin, J. C., Pathological inflammation in patients with COVID-19: a key role for monocytes and macrophages. *Nature reviews immunology* 2020, *20* (6), 355-362.
104. Ramlall, V.; Thangaraj, P. M.; Meydan, C.; Foox, J.; Butler, D.; Kim, J.; May, B.; De Freitas, J. K.; Glicksberg, B. S.; Mason, C. E., Immune complement and coagulation dysfunction in adverse outcomes of SARS-CoV-2 infection. *Nat. Med.* 2020, *26* (10), 1609-1615.
105. Bernard, I.; Limonta, D.; Mahal, L. K.; Hobman, T. C., Endothelium infection and dysregulation by SARS-CoV-2: evidence and caveats in COVID-19. *Viruses* 2020, *13* (1), 29.
106. Lee, I.-C.; Huo, T.-I.; Huang, Y.-H., Gastrointestinal and liver manifestations in patients with COVID-19. *J. Chin. Med. Assoc.* 2020.
107. Yachou, Y.; El Idrissi, A.; Belapasov, V.; Ait Benali, S., Neuroinvasion, neurotropic, and neuroinflammatory events of SARS-CoV-2: understanding the neurological manifestations in COVID-19 patients. *Neurol. Sci.* 2020, *41* (10), 2657-2669.
108. Lowery, S. A.; Sariol, A.; Perlman, S., Innate immune and inflammatory responses to SARS-CoV-2: Implications for COVID-19. *Cell Host Microbe* 2021, *29* (7), 1052-1062.
109. Boechat, J. L.; Chora, I.; Morais, A.; Delgado, L., The immune response to SARS-CoV-2 and COVID-19 immunopathology–current perspectives. *Pulmonology* 2021, *27* (5), 423-437.
110. Yoshikawa, T.; Hill, T.; Li, K.; Peters, C. J.; Tseng, C.-T. K., Severe Acute Respiratory Syndrome (SARS) Coronavirus-Induced Lung Epithelial Cytokines Exacerbate SARS Pathogenesis by Modulating Intrinsic Functions of Monocyte-Derived Macrophages and Dendritic Cells. *J. Virol.* 2009, *83* (7), 3039-3048.
111. Mulchandani, R.; Lyngdoh, T.; Kakkar, A. K., Deciphering the COVID-19 cytokine storm: systematic review and meta-analysis. *Eur. J. Clin. Invest.* 2021, *51* (1), e13429.
112. de Wilde, A. H.; Raj, V. S.; Oudshoorn, D.; Bestebroer, T. M.; van Nieuwkoop, S.; Limpens, R. W.; Posthuma, C. C.; van der Meer, Y.; Bárcena, M.; Haagmans, B. L., MERS-coronavirus replication induces severe in vitro cytopathology and is strongly inhibited by cyclosporin A or interferon-α treatment. *The Journal of general virology* 2013, *94* (Pt 8), 1749.
113. Miorin, L.; Kehrer, T.; Sanchez-Aparicio, M. T.; Zhang, K.; Cohen, P.; Patel, R. S.; Cupic, A.; Makio, T.; Mei, M.; Moreno, E., SARS-CoV-2 Orf6 hijacks Nup98 to block STAT nuclear import and antagonize interferon signaling. *Proceedings of the National Academy of Sciences* 2020, *117* (45), 28344-28354.

114. Katsura, H.; Sontake, V.; Tata, A.; Kobayashi, Y.; Edwards, C. E.; Heaton, B. E.; Konkimalla, A.; Asakura, T.; Mikami, Y.; Fritch, E. J., Human lung stem cell-based alveolospheres provide insights into SARS-CoV-2-mediated interferon responses and pneumocyte dysfunction. *Cell stem cell* 2020, *27* (6), 890-904. e8.
115. Lokugamage, K. G.; Hage, A.; de Vries, M.; Valero-Jimenez, A. M.; Schindewolf, C.; Dittmann, M.; Rajsbaum, R.; Menachery, V. D., Type I interferon susceptibility distinguishes SARS-CoV-2 from SARS-CoV. *J. Virol.* 2020, *94* (23), e01410-20.
116. Conti, P.; Caraffa, A.; Gallenga, C.; Ross, R.; Kritas, S.; Frydas, I.; Younes, A.; Ronconi, G., Coronavirus-19 (SARS-CoV-2) induces acute severe lung inflammation via IL-1 causing cytokine storm in COVID-19: a promising inhibitory strategy. *J. Biol. Regul. Homeost. Agents* 2020, *34* (6), 1971-1975.
117. Mason, R. J., Thoughts on the alveolar phase of COVID-19. *American Journal of Physiology-Lung Cellular and Molecular Physiology* 2020, *319* (1), L115-L120.
118. Costela-Ruiz, V. J.; Illescas-Montes, R.; Puerta-Puerta, J. M.; Ruiz, C.; Melguizo-Rodríguez, L., SARS-CoV-2 infection: The role of cytokines in COVID-19 disease. *Cytokine Growth Factor Rev.* 2020, *54*, 62-75.
119. Günther, A.; Ruppert, C.; Schmidt, R.; Markart, P.; Grimminger, F.; Walmrath, D.; Seeger, W., Surfactant alteration and replacement in acute respiratory distress syndrome. *Respir. Res.* 2001, *2* (6), 1-14.
120. Ahn, M.; Anderson, D. E.; Zhang, Q.; Tan, C. W.; Lim, B. L.; Luko, K.; Wen, M.; Chia, W. N.; Mani, S.; Wang, L. C., Dampened NLRP3-mediated inflammation in bats and implications for a special viral reservoir host. *Nature microbiology* 2019, *4* (5), 789-799.
121. Li, H.; Liu, L.; Zhang, D.; Xu, J.; Dai, H.; Tang, N.; Su, X.; Cao, B., SARS-CoV-2 and viral sepsis: observations and hypotheses. *The Lancet* 2020, *395* (10235), 1517-1520.
122. Herold, T.; Jurinovic, V.; Arnreich, C.; Lipworth, B. J.; Hellmuth, J. C.; von Bergwelt-Baildon, M.; Klein, M.; Weinberger, T., Elevated levels of IL-6 and CRP predict the need for mechanical ventilation in COVID-19. *J. Allergy Clin. Immunol.* 2020, *146* (1), 128-136. e4.
123. Domizio, J. D.; Gulen, M. F.; Saidoune, F.; Thacker, V. V.; Yatim, A.; Sharma, K.; Nass, T.; Guenova, E.; Schaller, M.; Conrad, C.; Goepfert, C.; de Leval, L.; Garnier, C. v.; Berezowska, S.; Dubois, A.; Gilliet, M.; Ablasser, A., The cGAS–STING pathway drives type I IFN immunopathology in COVID-19. *Nature* 2022, *603* (7899), 145-151.
124. Galani, I. E.; Triantafyllia, V.; Eleminiadou, E.-E.; Koltsida, O.; Stavropoulos, A.; Manioudaki, M.; Thanos, D.; Doyle, S. E.; Kotenko, S. V.; Thanopoulou, K., Interferon-λ mediates non-redundant front-line antiviral protection against influenza virus infection without compromising host fitness. *Immunity* 2017, *46* (5), 875-890. e6.
125. Alcami, A.; Koszinowski, U. H., Viral mechanisms of immune evasion. *Trends Microbiol.* 2000, *8* (9), 410-418.
126. Manzanares-Meza, L. D.; Medina-Contreras, O., SARS-CoV-2 and influenza: a comparative overview and treatment implications. *Bol. Med. Hosp. Infant. Mex.* 2020, *77*, 262-273.
127. Zhang, S.; Wang, L.; Cheng, G., The battle between host and SARS-CoV-2: Innate immunity and viral evasion strategies. *Mol. Ther.* 2022, *30* (5), 1869-1884.
128. Meyers, J. M.; Ramanathan, M.; Shanderson, R. L.; Beck, A.; Donohue, L.; Ferguson, I.; Guo, M. G.; Rao, D. S.; Miao, W.; Reynolds, D., The proximal proteome of 17 SARS-CoV-2 proteins links to disrupted antiviral signaling and host translation. *PLoS Pathog.* 2021, *17* (10), e1009412.

129. Gordon, D. E.; Hiatt, J.; Bouhaddou, M.; Rezelj, V. V.; Ulferts, S.; Braberg, H.; Jureka, A. S.; Obernier, K.; Guo, J. Z.; Batra, J., Comparative host-coronavirus protein interaction networks reveal pan-viral disease mechanisms. *Science* 2020, *370* (6521), eabe9403.
130. Tay, D. J. W.; Lew, Z. Z. R.; Chu, J. J. H.; Tan, K. S., Uncovering Novel Viral Innate Immune Evasion Strategies: What Has SARS-CoV-2 Taught Us? *Front. Microbiol.* 2022, *13*.
131. Gordon, D. E.; Jang, G. M.; Bouhaddou, M.; Xu, J.; Obernier, K.; White, K. M.; O'Meara, M. J.; Rezelj, V. V.; Guo, J. Z.; Swaney, D. L., A SARS-CoV-2 protein interaction map reveals targets for drug repurposing. *Nature* 2020, *583* (7816), 459-468.
132. Banerjee, A.; El-Sayes, N.; Budylowski, P.; Jacob, R. A.; Richard, D.; Maan, H.; Aguiar, J. A.; Demian, W. L.; Baid, K.; D'Agostino, M. R., Experimental and natural evidence of SARS-CoV-2-infection-induced activation of type I interferon responses. *Iscience* 2021, *24* (5), 102477.
133. Thoms, M.; Buschauer, R.; Ameismeier, M.; Koepke, L.; Denk, T.; Hirschenberger, M.; Kratzat, H.; Hayn, M.; Mackens-Kiani, T.; Cheng, J., Structural basis for translational shutdown and immune evasion by the Nsp1 protein of SARS-CoV-2. *Science* 2020, *369* (6508), 1249-1255.
134. Davalos, D.; Akassoglou, K. In *Fibrinogen as a key regulator of inflammation in disease*, Semin. Immunopathol., Springer: 2012; pp 43-62.
135. Xu, H.; Akinyemi, I. A.; Chitre, S. A.; Loeb, J. C.; Lednicky, J. A.; McIntosh, M. T.; Bhaduri-McIntosh, S., SARS-CoV-2 viroporin encoded by ORF3a triggers the NLRP3 inflammatory pathway. *Virology* 2022.
136. Swanson, K. V.; Deng, M.; Ting, J. P.-Y., The NLRP3 inflammasome: molecular activation and regulation to therapeutics. *Nature Reviews Immunology* 2019, *19* (8), 477-489.
137. Hayn, M.; Hirschenberger, M.; Koepke, L.; Nchioua, R.; Straub, J. H.; Klute, S.; Hunszinger, V.; Zech, F.; Bozzo, C. P.; Aftab, W., Systematic functional analysis of SARS-CoV-2 proteins uncovers viral innate immune antagonists and remaining vulnerabilities. *Cell Rep.* 2021, *35* (7), 109126.
138. Marquez-Miranda, V.; Rojas, M.; Duarte, Y.; Diaz-Franulic, I.; Holmgren, M.; Cachau, R. E.; Gonzalez-Nilo, F. D., Analysis of SARS-CoV-2 ORF3a structure reveals chloride binding sites. *bioRxiv* 2020.
139. Piret, J.; Boivin, G., Viral interference between respiratory viruses. *Emerg. Infect. Dis.* 2022, *28* (2), 273.
140. Beyer, D. K.; Forero, A., Mechanisms of Antiviral Immune Evasion of SARS-CoV-2. *J. Mol. Biol.* 2022, *434* (6), 167265.
141. Fuss, C.; Palmaz, J. C.; Sprague, E. A., Fibrinogen: structure, function, and surface interactions. *J. Vasc. Interv. Radiol.* 2001, *12* (6), 677-682.
142. Miao, G.; Zhao, H.; Li, Y.; Ji, M.; Chen, Y.; Shi, Y.; Bi, Y.; Wang, P.; Zhang, H., ORF3a of the COVID-19 virus SARS-CoV-2 blocks HOPS complex-mediated assembly of the SNARE complex required for autolysosome formation. *Dev. Cell* 2021, *56* (4), 427-442. e5.
143. Jiang, H.-w.; Zhang, H.-n.; Meng, Q.-f.; Xie, J.; Li, Y.; Chen, H.; Zheng, Y.-x.; Wang, X.-n.; Qi, H.; Zhang, J., SARS-CoV-2 Orf9b suppresses type I interferon responses by targeting TOM70. *Cell. Mol. Immunol.* 2020, *17* (9), 998-1000.
144. Li, J.-Y.; Liao, C.-H.; Wang, Q.; Tan, Y.-J.; Luo, R.; Qiu, Y.; Ge, X.-Y., The ORF6, ORF8 and nucleocapsid proteins of SARS-CoV-2 inhibit type I interferon signaling pathway. *Virus Res.* 2020, *286*, 198074.
145. Liu, X.-Y.; Wei, B.; Shi, H.-X.; Shan, Y.-F.; Wang, C., Tom70 mediates activation of interferon regulatory factor 3 on mitochondria. *Cell Res.* 2010, *20* (9), 994-1011.

146. Terracciano, R.; Preianò, M.; Fregola, A.; Pelaia, C.; Montalcini, T.; Savino, R., Mapping the SARS-CoV-2–host protein–protein interactome by affinity purification mass spectrometry and proximity-dependent biotin labeling: A rational and straightforward route to discover host-directed anti-SARS-CoV-2 therapeutics. *Int. J. Mol. Sci.* 2021, *22* (2), 532.
147. Fierabracci, A.; Arena, A.; Rossi, P., COVID-19: A review on diagnosis, treatment, and prophylaxis. *Int. J. Mol. Sci.* 2020, *21* (14), 5145.
148. Stewart, C. E.; Torr, E. E.; Mohd Jamili, N. H.; Bosquillon, C.; Sayers, I., Evaluation of differentiated human bronchial epithelial cell culture systems for asthma research. *J. Allergy* 2012, *2012*.
149. Tseng, C.-T. K.; Tseng, J.; Perrone, L.; Worthy, M.; Popov, V.; Peters, C. J., Apical entry and release of severe acute respiratory syndrome-associated coronavirus in polarized Calu-3 lung epithelial cells. *J. Virol.* 2005, *79* (15), 9470-9479.
150. Shen, B.; Finkbeiner, W.; Wine, J.; Mrsny, R.; Widdicombe, J., Calu-3: a human airway epithelial cell line that shows cAMP-dependent Cl-secretion. *American Journal of Physiology-Lung Cellular and Molecular Physiology* 1994, *266* (5), L493-L501.
151. Foster, K. A.; Avery, M. L.; Yazdanian, M.; Audus, K. L., Characterization of the Calu-3 cell line as a tool to screen pulmonary drug delivery. *Int. J. Pharm.* 2000, *208* (1-2), 1-11.
152. Kanimozhi, G.; Pradhapsingh, B.; Pawar, C. S.; Khan, H. A.; Alrokayan, S. H.; Prasad, N. R., SARS-CoV-2: pathogenesis, molecular targets and experimental models. *Front. Pharmacol.* 2021, *12*.
153. Vénéreau, E.; Ceriotti, C.; Bianchi, M. E., DAMPs from cell death to new life. *Front. Immunol.* 2015, *6*, 422.
154. Haghi, M.; Young, P. M.; Traini, D.; Jaiswal, R.; Gong, J.; Bebawy, M., Time-and passage-dependent characteristics of a Calu-3 respiratory epithelial cell model. *Drug Dev. Ind. Pharm.* 2010, *36* (10), 1207-1214.
155. Aghapour, M.; Raee, P.; Moghaddam, S. J.; Hiemstra, P. S.; Heijink, I. H., Airway epithelial barrier dysfunction in chronic obstructive pulmonary disease: role of cigarette smoke exposure. *Am. J. Respir. Cell Mol. Biol.* 2018, *58* (2), 157-169.
156. Foster, K. A.; Oster, C. G.; Mayer, M. M.; Avery, M. L.; Audus, K. L., Characterization of the A549 cell line as a type II pulmonary epithelial cell model for drug metabolism. *Exp. Cell Res.* 1998, *243* (2), 359-366.
157. Zanoni, I.; Granucci, F.; Broggi, A., Interferon (IFN)-λ takes the helm: immunomodulatory roles of type III IFNs. *Front. Immunol.* 2017, *8*, 1661.
158. Thomson, S. J.; Goh, F. G.; Banks, H.; Krausgruber, T.; Kotenko, S. V.; Foxwell, B. M.; Udalova, I. A., The role of transposable elements in the regulation of IFN-λ1 gene expression. *Proceedings of the National Academy of Sciences* 2009, *106* (28), 11564-11569.
159. Bugge, M.; Bergstrom, B.; Eide, O. K.; Solli, H.; Kjønstad, I. F.; Stenvik, J.; Espevik, T.; Nilsen, N. J., Surface Toll-like receptor 3 expression in metastatic intestinal epithelial cells induces inflammatory cytokine production and promotes invasiveness. *J. Biol. Chem.* 2017, *292* (37), 15408-15425.
160. Laura, G.; Liu, Y.; Fernandes, K.; Willis-Owen, S. A. G.; Ito, K.; Cookson, W. O.; Moffatt, M. F.; Zhang, Y., ORMDL3 regulates poly I:C induced inflammatory responses in airway epithelial cells. *BMC Pulm. Med.* 2021, *21* (1), 167.
161. Smith, S. M.; Wunder, M. B.; Norris, D. A.; Shellman, Y. G., A simple protocol for using a LDH-based cytotoxicity assay to assess the effects of death and growth inhibition at the same time. *PLoS One* 2011, *6* (11), e26908.

162. Berridge, M. V.; Herst, P. M.; Tan, A. S., Tetrazolium dyes as tools in cell biology: new insights into their cellular reduction. *Biotechnol. Annu. Rev.* 2005, *11*, 127-152.
163. Galluzzi, L.; Aaronson, S. A.; Abrams, J.; Alnemri, E. S.; Andrews, D. W.; Baehrecke, E. H.; Bazan, N.; Blagosklonny, M. V.; Blomgren, K.; Borner, C., Guidelines for the use and interpretation of assays for monitoring cell death in higher eukaryotes. *Cell Death Differ.* 2009, *16* (8), 1093-1107.
164. Kroemer, G.; Galluzzi, L.; Vandenabeele, P.; Abrams, J.; Alnemri, E. S.; Baehrecke, E.; Blagosklonny, M.; El-Deiry, W.; Golstein, P.; Green, D., Classification of cell death: recommendations of the Nomenclature Committee on Cell Death 2009. *Cell Death Differ.* 2009, *16* (1), 3-11.
165. Bianchi, F.; Alexiadis, S.; Camisaschi, C.; Truini, M.; Centonze, G.; Milione, M.; Balsari, A.; Tagliabue, E.; Sfondrini, L., TLR3 expression induces apoptosis in human non-small-cell lung cancer. *Int. J. Mol. Sci.* 2020, *21* (4), 1440.
166. Taura, M.; Fukuda, R.; Suico, M. A.; Eguma, A.; Koga, T.; Shuto, T.; Sato, T.; Morino-Koga, S.; Kai, H., TLR3 induction by anticancer drugs potentiates poly I: C-induced tumor cell apoptosis. *Cancer Sci.* 2010, *101* (7), 1610-1617.
167. Palchetti, S.; Starace, D.; De Cesaris, P.; Filippini, A.; Ziparo, E.; Riccioli, A., Transfected poly (I: C) activates different dsRNA receptors, leading to apoptosis or immunoadjuvant response in androgen-independent prostate cancer cells. *J. Biol. Chem.* 2015, *290* (9), 5470-5483.
168. Kübler, K.; tho Pesch, C.; Gehrke, N.; Riemann, S.; Daßler, J.; Coch, C.; Landsberg, J.; Wimmenauer, V.; Pölcher, M.; Rudlowski, C., Immunogenic cell death of human ovarian cancer cells induced by cytosolic poly (I: C) leads to myeloid cell maturation and activates NK cells. *Eur. J. Immunol.* 2011, *41* (10), 3028-3039.
169. Chen, H.; Wang, D. L.; Liu, Y. L., Poly (I: C) transfection induces mitochondrial-mediated apoptosis in cervical cancer. *Mol. Med. Report.* 2016, *13* (3), 2689-2695.
170. Barber, G. N., STING: infection, inflammation and cancer. *Nature Reviews Immunology* 2015, *15* (12), 760-770.
171. Rui, Y.; Su, J.; Shen, S.; Hu, Y.; Huang, D.; Zheng, W.; Lou, M.; Shi, Y.; Wang, M.; Chen, S., Unique and complementary suppression of cGAS-STING and RNA sensing-triggered innate immune responses by SARS-CoV-2 proteins. *Signal transduction and targeted therapy* 2021, *6* (1), 1-11.
172. Wang, W.; Zhou, Z.; Xiao, X.; Tian, Z.; Dong, X.; Wang, C.; Li, L.; Ren, L.; Lei, X.; Xiang, Z., SARS-CoV-2 nsp12 attenuates type I interferon production by inhibiting IRF3 nuclear translocation. *Cell. Mol. Immunol.* 2021, *18* (4), 945-953.
173. Han, L.; Zhuang, M. W.; Deng, J.; Zheng, Y.; Zhang, J.; Nan, M. L.; Zhang, X. J.; Gao, C.; Wang, P. H., SARS-CoV-2 ORF9b antagonizes type I and III interferons by targeting multiple components of the RIG-I/MDA-5–MAVS, TLR3–TRIF, and cGAS–STING signaling pathways. *J. Med. Virol.* 2021, *93* (9), 5376-5389.
174. Le Bert, N.; Clapham, H. E.; Tan, A. T.; Chia, W. N.; Tham, C. Y. L.; Lim, J. M.; Kunasegaran, K.; Tan, L. W. L.; Dutertre, C.-A.; Shankar, N.; Lim, J. M. E.; Sun, L. J.; Zahari, M.; Tun, Z. M.; Kumar, V.; Lim, B. L.; Lim, S. H.; Chia, A.; Tan, Y.-J.; Tambyah, P. A.; Kalimuddin, S.; Lye, D.; Low, J. G. H.; Wang, L.-F.; Wan, W. Y.; Hsu, L. Y.; Bertoletti, A.; Tam, C. C., Highly functional virus-specific cellular immune response in asymptomatic SARS-CoV-2 infectionSARS-CoV-2–specific T cells in asymptomatic. *J. Exp. Med.* 2021, *218* (5).

175. Que, Y.; Hu, C.; Wan, K.; Hu, P.; Wang, R.; Luo, J.; Li, T.; Ping, R.; Hu, Q.; Sun, Y.; Wu, X.; Tu, L.; Du, Y.; Chang, C.; Xu, G., Cytokine release syndrome in COVID-19: a major mechanism of morbidity and mortality. *Int. Rev. Immunol.* 2022, *41* (2), 217-230.

Supplementary

RIPA Buffer Recipe

Buffer	Stock solution	Total volume
Lysis buffer (2x) *keep in -20 oC **dilute 1:1 with fresh benzonase and proteinase inhibitor solution before using*	 Glycerol 87% NaF 0.5M Tris/HCl (pH 8.0) 1M EDTA (pH 8.0) 0.2M EGTA 0.2M NaCl 5M Triton X-100 10% Na3VO4 0.2M Sodium Deoxycholate 10% MiliQ water	for 100 mL: 23 mL 20 mL 10 mL 1 mL 1 mL 15.4 mL 20 mL 1 mL 10 mL Up to 100 mL
Benzonase and proteinase inhibitor cocktail solution **make before use*	 Benzonase 0.25 U/ml Proteinase inhibitor cocktail MiliQ water	for 5 mL: 1.3 µL 1 tablet 5 mL

Supplementary Table 1. Components of RIPA buffer employed for the lysis of cells and protein extraction prior to their WB analysis.

Molecular weights of SARS-CoV-2 viral proteins

SARS-CoV-2 viral protein	Molecular Mass (kDa)
ORF3a	31.1
ORF6	7.3
ORF9b	10.8

Supplementary Table 2. Molecular weight (kDa) of transfected SARS-CoV-2 viral proteins, compared to Krogan's laboratory.

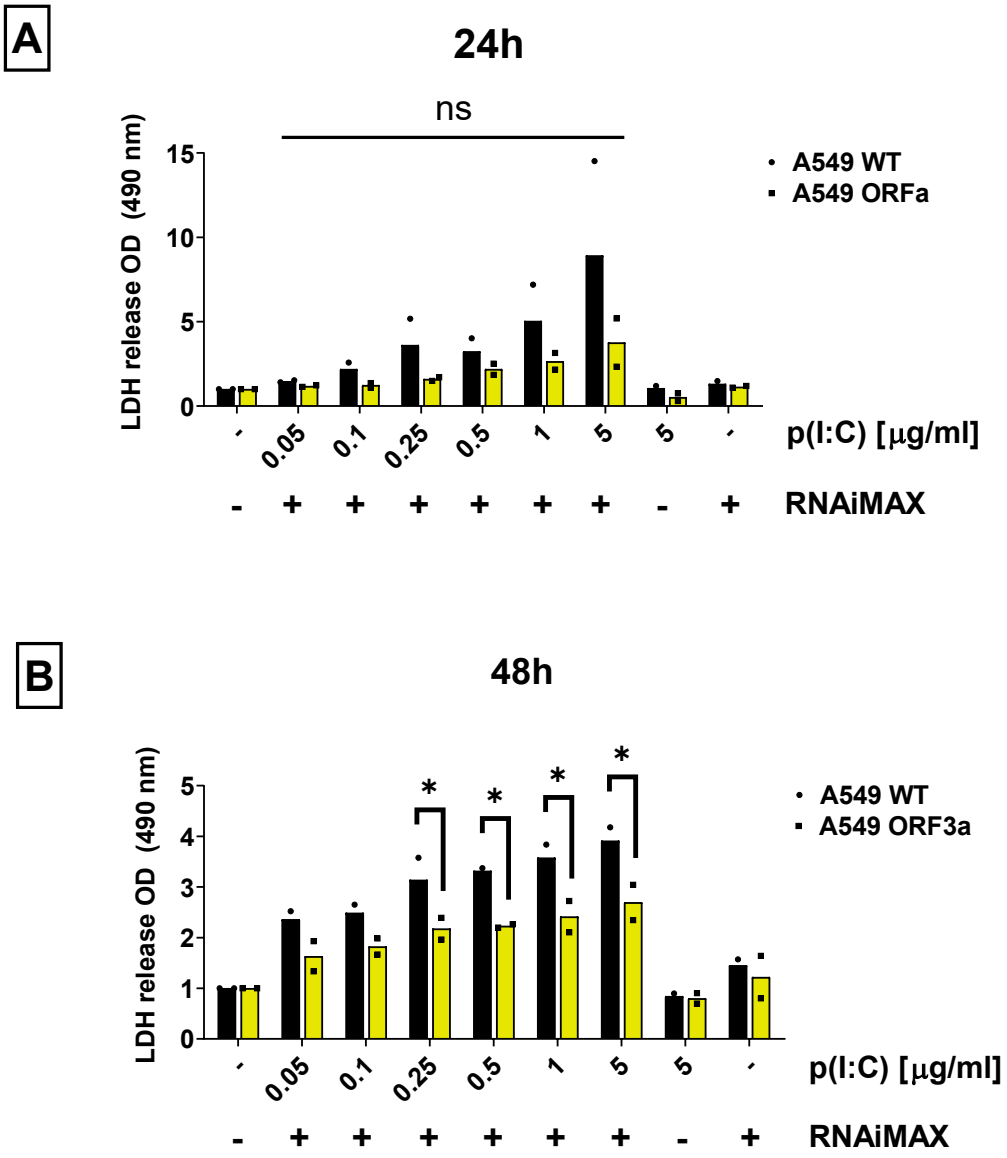

Supplementary Figure 1. LDH release from wild-type and SARS-CoV-2 ORF3a expressing A549 cell lines in response to RIG-I/MDA5 stimulation. *LDH release into culture supernatants from wild-type and ORF3a-transduced A549 cells untreated or stimulated with poly(I:C) + lipofectamine RNAiMAX after incubation for 24 (**A**) and 48 hours (**B**). Cells were seeded the day before stimulation with poly(I:C) + lipofectamine RNAiMAX. Stimulation with poly(I:C) or RNAiMAX alone (twice the volume used for stimulation with the highest poly(I:C) concentration) was included as an experimental control. Untreated controls were incubated with CCM. Doxycycline (0.5 µg/ml) was added to the CCM of A549 ORF3a-transduced cell line. After incubation for 24 (**A**) and 48 hours (**B**), cell supernatants were collected. Absorbance was quantified at 490 nm and 655 nm and subtracted. Results were normalised to the untreated control and show means of technical duplicates from two biological duplicates. Differences in treatment response in both cell lines were assessed by two-way ANOVA with Tukey correction. ns $p>0.05$, * $p\leq0.05$.*

Daniel Margarido Galán

Investigating the immunomodulatory effects of SARS-CoV-2 proteins ORF3a, ORF6 and ORF9b

NTNU
Norwegian University of
Science and Technology